



universität
wien

DISSERTATION

Titel der Dissertation

Compartmental Modeling for the Volatile Organic Compound Isoprene in Human Breath

Verfasserin

Helin Koç Rauchenwald

angestrebter akademischer Grad

Doktorin der Naturwissenschaften (Dr. rer. nat.)

Wien, im September 2011

Studienkennzahl lt. Studienblatt: A 091 405

Dissertationsgebiet lt. Studienblatt: Mathematik

Betreuerin / Betreuer: ao. Univ.-Prof. Gerald Teschl, Univ.-Doz. Karl Unterkofler

Abstract

Mathematics subject classification: 92C45, 92C35, 93C10, 93B30

Keywords: *breath gas analysis, volatile organic compounds, modeling, isoprene.*

The interest in the diagnostic potential of volatile organic compounds (VOCs) in breath increases as a result of constantly improving modern analyzing techniques. Unfortunately, physicians have paid little attention to a causal mathematical description of the underlying physiological processes yet. Even if mathematical models are idealized representations of the reality, their impact on combining all the information and in prediction is undisputable.

The emphasis of this work was to derive a mechanical description of the physiological processes governing the gas exchange dynamics of isoprene under physical exercise. Isoprene has been classified in the group of biomarkers and can be seen as a prototypic example of low-soluble substances concerning its gas exchange mechanisms. Modern mass spectrometric techniques allow its online quantification in exhaled breath in real time.

Describing short-term effects is crucial to get a deeper understanding of the determining factors of the underlying mechanisms. Changes in physiology occurring during physical exercise, such as increased ventilation and increased cardiac output, offer an opportunity to examine and understand the exchange processes that determine absorption, desorption, and distribution of this important volatile organic compound. Thus, for the present work cycling exercises on a medical ergometer were carried out and an experimental setup allowing parallel and real-time measurements of exhaled isoprene time-courses in conjunction with physiological parameters was used to collect relevant information for modeling purposes.

Isoprene concentrations show a distinct peak shaped response to exercise, which has been recognized before by several investigators. The existing model describing exhaled dynamics of isoprene in response to exercise is able to explain its dynamics only on the basis of physiological assumptions, which contradict physiological facts and real-time measurements. As conventional knowledge suggests isoprene is expected to be sensitive to the regional inhomogeneities in the lung due to its low solubility in blood. For this reason, we focused our attention onto various existing lung models first, which take into account regional inhomogeneities of the lung. However, such representations also fail to describe the observed data. On the contrary, experimental evidence suggests a relationship between muscle compartment activity and isoprene excretion. The first known physiological model developed for isoprene exposure studies assumes a production of isoprene in the liver as the solely source of isoprene in the human body and fails to describe its exchange dynamics under physical exercise. Based on this model, we derived

a compartment model, which suggests a metabolic activity of the skeletal muscles. The new model is capable to explain the observed isoprene profiles within a range of acceptable parameter sets.

Even if further investigations are necessary to consolidate this hypothesis, several findings about isoprene, such as the linkage of its output to age and statin therapy, and the effect of bilateral deficit when switching from two-legged to one-legged exercise appear to fit into this hypothesis.

Chapter 1 of this thesis briefly summarizes the motivation behind the breath gas analytical investigations, experimental setup used for the experiments, and classical theory of pulmonary gas exchange.

Chapter 2 concerns the derivation of compartmental mass balance equations used in physiological modeling.

Chapter 3 covers the description of mathematical and numerical methods for qualitative and quantitative analysis of modeling and parameter estimation processes.

The first 5 sections of chapter 4 represent existing modeling approaches and discuss their physiological relevance. Subsequently, some insightful experiments are presented which lead to the new model developed by our research group. This model has been refined and a more specific location of isoprene, namely skeletal muscles is suggested.

The appendices summarize fundamental physical principles underlying the derivation of physiologically based models and parameter values.

Zusammenfassung

Der menschliche Atemluft enthält hunderte von flüchtigen Spurenelementen, die entweder im Organismus als Folge von biochemischen und metabolischen Prozessen entstehen, oder von der Umwelt absorbiert werden. Der Quantifizierung von flüchtigen organischen Spurenelementen (VOCs) im menschlichen Atem wird ein diagnostisches Potential zugeschrieben. Atemgasanalyse ist die wissenschaftliche Untersuchung der Atemluft und ihre Hauptmotivation ist die Suche nach Marker-Substanzen, die als Indikatoren von pathophysiologischen Erkrankungen dienen können.

Aufgrund ihrer nicht-invasiven Natur haben atemgasanalytische Untersuchungen in den letzten Jahren enorm an Interesse gewonnen. Allerdings ist der nicht-invasive Test noch in Entwicklung und hat in der klinischen Routine noch nicht Eingang gefunden. Neben Problemen bezüglich der Standardisierung der Atemluftabnahme und der Analysemethoden, verhindert das unzureichende Wissen über die Herkunft und die biochemischen Prozesse dieser Substanzen die Anwendung der Atemtests.

Die physiologisch basierte mathematische Modellierung spielt bei der quantitativen Analyse der experimentellen Daten eine entscheidende Rolle. Ihre Aufgabe ist es, eine mechanische Beschreibung der zugrundeliegenden physiologischen Phänomene unter Berücksichtigung aller relevanten experimentellen Daten zu liefern. Somit ermöglicht die mathematische Modellierung einerseits ein detailliertes Verständnis der physiologischen Vorgänge und kann andererseits aufgrund dessen bei der Standardisierung und Entwicklung der Atemluftentnahmemethoden eine wichtige Rolle spielen. Die Arbeit konzentriert sich auf Isopren, welches eine der wichtigsten organischen Substanzen in der menschlichen Atemluft ist. Das Ziel der vorliegenden Arbeit war, den quantitativen Zusammenhang zwischen den Atemluftkonzentration und der zugrundeliegenden endogenen Blut/und Gewebekonzentrationen von Isopren zu beschreiben. Um die Kurzzeiteffekte der relevanten physiologischen Faktoren (sowie Blutfluss und Atemfluss) zu bestimmen, wurden Echtzeitmessungen unter Ergometerbelastung durchgeführt. Die herkömmlichen Modelle, die sich hauptsächlich auf die funktionellen Änderungen der Lunge konzentrieren, sind nicht in der Lage, eine physiologisch relevante Beschreibung der experimentellen Daten zu liefern. Im Gegensatz dazu wurde ein neues Modell auf Basis einer peripheren Herkunft von Isopren von unserer Arbeitsgruppe entwickelt. Die neue Hypothese wurde in der vorliegenden Arbeit durch weitere Experimente bekräftigt und das zugrundeliegende Modell verfeinert, was uns zu der Schlussfolgerung führte, dass die Skelettmuskeln eine wichtige Rolle bei der Isoprenformation spielen.

Diese Hypothese wirft ein neues Licht auf die bisherigen Untersuchungen und eröffnet neue Diskussions- und Interpretationsmöglichkeiten über die Herkunft von Isopren.

Keywords: Breath gas analysis, isoprene, volatile organic compounds, modeling

Acknowledgements

I want to thank my advisors Karl Unterkofler and Gerald Teschl for their professional support. Also I am very grateful to Anton Amann and Julian King for the close collaboration within a theoretical and experimental framework, and for all the fruitful discussions.

Contents

1	Introduction	3
1.1	Breath Gas Analysis and The Need for Modeling	3
1.2	A Survey on Physiological Relevant Facts	8
1.2.1	Cardiovascular and respiratory responses to dynamical exercise	8
1.2.2	Isoprene	9
1.2.3	Acetone	11
1.3	Real Time Measurements	12
1.4	Modeling Pulmonary Gas Exchange	15
2	Physiological Modeling	19
2.1	Compartmental Mass Transport	19
2.2	Respiratory Gas Exchange	21
2.2.1	Mass Balance Equation	21
2.3	Gas Exchange in Systemic Compartments	23
3	Model Structure and Properties	26
3.1	Qualitative Properties of the Model	27
3.1.1	Existence and Uniqueness of Solutions	27
3.1.2	Continuous Dependence on Initial Conditions and Parameters	29
3.1.3	Stability of Equilibrium Points	30
3.1.4	Compartmental Systems	32
3.2	Optimization and Parameter Identifiability	36
3.2.1	A Priori Observability/Identifiability	37
3.2.2	Nonlinear Least Squares Optimization	39
3.2.3	General Gradient Based Algorithms	41
3.2.4	Constrained Nonlinear Optimization	43
3.2.5	A Posteriori Identifiability	44
3.2.6	Qualitative Analysis of Parameter Estimates	46
4	Modeling Isoprene	49
4.1	A Five Compartment Physiological Toxicokinetic Model	51

4.2	A Serial Model of the Lung	55
4.3	A Parallel Model of the Lung	59
4.4	Stratified Inhomogeneity	63
4.5	Discussion to the Aforecited Models	65
4.6	Revealing Information from Experiments	66
	4.6.1 A first three compartment model for isoprene	69
4.7	A Five Compartment Model	72
4.8	Discussion and Conclusions	83
A	Physical Preliminaries	85
	A.1 The Ideal Gas Law	85
	A.2 Diffusion and Solubility of Gases	86
	A.3 Unit Conversion Factors for Concentrations	88
B	Parameter Values	89
	B.1 Physiological Parameters	89
	B.2 Model Parameters	90
C	Symbols and Abbreviations	92
	Bibliography	92
	Curriculum Vitae	102

Chapter 1

Introduction

1.1 Breath Gas Analysis and The Need for Modeling

The linkage of human breath composition to health and disease has been noticed long since. Our current day understanding of the diagnostic potential of breath gas can be traced back to antiquity as demonstrated by Hippocrates in his treatise on breath aroma and disease [26].

In 1784 Lavoisier and Laplace showed that respiration consumes oxygen and eliminates carbon dioxide. In the mid 1880s Nebelsthal discovered the relation between breath acetone and diabetics, and in 1874 Anstie isolated ethanol from breath, which is the basis of breath alcohol testing today [26, 69]. However, a major breakthrough in the scientific study of breath started in the 1970s when Linus Pauling demonstrated the existence of more than 250 unique substances in exhaled breath [84]. Since then, breath gas analysis has rapidly evolved as a new diagnostic tool in medical testing for respiratory and systemic diseases.

Besides oxygen and carbon dioxide, human breath contains elemental gases like nitric oxide, carbon monoxide, and a multitude of volatile organic substances. The small inorganic molecule nitric oxide (NO) is predominantly generated in the bronchial system and is subject to several medical investigations since it has been recognized as a mediator of numerous physiological processes and as a marker of airway inflammation. The significant role of NO in vasodilation of blood vessels has been proved in the Nobel prize-winning work by Furchgott, Ignarro and Murad, which nowadays has reached clinical applications [14, 57]. Volatile organic compounds (VOCs) are a large group of carbon-based (hence organic) chemicals which include a very wide range of individual substances, such as aldehydes, halocarbons, oxygenates, ketones, and hydrocarbons. Volatility indicates that the gases mentioned have high vapor pressure under normal conditions (at room temperature), and thus can significantly vaporize and enter the exhaled air.

The initial technical difficulties in detection and identification of VOCs in exhaled breath have been for the most part overcome due to the development of very sensitive modern analyzing-techniques (such as mass spectrometry (MS), gas chromatography (GC) and gas spectrometry mass spectrometry (GC-MS)) in the last three decades. Now more than 200 VOCs can be detected at trace level down to the parts-per-trillion (ppt) range in human breath [4, 12, 39, 60, 64, 84, 85].

For VOCs, sampling and analysis of breath is preferred to direct measurement from blood samples, because breath collection is non-invasive and can be carried out as often as desirable. This has led to an increased interest of the physiological meaning of VOCs and correlations of their concentrations with patients' clinical conditions.

While exogenous VOCs are absorbed from the environment by inhalation, ingestion or skin contact and thus are of interest for quantifying the body burden in response to environmental exposure [7, 86], endogenous VOCs originate from biochemical and metabolic processes in the human body. It is believed that the concentration of blood-borne VOCs in exhaled breath is a reflection of their concentration in blood through gas exchange in the blood/breath interface in the lungs (due to their volatility, the kinetics of VOCs can be approximated according the substance solubilities), therefore some systemic diseases accompanied by metabolic and oxidative stress alter the pattern of exhaled VOCs concentrations [73]. Among others, breast cancer, diabetes mellitus, lipid preoxidation, heart, liver and renal diseases have been investigated in association with exhaled VOC profiles. Table 1.1 provides a selected list of VOCs and related disorders and/or clinical applications. References and a more detailed list can be found in [69].

Even if the major motivation behind breath gas analytical investigations is the search for potential biomarkers of pulmonary diseases and pathophysiological disorders, there are a number of further applications. The ability of continuous and on-line analysis (i.e., by means of proton-transfer-mass-spectrometry (PTR-MS)) of exhaled breath [1, 6, 52–55] renders ongoing information on the current metabolic and physiological state of an individual. Hence, it opens new areas of future applications like dynamic assessments of normal physiological function or pharmacodynamics [3] and optimal control of narcosis in anesthesiology [95].

Despite the promising diagnostic, prognostic and predictive potential of biomarkers, breath analysis is a young field of research and has not yet been widely accepted in clinical routine. Breath sampling, in particular, is far from being a standardized procedure due to the numerous confounding factors biasing the concentrations of volatiles in breath [2]. These factors are related to both breath sampling protocols as well as complex chemical and physiological mechanisms underlying biochemical pathways and exhalation kinetics of VOCs. Even under resting conditions breath concentrations of VOCs can strongly be influenced by specific physiological parameters

(such as cardiac output and breathing patterns), depending on the physical-chemical properties of the compound under study [10, 22].

Breath marker	Conditions
ethane	lipid preoxidation, oxidative stress, breast cancer, heart transplant rejection
pentane	lipid preoxidation, breast cancer
isoprene	lung cancer, breast cancer, hypercholesterolemia, oxidative stress
acetone	diabetes mellitus, ketosis, halitosis
acetaldehyde	lung cancer, alcohol consumption
methanol	overgrowth of intestinal bacterial flora
ethanol	overgrowth of intestinal bacterial flora, alcohol consumption
2-propanol	acetone reduction by bacterial flora, lung cancer, breast cancer, stomach cancer
dimethylsulfide	Intestinal bacterial flora, liver disorders, oral infection
ammonia	uremia, peptic ulcer, kidney disease
benzene	lung cancer, breast cancer, smoke exposure
ethylene	anesthetics inhalation

Table 1.1 – A selected list of breath biomarkers and related disorders [69].

In order to obtain diagnostically conclusive results, a thorough understanding of the physiological events and phenomena affecting exhaled VOC levels as well as an appropriate choice of breath sampling conditions and protocols are essential.

For illustration of this point, consider the population study result in Figure 1.1, which may suggest the detection of lung cancer patients on the basis of decreased isoprene levels in end-tidal breath.

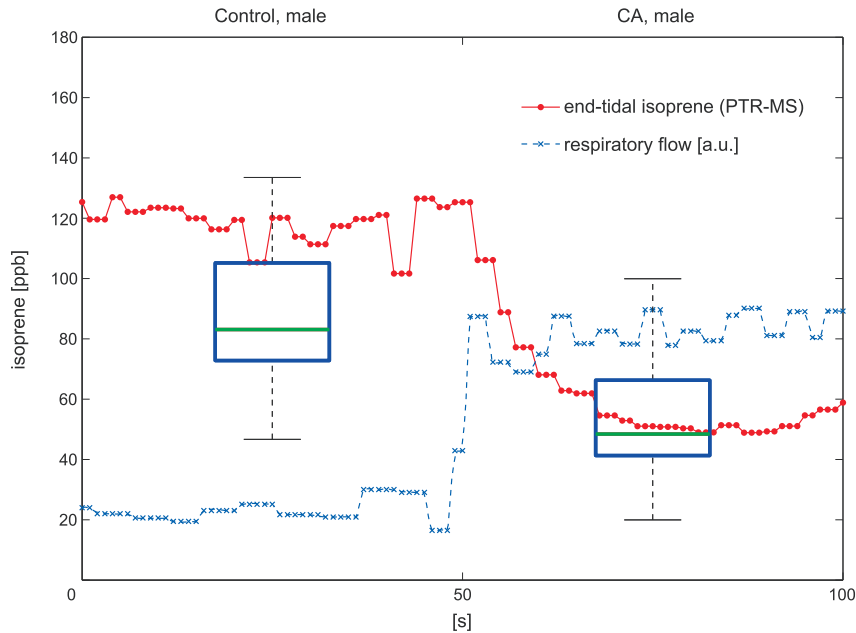


Figure 1.1 – Overlay depicting the variability of end-tidal isoprene concentrations during hyperventilation of one single volunteer as compared to the population boxplots associated with healthy test subjects and lung cancer patients, cf. [12].

Effectively, from the respective boxplots a tentative threshold value of about 70 ppb differentiating between lung cancer patients and healthy volunteers might be established. It should be noted, however, that from a procedural point of view this observation will be of limited use, since any further attempt to classify a specific individual will strongly depend on the hemodynamic and respiratory status of the test subject investigated. Correspondingly, by measuring end-tidal isoprene levels with breath-to-breath resolution (cf. [53]), it can be demonstrated that a normal healthy volunteer at rest might easily switch between the two groups defined above merely by changing his breathing pattern, e.g., by breathing faster or by increasing tidal volume. Doing so leads to an instantaneous drop of breath isoprene levels, thereby hampering an unambiguous classification of this volunteer. Such issues are further aggravated by the fact that human subjects tend to hyperventilate when they are asked to breathe normally and provide a breath sample [91]. Consequently, any screening study results like the one above must be complemented by information on their variability with changes of

ventilation, blood flow or pre-measurement conditions.

This paradigmatic example shows that a proper quantitative assessment of the underlying exhalation kinetics is mandatory when aiming at the successful introduction of a clinically applicable breath test.

In this context, mathematical modeling and simulation can be employed for capturing the decisive quantitative features of the observable data. The primary task of mathematical modeling hence is to provide a mechanistic description of the physiological phenomena governing the VOC under scrutiny using all the experimental evidence available. Once such a model has been developed it becomes possible to understand the key relationships underlying the physiological behavior of the compound and to identify its defining parameters. Such a quantitative approach can aid substantially in preventing misinterpretations of experimental results and in discovering errors and omissions in earlier interpretations. Furthermore, these analyses can guide the standardization and establishment of new sampling protocols, avoiding potential confounding factors and maximizing the information content of experimental results.

In the present work, we aim to establish the quantitative relationship between breath and the underlying endogenous blood/tissue concentrations of isoprene. Beside the determination of physiological factors influencing the gas exchange dynamics, an exhaustive understanding of the physiological phenomenon can be achieved by describing the short-term effects of exhaled dynamics in response to varying physiological conditions, which is mimicked here by ergometer exercises.

In our experiments we have focused on two endogenous VOCs, isoprene and acetone, which have received wide attention in the field of exhaled breath analysis. These two compounds have contrasting physical-chemical properties (isoprene is strongly lipophilic whereas acetone is hydrophilic) and thus can be considered as representative examples in a broad spectrum for modeling. While acetone will serve as an example for comparison and complement in this part of the thesis, we refer to King et al. [55] for a corresponding model and detailed analysis regarding acetone.

In the following we will briefly review some of the most important facts that have provided a deeper understanding on the involved mechanisms influencing the dynamics of isoprene and acetone in exhaled breath.

1.2 A Survey on Physiological Relevant Facts

1.2.1 Cardiovascular and respiratory responses to dynamical exercise

Physical exercise triggers a coordinated response of the respiratory and cardiovascular systems. Due to the increasing activity and demands of skeletal muscles, exercise increases the demand for oxygen and the production of carbon dioxide. To meet this increased demand, three primary physiological changes take place: increased ventilation, increased cardiac output and redistribution of cardiac output to enhance perfusion of exercising muscles.

The volume of fresh air moved into the lung from outside the body and the volume of blood pumped by the heart per unit of time are referred to as *ventilation* and *cardiac output*, respectively.

The increase in ventilation is nearly linear to both oxygen consumption and carbon dioxide production up to a level of 60% of the subject's maximal work capacity. Above that level, ventilation increases faster than oxygen consumption but continues to rise proportionally to the increase in carbon dioxide production [62]. Even during mild to moderate exercise (aerobic metabolism) the immediate increase in ventilation occurs too quickly to be a response to alterations in metabolism or changes in the blood gases [62] and therefore requires some other sensory input or central nervous system mechanisms to be responsible. Two possibilities to explain this response are neurally derived stimuli (feedforward control mechanism, a learned response to exercise) and humorally derived stimuli (feedback response to exercise, blood-borne stimuli) [42]. During heavy exercise (anaerobic threshold) the respiratory drive may involve increased sensory inputs to the central venous system which may be important in producing the additional increase in ventilation [42].

Although the reason for the abrupt increase in ventilation at the beginning of dynamical exercise remains uncertain, its presence is beyond doubt and has been demonstrated by several investigators (see e.g., [42,62,67,118]). The increase in ventilation is usually a result of increases in both tidal volume and breathing frequency. Initially, the tidal volume increases more than the breathing frequency, but as metabolic acidosis develops, the increase in breathing frequency predominates [62].

Cardiac output increases linearly with oxygen consumption during exercise. This normally occurs more as a result of an anatomically mediated increase in the heart rate than from an increase in stroke volume. The mean systemic pressure increases which in turn raises the pressure gradient for venous return and local vasodilatation in the contracting muscles. As a consequence the increased cardiac output is distributed preferentially to these muscles [119]. Overall, cardiac output becomes more effective in supplying exercising muscles with oxygen and metabolic substrates and in removing

waste products. Increased perfusion of skin helps to remove the excess body heat generated during exercise [42].

While overall ventilation can increase by approximately 20-fold during maximal exercise, the heart increases its output by only about five times that of its normal resting output. Therefore, it is the cardiovascular system rather than the respiratory system that is the limiting factor in exercise of healthy people.

1.2.2 Isoprene

Isoprene, also known as 2-methyl-1, 3-butadiene (CAS number 78-79-5), is a volatile liquid organic hydrocarbon with a boiling point of 34 °C, a high vapor pressure of 60.7 kPa at 20 °C, and a molar mass of 68.11 g/mol. It is used primarily for the synthesis of isoprene rubber and of copolymers with styrene or with isobutene yielding rubbers with special properties [30].

Isoprene is a significant biosynthetic compound produced by plants, animals and bacteria. It is a fundamental structure of isoprenoid biochemicals, which include cholesterol, other sterols, carotenoids, and Vitamin A. In human breath isoprene is the major hydrocarbon component [34] with concentrations of around 100 ppb [53, 59, 111] during rest. A circadian rhythm of breath isoprene with an increase during the night has been observed [17, 73].

Breath isoprene concentrations have been reported to be non-detectable in the breath of neonates, while steadily increasing in teenagers and reaching a plateau level in the middle age [90, 103]. In young children exhaled breath isoprene is demonstrably lower than in adults by a factor of about 2.4 [65]. Moreover, isoprene levels in older people appear to decrease [59, 90].

The origin of human isoprene has been attributed to the mevalonate pathway of cholesterol biosynthesis [24, 105]. Cholesterol is synthesized practically in all our cells, however only the biosynthesis in the liver is supposedly of crucial importance for the metabolism, which emphasises a hepatic production of isoprene.

The biosynthesis of cholesterol is a complicated process, but it can be simplified to the following steps: Acetyl CoA (citric acid cycle) is a product of the metabolism of any source of energy, be it protein, fat, or carbohydrate. Initially three molecules of Acetyl-CoA are formed to mevalonate (mevalonic acid) which is the rate-determining step for the whole biosynthesis and is the site of action for statins. Mevalonate is then converted to form activated isoprene. Six active isoprene molecules form squalene and finally squalene is converted to cholesterol [44].

The synthesis of mevalonate from which isoprene is derived is inhibited by statins. Statin drugs ("cholesterol-lowering" drugs) inhibit the synthesis of mevalonate as has been demonstrated for lovastatin by Stone et al. [105] and for atorvastatin by Karl et al. [50]. The latter have shown that drug administration results in a proportionally decline of breath isoprene concen-

tration and the serum cholesterol levels and that cholesterol feeding, which suppresses mevalonate formation, also lowers breath isoprene concentration. In addition, cholesterol synthesis appears to occur mostly at night [75]. That is why it is believed that isoprene concentration measurements could potentially be used for mass screening for lipid disorders and to improve the care of patients suffering from disorders in cholesterol metabolism, such as hypercholesterolemia.

On the other hand, several studies have pointed out that the effects of statins extend beyond their cholesterol-lowering capacity. *Myopathy* is used as a general term for diseases of the muscles. Myotoxic effects have been reported to be a major adverse reaction to statin therapy, leading to the inhibition of skeletal muscle activity and cell injury [27, 29, 116].

The extent to which the mevalonate pathway accounts for isoprene formation under physiological conditions is still a matter of debate [73, 107]. In particular, the above-mentioned pathway rests on the acid-catalyzed solvolysis of dimethylallyl-diphosphate in the liver which may be insignificant at physiological pH values [100, 101].

Other aforementioned clinical applications of breath isoprene relate to end-stage renal disease (ESDR) [66], heart failure [71], acute myocardial infarction [72] and lung cancer [12]. A brief overview of the potential applications of breath isoprene as a biomarker can be found in [96].

Isoprene is metabolized to monoepoxide and diepoxide intermediates by liver microsomal cytochrome P450-dependent monooxygenases from several species, including humans. Detoxification of these intermediates may occur by hydrolysis (a chemical reaction or process in which a chemical compound is broken down by reaction with water) catalyzed by epoxide hydrolase or conjugation with glutathione catalyzed by glutathione-S-transferase [81].

Due to its volatility and low affinity for blood as reflected by a small blood:gas partition coefficient $\lambda_{b:air} = 0.75$ at body temperature [30], isoprene exchange occurs mainly in the lung (see Section 1.4). Physical activity causes strong changes in isoprene concentration in exhaled breath of humans [50, 53, 99]. Real time measurements during moderate workload ergometer challenges have been investigated by Karl et al. [50] and King et al. [53] demonstrating an initial increase of breath isoprene in the first minute of exercise by a factor of about 2 – 3 in mixed exhaled breath [50], and by a factor of about 3 – 4 in end-tidal breath [53], respectively. Because of these characteristic rest-to-work transitions isoprene concentration in exhaled breath might be interpreted as a potentially sensitive indicator for fluctuations of blood and respiratory flow and can therefore be viewed as a candidate for future assessments of hemodynamics, pulmonary function and gas exchange patterns via observed exhaled behavior.

1.2.3 Acetone

Acetone, also known as 2-propanone (or dimethyl ketone, β -keto-propane, pyroacetic ether, CAS number 67-64-1) is a volatile, highly flammable liquid with a boiling point of 56 °C, a vapor pressure of 24 kPa at 20 °C, and a molar mass of 58.08 g/mol. Acetone is commercially produced by fermentation of corn or from isopropyl alcohol, cumene or propane either as the main product or as a by-product of chemical reactions [49].

Acetone is one of the most abundant compounds in human breath with typical exhaled breath concentrations in the range of 500-1000 ppb in adults [53, 98, 110]. So far no influences of sex, age, and BMI on breath concentrations in adults could be detected [98].

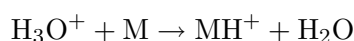
In mammals ^{14}C -carbons of labeled acetone have been found in liver glycogen, urea, cholesterol, fatty acids and a substantial amount of ^{14}C -carbons has been recovered in vivo in exhaled carbon dioxide [49, 87] indicating a metabolism of acetone intermediates. The two sources of acetone production in the body are the decarboxylation of acetoacetate and the dehydrogenation of isopropanol. The former compound seems to be the major source of acetone in mammals and arises from either lipolysis or amino acid degradation [49]. Metabolic elimination occurs by conversion of acetone into acetol by a cytochrome P450 isozyme. This isozyme is present in a wide variety of tissues such as liver, kidney, spleen, and intestines [49].

Breath acetone increases during starvation-induced and diabetic ketonemia [87, 106], fasting, and high-fat diets [32, 78, 79]. Breath and plasma acetone concentrations are nearly proportional [87], therefore breath acetone is a suggested marker for monitoring the ketotic state of an individual. Acetone has been used to assess the blood glucose level during a glucose load by Galassetti et al. [33]. Additionally, elevated breath acetone levels have been associated with congestive heart failure [58].

Acetone has a high water solubility, i.e., a blood:gas partition coefficient $\lambda_{\text{b:air}} = 340$ at body temperature [10]. As demonstrated by Anderson et al. [9, 10] this feature causes that upper airways take the primary role in acetone gas exchange. The airway interaction leads to a decreased relative elimination (expressed as the rate mixed venous to mixed alveolar partial pressure or concentration) and thus to an underestimation of blood gas levels. Rebreathed air (isothermal rebreathing) has shown to be a consistent and representative measure of alveolar air concentration for acetone, while end exhaled air of tidal breathing and prolonged expiration lead to an underestimation of alveolar air concentration by 30% and 20%, respectively [10]. Senthilmohan et al [99] reported slightly increased values under physical exercise. King et al [53] showed that exhaled acetone concentration during exercise closely resembles the profile of alveolar ventilation.

1.3 Real Time Measurements

The range of measurement techniques employed for breath gas analytical investigations is extremely diverse and each method comes with its specific strengths and weaknesses [5, 18]. Within the present setting, we will mainly focus on direct mass spectrometric techniques such as proton-transfer-reaction mass spectrometry (PTR-MS). In brief, the latter has proven to be a sensitive method for the quantification of volatile molecular species M on the basis of chemical ionization within a drift chamber. More specifically, it takes advantage of the proton transfer



from hydronium precursor ions originating from an adjoint hollow cathode. Specifically, this reaction scheme is selective to VOCs with proton affinities higher than water (166.5 kcal/mol), thereby avoiding the ionization of the bulk composition exhaled air, N_2 , O_2 , and CO_2 . Count rates of the nascent product ions MH^+ or fragments thereof appearing at specified mass-to-charge ratios m/z can subsequently be converted into absolute concentrations of the investigated compounds. Further details on quantification can be found in [98].

A major hallmark of PTR-MS is its *real-time* capability, allowing for the concentration measurement of VOCs with breath-by-breath resolution (i.e., on a time-scale of less than 0.5 s). The possibility of generating high frequency data can be viewed as an essential requirement for relating short-term changes in breath VOC concentrations to quick physiological variations (e.g., in blood or ventilatory flow). An experimental setup combining real-time PTR-MS trace gas measurements with data streams reflecting hemodynamic and respiratory parameters is shown in Figure 1.2.

The setup consists of five central parts:

- a hemodynamical monitor (Task Force Monitor) measuring heart rate, heart minute volume, blood pressure, etc, on the basis of standard ECG leads and transthoracic impedance cardiography (ICG),
- a spirometer (Medikro SpiroStar) measuring the volumetric flow rate when breathing through a flow transducer of some form (e.g., a head mask),
- a heated, chemically inert gas sample line leading from the flow transducer to the mass spectrometer,
- a medical semi-supine cycle ergometer for imposing certain workloads on the test subject,
- the PTR-MS for measurement of volatile compounds in exhaled breath.

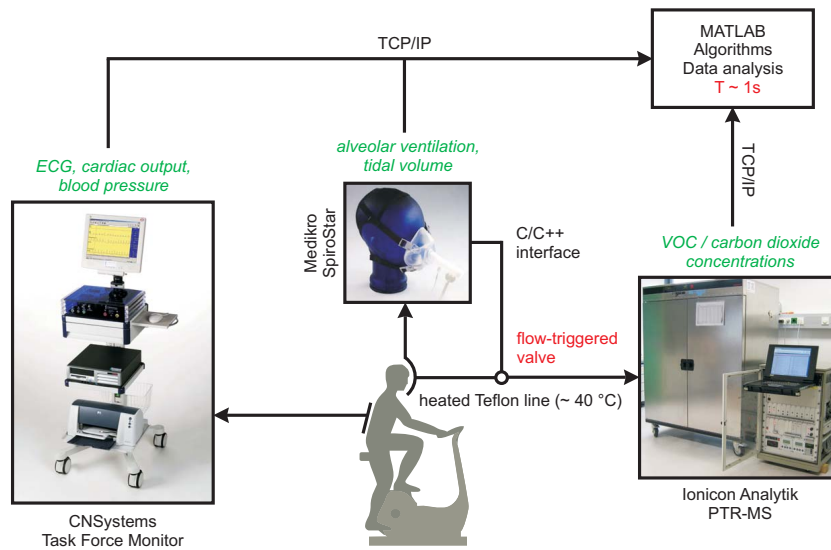


Figure 1.2 – Experimental setup used for obtaining VOC profiles in conjunction with a number of physiological parameters [53].

Items in *italic* correspond to measurable variables. A selective and automated analysis of predefined (e.g., end-tidal) breath segments is achieved by flow-triggered sample extraction.

The test subject freely inhales/exhales through a flow transducers mouth-piece, which is connected to a silicone head mask covering mouth and nose. A detailed description of the experimental setup is given in [53]. The volume of air inhaled or exhaled during normal breathing is called *tidal volume*. A small proportion of the tidal volume contains the total volume of the conducting airways, which do not contribute to gas exchange and it is therefore called *anatomical dead space*. The respiratory flow effectively taking part in pulmonary gas exchange (\dot{V}_A) is described by

$$\dot{V}_A = \dot{V}_E - \dot{V}_D, \quad (1.1)$$

where \dot{V}_E represents the total minute ventilation and \dot{V}_D represents the total dead space ventilation. While the measured VOC concentrations during normal tidal breathing will provide the average composition of all the breath sampled, end-tidal concentrations (the concentrations in the end-exhalation volume) will approach the alveolar concentrations.

The above-mentioned instrumentation allows for the measurement of end-tidal VOC concentration profiles. Respiratory flow is monitored continuously during tidal breathing, which allows for a reliable breath-by-breath detection of each end-tidal segments. Parallel to the breath measurements several decisive physiological factors during rest, exercise challenges on a cycle ergometer, and in a sleep laboratory setting can be performed.

Such synchronized data streams are shown in Figure 1.3 and represent an indispensable phenomenological basis pertinent to any quantitative modeling approach. The data streams presented are taken from the study cohort in [53] and are obtained from a single study subject during three different exercise protocols on an ergometer. While an immediate and simultaneous increase in alveolar ventilation and cardiac output can be observed in all protocols at the onset of exercise, isoprene and acetone concentrations show different profiles according to their physiochemical properties influencing their gas-exchange dynamics.

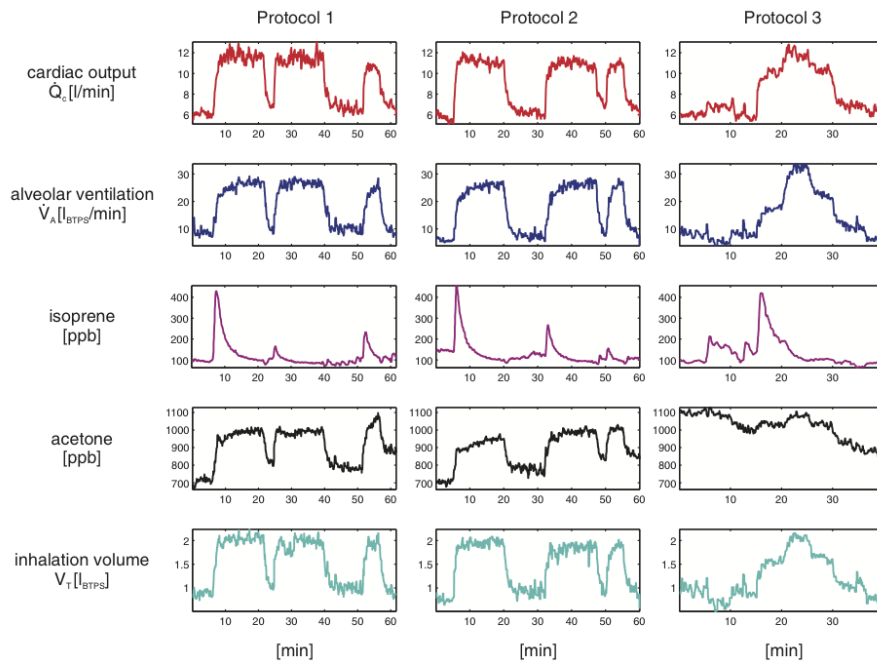


Figure 1.3 – Typical results for one single test subject (male, 26 years)

Protocol 1: 5 min resting - 15 min exercise (75 W) - 3 min resting - 15 min exercise (75 W) - 12 min resting - 5 min exercise (75 W) - 5 min resting,

Protocol 2: 5 min resting - 15 min exercise (75 W) - 12 min resting - 15 min exercise (75 W) - 3 min resting - 5 min exercise (75 W) - 5 min resting,

Protocol 3: 5 min resting - 5 min supine position - 5 min resting - 5 min exercise (50 W) - 5 min exercise (100 W) - 5 min exercise (50 W) - 10 min resting)

1.4 Modeling Pulmonary Gas Exchange

In the basic model describing the pulmonary gas exchange of blood borne inert¹ gases, the lung is assumed to be a homogenous single compartment with an effective fixed storage volume \tilde{V}_A of the gas considered. The effective storage volume is larger than the gaseous volume of the lung because there is also gas dissolved in the lung tissue (for the exact definition see Section 2.2.1). The rate of accumulation of gas in this volume equals the difference between the transport into and out of this volume due to alveolar ventilation \dot{V}_A and pulmonary perfusion (or cardiac output) \dot{Q}_c , which are modeled as continuous² and equal in inflow and outflow. This relationship is described by the following mass balance equation (see, Section 2.2.1)

$$\tilde{V}_A \frac{dC_A(t)}{dt} = \dot{Q}_c(t) (C_{\bar{v}}(t) - C_a(t)) + \dot{V}_A(t) (C_I - C_A(t)) \quad (1.2)$$

in which $C_{\bar{v}}$, C_a , C_I , and C_A are concentrations in mixed venous blood, arterial blood, inspired air, and alveolar air, respectively. Here, the gas concentration in inspired air is considered to be constant, while the expired air is assumed to have the same concentration as the alveolar air. Moreover, it is assumed that there is no diffusion limitation between pulmonary blood and alveolar air implying that arterial blood and alveolar gas are in equilibrium according to Henry's Law (see Section A.2)

$$C_a = C_A \lambda_{b:air}, \quad (1.3)$$

where $\lambda_{b:air}$ denotes the dimensionless partition coefficient between capillary blood and alveolar air.

For an inert gas which is not present in the inspired air, i.e., $C_I = 0$, equations (1.2) and (1.3) yield the well known equation derived by Farhi [28] for steady state conditions

$$C_A = \frac{C_{\bar{v}}}{\lambda_{b:air} + \dot{V}_A/\dot{Q}_c}. \quad (\text{Farhi's equation}) \quad (1.4)$$

It expresses the fact that the concentration of an inert gas in the alveolar air depends on the mixed venous concentration $C_{\bar{v}}$, the dimensionless blood:air partition coefficient $\lambda_{b:air}$, and the ventilation perfusion ratio \dot{V}_A/\dot{Q}_c . As it can be easily seen from this equation, low soluble gases such as isoprene are greatly influenced even by small fluctuations in ventilation or pulmonary perfusion, while highly soluble gases such as acetone are not affected at all. This compound-specific response to changes in ventilation and pulmonary perfusion can also be seen in Figure 1.3. At the onset of exercise, a

¹Here, the word *inert* refers to the property that the gas does not react chemically with blood, and therefore is present only in physical solution

²That means that we take averages over a time period.

peak-shaped profile of the end-tidal isoprene concentration can be observed, whereas end-tidal acetone concentrations closely resembles the profile of the alveolar ventilation.

There are two essential assumptions involved in the model of Farhi (1.4). First, the diffusion across the alveolar membrane separating the capillary blood from alveolar air space is not rate-limiting for alveolar gas exchange, such that a complete concentration equilibrium is attained in the lung at every instant. Although this assumption may be doubtful for gases of big molecular weight and high solubility in blood, for inert gases it is fungible [31, 113]. Second, the gases are well-mixed within the alveolar space. However, theoretical evidence appears to favor the existence of inhomogeneities throughout the normal lung [42, 118].

The ventilation-perfusion ratio (\dot{V}_A/\dot{Q}_c) refers to the ratio of alveolar air to capillary blood received from an alveolar region and it can differ between distinct regions of the lung. This is mainly caused by effects of gravity, which results in a systemic gradient in both, ventilation and perfusion. Due to the effects of hydrostatic pressure on the freely distensible pulmonary vessels, the lower lung regions get a substantially larger blood flow than the upper regions. The ventilation is also greater in the lower regions, because alveolar ventilation depends on the difference between the maximum and minimum volume of the alveolus during the breathing cycle, which is greater in the lower regions. However, these effects do not exactly balance such that the \dot{V}_A/\dot{Q}_c -ratio varies throughout the lung. Two well-known theories regarding to the inhomogeneous lung refer to *parallel* and *serial* (stratified) inhomogeneities.

We now take into account an inhomogeneous lung consisting of regions with different \dot{V}_A/\dot{Q}_c -ratios, which are connected in parallel. Considering the steady state relationship (1.4) for each different lung region, we see that the lung eliminates various gases in different proportions. The ratios of mixed arterial to mixed venous concentration (C_a/C_v) and mixed alveolar to mixed venous concentration (C_A/C_v) are defined as *retention* and *excretion*, respectively. In an inhomogeneous lung, regions with a low \dot{V}_A/\dot{Q}_c -ratio particularly increase the retention of low soluble gases, while, conversely, regions with a high \dot{V}_A/\dot{Q}_c -ratio will mainly affect the retention of highly soluble gases. This is also the basis for the Multiple Inert Gas Elimination Technique (MIGET) introduced by Wagner [114] to determine a virtually continuous \dot{V}_A/\dot{Q}_c distribution of the inhomogeneous lung (compartments connected in parallel) by the simultaneous elimination of six different inert gases with various solubilities.

Although MIGET is a useful technique for quantifying the ventilation-perfusion inequality and pulmonary shunting, it has been shown by Olszowka [82] that the calculated \dot{V}_A/\dot{Q}_c distribution using MIGET is not unique and it is not necessarily the correct distribution since a number of considerably different distributions may account for a given set of retention data. We will

discuss the \dot{V}_A/\dot{Q}_c - inhomogeneity of the lung by means of a simple three compartment model concerning isoprene in Chapter 4.

On the other hand, the term stratified inhomogeneity designates longitudinal or serial concentration gradients in the airways due to incomplete mixing of inspired with resident gas present in the lung in contrast to the regional inhomogeneities implying concentration differences between parallel lung regions. According to this theory developed by Scheid et al [97], convection is the dominant transport mechanism in the upper airways while axial diffusion is determining the gas exchange in terminal regions of the lung so that there exists a diffusion limitation expressed in terms of diffusion conductance (D), which is proportional to the diffusion constant of the gas considered in the gaseous medium and is therefore specific for the gas species. Stratified inhomogeneity reduces gas exchange efficiency by producing an increase in retention and decrease in excretion of gases eliminated from the blood, both effects being dependent upon the gas diffusivity and blood solubility [42]. Regarding acetone, the diffusion conductance D describes the diffusion limitation between the bronchial lining and alveolar space, while for isoprene it refers to the diffusion limitation between proximal and axial regions of the alveolar space. We will study the latter in Chapter 4.

Furthermore, in these aforementioned studies, the gas exchange mechanism is restricted to the alveolar space by the assumption that no inert gas is added to or withdrawn from the alveolar gas as it flows through the airways during expiration. This is not true for highly soluble gases which may readily dissolve in the bronchial lining and in the blood of bronchial circulation. Anderson et al [9] have demonstrated that the blood:air partition coefficient, $\lambda_{b:air}$, is a very important factor to determine the location of the gas exchange in the lungs (airways versus alveoli). They have found that low soluble gases (referred to as *non-polar* gases) with $\lambda_{b:air} \leq 10$ exchange almost solely in the alveoli, whereas for gases of high solubility (*polar* gases) with $\lambda_{b:air} > 10$ the gas exchange in the airways plays the dominant role, so that diffusion of gas through the airway tissue, bronchial blood flow, or inspired air conditions are the important factors determining pulmonary gas exchange³. Also the measure of heterogeneity of \dot{V}_A/\dot{Q}_c may be affected by the same factors that affect the airway gas exchange.

According to their solubilities, it can be assumed that isoprene exchange occurs almost exclusively in the alveoli whereas the majority of acetone exchange takes place within the conducting airways rather than in the alveoli, which makes the acetone gas exchange mechanism less sensitive to the regional inhomogeneities of the lung.

³Due to the high water content of blood, generally a strong correlation is assumed between water:air and blood:air partition coefficients for polar gases and both are used interchangeable.

To describe the breath isoprene dynamics under physical exercise, some of the aforementioned modeling approaches will be studied in Chapter 4, starting with the first developed physiologically based model for isoprene by Filser et al. [30]. First, we will focus our interest on models considering functional mechanisms of the lung, namely the serial lung model suggested by Karl et al. [50], a three compartment parallel lung model (see, e.g., [43, 45]) with regional ventilation-perfusion inhomogeneities, and a serial inhomogeneous lung model in terms of stratified inhomogeneity as suggested by Scheid [97]. Subsequently, some insightful experimental results are presented which lead to a new interpretation of the physiological formation of isoprene and the first three compartment model developed by our research group [52]. This model will be then refined to capture the original compartmental segmentation suggested by Filser and to explain further experiments.

Chapter 2

Physiological Modeling

2.1 Compartmental Mass Transport

Gas exchange processes in the human body involve the study of mass transport phenomena between different parts of the organism, which are interconnected through the circulatory system. Physiologically based compartment models have been widely used for this purpose to describe the time-dependent distribution, absorption, metabolism and elimination of a substance among different tissues. In general, one can always perform a detailed analysis of the transport mechanism up to microvessels and cells level, however, such an analysis requires a great deal of effort. On the one hand, all the relevant information about the geometric structure and transport properties are not available. On the other hand, such detailed considerations render the numerical solutions expansive, are thus often unnecessary, even impossible.

For this compelling reasons compartment models are mostly based on the transport analysis at the organ level, where the compartments are defined from physical properties corresponding either to specific, localized anatomic structures (like lung, liver, kidney, etc.) or to type of tissues (such as fat, muscle, viscera, bone, etc.) that are distributed throughout the body [8, 20, 30, 77]. In most physical models all tissue of any given type is combined to form a lumped compartment, as for example all fat in the body is lumped into a single compartment with a total fat volume and total fat blood flow. A typical example is shown in Figure (2.1).

Within the scope of the present work, we will confine ourselves to the kinetically homogenous compartments regarding the systemic part of the body, whereas spatially inhomogenous compartments of the respiratory tract will also lie of the field of interest.

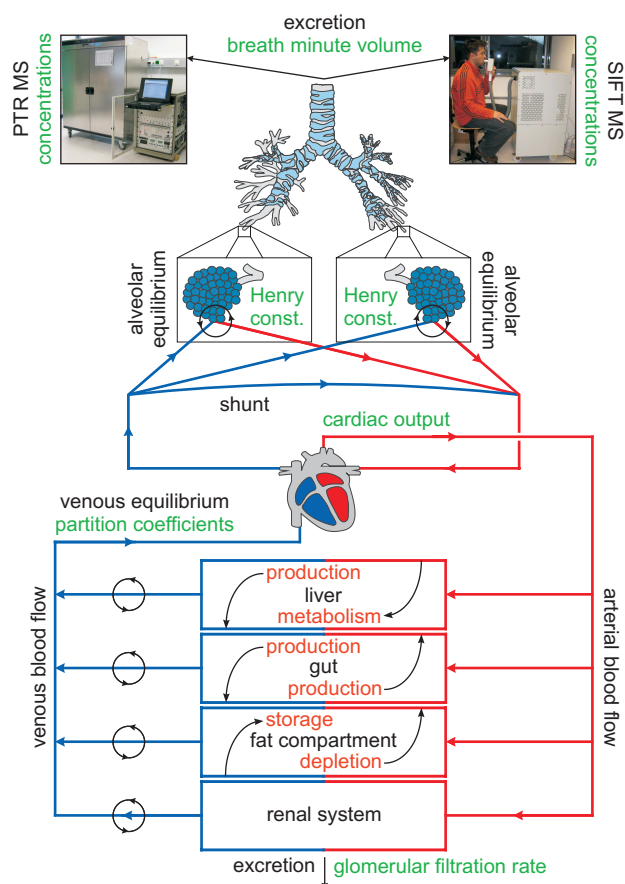


Figure 2.1 – Physiologically based compartment model for the distribution of an endogenous volatile organic compound within the human body.

The transport processes within these predefined compartments are specified by the laws of physics, i.e., the conservation of mass, stating that the rate of accumulation of mass in each compartment equals the difference between the transport of mass into the compartment and out of the compartment. In physiological compartment models, the concentrations are treated as continuous and thus the time-dependent course of compound in each compartment is described by a mass-balance differential equations. Pharmacological and physiochemical knowledge about the mechanism of transport, sites of action, binding and solubility, etc. together with physiological data (determining tissue volumes and blood flow rates) are used to formulate the model equations.

2.2 Respiratory Gas Exchange

The lung is responsible for the gas exchange between the outside environment and blood. This happens by means of ventilation, perfusion and diffusion. Inhaled air passes along a branching network of progressively narrower, shorter, and more numerous airways that end in smaller sacs called *alveoli*. There are about 500 million alveoli in the human lung each with an average diameter of about $300 \mu\text{m}$ at 75 % of maximum lung volume providing a very large surface area (approximately 70 m^2) for gas exchange [118].

The pulmonary circulation carries the entire cardiac output of blood from the right ventricle to the lungs for gas exchange. The main pulmonary artery branches successively down to the the pulmonary capillaries. Pulmonary capillaries (about 5 to $7 \mu\text{m}$ in radius) track along the alveolar walls, passing several alveoli before the blood is collected in the venous system.

Pulmonary capillaries form a continuous network in the alveolar walls throughout a lobe. When distended by intravascular pressure, they are so numerous that blood flows almost as an unbroken sheet between the airspaces. "Sheet flow" reduces vascular resistance and optimizes gas exchange. When the pressure difference between the inside and outside of the vessels (transmural pressure) is low, some of the capillary segments are closed, but they are easily opened and recruited into the pulmonary vascular bed by a transmural pressure increase. The open capillaries distend when their transmural pressure rises, as when cardiac output increases [42].

In the lung, gas exchange occurs via passive diffusion along a partial pressure gradient across the alveolocapillary membrane. The relative thinness (about 0.1 to $0.5 \mu\text{m}$) of this membrane allows for easy gas exchange.

2.2.1 Mass Balance Equation

To establish the conservation of mass, we consider a control volume of constant size of the capillary blood (V_D) that is bounded by alveolar air space, where gas exchange occurs by the blood flow and the diffusion between capillary blood and alveolar air. In the following, C_b and C_g denote the concentrations, P_b and P_g the partial pressures of the substance in blood and gaseous phase, respectively.

For the control volume V_D , the mass of the dissolved gas contained in this volume at any time is

$$\int_0^{V_D} C_b(v, t) dv.$$

The gas exchange between alveolar air and capillary blood is described by a diffusion term with the assumption that the flow is linearly proportional to the difference in partial pressures in gas (P_g) and in blood (P_b) across

the interface and thus

$$q(v, t) = D_L(P_b(v, t) - P_g(v, t)), \quad (2.1)$$

where D_L is the diffusing capacity of the lung and includes the area, thickness, and diffusion properties of the sheet and gas concerned (see Appendix A.2). The net flux $q(v, t)$ due to diffusion is negative when gas is flowing from the dissolved phase to the gaseous phase. Since mass is conserved, we have

$$\frac{d}{dt} \int_0^{V_D} C_b(v, t) dv = \dot{Q}_c(t) (C_b(0, t) - C_b(V_D, t)) - \int_0^{V_D} q(v, t) dt, \quad (2.2)$$

where $\dot{Q}_c(t)$ is the blood flow in the capillary at any time and is independent of v .

Differentiating (2.2) with respect to V_D and replacing V_D by v and then using (2.1), we obtain

$$\frac{d}{dt} C_b(v, t) + \dot{Q}_c(t) \frac{d}{dv} C_b(v, t) = -D_L(P_b(v, t) - P_g(v, t)). \quad (2.3)$$

Similar to (2.3), a mass balance equation for the gas contained in a constant volume V'_D of alveolar air space

$$\frac{d}{dt} C_g(v, t) + \dot{V}_A(t) \frac{d}{dv} C_g(v, t) = D_L(P_b(v, t) - P_g(v, t)), \quad (2.4)$$

where $\dot{V}_A(t)$ denotes the air flow through the borders of the volume, since for the gas in the volume transport is by the air flow and the diffusion between the capillary blood and the gas in alveolar space. Equations (2.3) and (2.4) can be combined to give

$$\frac{d}{dt} C_b(v, t) + \frac{d}{dt} C_g(v, t) = -\dot{Q}_c(t) \frac{d}{dv} C_b(v, t) - \dot{V}_A(t) \frac{d}{dv} C_g(v, t). \quad (2.5)$$

Gas Exchange in One Alveolus

We consider each differential volume of the alveolar air space as an alveolus. Although C_g may vary with anatomic site in each alveolus, for simplicity spatial gradients in concentrations are usually neglected, i.e., each alveolus is assumed to be *homogenous* (or *well-mixed*, that is as if the alveolus is stirred rapidly and the concentrations of all species in the alveolus remain homogenous). Due to the high gas exchange efficiency of the lung diffusion is assumed to be fast compared to the other dynamics influencing the

system and an equilibration of the gas in alveolus with capillary blood is achieved (in the absence of chemical bindings with blood) instantly according to Henry's Law (A.2). As an implication of the *Mean Value Theorem* of analysis and denoting the constant concentration of the gas in inspired air by C_I from Equation (2.5) we get

$$\frac{d}{dt}C_b(v, t) = -\dot{Q}_c(t)\frac{d}{dv}C_b(v, t) + \frac{\dot{V}_A(t)}{V'_D} \left(C_I - \frac{C_b(v, t)}{\lambda_{b:\text{air}}} \right), \quad (2.6)$$

where $\lambda_{b:\text{air}}$ is the dimensionless partition coefficient between concentrations in blood and in alveolus.

Gas Exchange Between Homogenous Compartments

A further approach to gas exchange modeling is to regard the alveolar capillaries also as a homogenous compartment with a constant mean concentration. According to this the gas exchange unit consist of two homogenous compartments representing alveolar air and capillary blood. A permanent diffusion equilibrium holds between these two compartments, i.e., C_b as well as C_g instantaneously approach their steady state values. Due to this assumption the diffusion terms on the right hand sides of equations (2.3) and (2.4) equals zero. By denoting $C_b(0, t) = C_{b,\text{in}}(t)$ and $C_\star(V_D, t) = C_{\star,\text{out}}(t)$ ¹ the combination of (2.3) and (2.4) simplifies to the following ordinary differential equation (ODE) which depends only on time

$$\tilde{V}_D \frac{d}{dt}C_g(t) = \dot{Q}_c(t) (C_{b,\text{in}}(t) - C_{b,\text{out}}(t)) + \dot{V}_A (C_I - C_{g,\text{out}}(t)). \quad (2.7)$$

The factor $\tilde{V}_D := V'_D + V_D\lambda_{b:\text{air}}$ can be interpreted as "effective" volume of the combined compartment.

2.3 Gas Exchange in Systemic Compartments

In physiologically based compartment models the systemic part of the body is subdivided in organs or tissues as mentioned before. These compartments are connected by blood flow in parallel. The rational selection of the size and number of compartments depends on the specific compound. A wide spectrum of approaches from detailed models containing all known factors influencing the system to more simplified models eliminating some organs or representing them in a lumped compartment can be chosen without losing the ability to describe specific datasets.

¹here \star denotes g or b

Compartments are considered to consist of three well-mixed subcompartments representing the vascular part through which the compartment is perfused with blood, cellular space comprising the cells of the organ, and an interstitial space connecting them. Mass transfer between these compartments occurs by diffusion. When one of the steps in mass transport is rate limiting, e.g., diffusion between the subcompartments occurs very rapid compared to the perfusion rate to the tissue (*flow-limited* assumption), the compartment may be simplified from the three-subcompartment model to a model with one or two subcompartments (for a detailed description see [35]). We will use here the latter approach of one perfusion limited well-mixed compartment assuming a rapid diffusion equilibrium between the vascular, interstitial, and cellular compartments. The compound enters the compartment in the arterial blood and leaves it in the venous blood. Due to the diffusion equilibrium across the tissue membranes, the venous blood leaving the compartment is considered to be in equilibrium with the compartmental concentration at every instant. The relationship between the single compartment concentration (C) and effluent venous blood (C_v)

$$C_v = \lambda_{b:t} C \quad (2.8)$$

is called venous equilibrium assumption, where $\lambda_{b:t}$ is the partition coefficient between blood and compartment. This assumption is referred to as *blood-flow-limited* uptake.

In some compartments, metabolic activities such as production and metabolic elimination may take place, thus gain or loss of the compound should be considered. Tissue retention of organic compounds is related to blood:tissue partition coefficients $\lambda_{b:t}$ and the presence of specific binding proteins in the tissues. Elimination is regulated by pulmonary dynamics for exhalation, by kinetic constants of metabolizing enzymes (found principally in liver), and to a much lesser extent by renal filtration mechanisms [8]. Metabolic elimination is usually described either by first order kinetic or saturable *Michaelis Menten* kinetic. In case of high concentrations of compound in inhaled air, the saturable metabolic elimination in compartment is given by

$$\frac{V_{\max} \lambda_{b:t} C}{K_m + \lambda_{b:t} C} \quad (2.9)$$

with a maximum rate of metabolism for this compound V_{\max} and Michaelis-constant K_m . Here, C denotes the compartmental concentration of the compound and $\lambda_{b:t}$ is the compartment specific blood:tissue partition coefficient.

If the ambient is nearly free of the substance, the rate of metabolic elimination is approximated by

$$\frac{V_{\max}}{K_m} \lambda_{b:t} C = k_{\text{met}} \lambda_{b:t} C, \quad (2.10)$$

where k_{met} denotes the rate of metabolic elimination.

The mass balance equation for a compartment with a constant production rate and a metabolic elimination described by linear kinetic reads

$$\tilde{V} \frac{dC(t)}{dt} = q \dot{Q}_c(t) (C_a(t) - \lambda_{b:t} C(t)) - k_{\text{met}} \lambda_{b:t} C(t) + k_{\text{pr}}, \quad (2.11)$$

where C_a is the arterial concentration, q is the fractional flow rate of blood to the tissue compartment, and k_{pr} is the production rate. The effective compartment volume is defined by $\tilde{V} := V + V_{t,b} \lambda_{b:t}$ with tissue volume V and blood volume contained in the tissue compartment $V_{t,b}$.

As defined in Equation (2.8), the term $\lambda_{b:t} C$ determines the concentration of venous blood leaving the compartment. Thus, the total mixed venous concentration is calculated by blood flow-weighted averaging of all considered compartments. By a number of N compartments, the total mixed venous concentration reads

$$C_{\bar{v}}(t) = \sum_N q_N \lambda_{b,N} C_N(t). \quad (2.12)$$

Chapter 3

Model Structure and Properties

The essence of the modeling process is to derive a mechanical description of the underlying real system, which delivers the best possible understanding of the biological phenomenon, allows all the known experimental data to be taken into account and makes it possible to understand what components and interactions are important in the originating complex system. Once such a model structure is chosen, one is usually confronted with the identification of model parameters, which could not be directly measured and have to be estimated from measured data. In the following we will review some methodological aspects of the modeling process and parameter estimation.

In the context of VOC modeling, compartmental considerations as described in Chapter 2 together with an appropriate input-output configuration and a fully determined set of parameters corresponding to the system will lead to the following deterministic description of the underlying physical system

$$\dot{\mathbf{x}} = \mathbf{f}(t, \mathbf{x}, \mathbf{u}, \mathbf{p}), \quad \text{with } \mathbf{x}(t_0) = \mathbf{x}_0, \quad (3.1)$$

$$y = h(t, \mathbf{x}, \mathbf{u}, \mathbf{p}), \quad (3.2)$$

where the state variable \mathbf{x} evolves in an open set \mathcal{D} of the n -dimensional space \mathbb{R}^n , $y \in \mathbb{R}$ is the measurement (or output), $\mathbf{u} \in \mathbb{R}^r$ is the known system input vector, and $\mathbf{p} \in \mathbb{R}^q$ is the constant parameter vector. The observation interval is denoted by $\mathcal{I} = [t_0, t_1]$.

In the present context, \mathbf{x} typically reflects molecular concentrations of the trace gas under consideration within the blood/tissue compartments introduced, \mathbf{u} describes external (constant or time-varying) inputs (like flows, temperature, etc.), and the constant unknown parameter vector consists of in vivo kinetic rate constants (like production rates or metabolic elimination rates) or compartment volumes to be estimated. The scalar *measurement*

equation (3.2) contains the information on the model dynamics collected by experiments according to a fixed experimental setup.

In the following we assume that $\mathbf{f}(\cdot)$ and $h(\cdot)$ are continuous in t and continuously differentiable with respect to state \mathbf{x} and parameters \mathbf{p} . The external input vector \mathbf{u} is postulated to be uniformly bounded over \mathcal{I} . Some constraints according to the model structure are usually available

$$\mathbf{g}(t, \mathbf{x}, \mathbf{u}, \mathbf{p}) \geq 0, \quad (3.3)$$

where g is a vector of polynomial functions describing all the algebraic (linear or nonlinear) equality and inequality constraints among the components of \mathbf{x} , \mathbf{u} and \mathbf{p} , which are known a priori.

The equations (3.1)-(3.3) define a *complete constrained structure*. On the basis of measurements, the task is to determine the unknown initial state \mathbf{x}_0 and the constant parameter vector \mathbf{p} .

3.1 Qualitative Properties of the Model

The solution of the initial value problem (3.1) has to fulfill some qualitative requirements, like existence, uniqueness, continuous dependence on initial conditions, and continuous dependence on parameters, for the model to be a useful description of a physical system.

Let us consider the general state equation (given, e.g., by substituting the inputs which are specified as a function of t), where $\mathbf{f} : \mathcal{I} \times \mathcal{D} \rightarrow \mathbb{R}^n$ is continuous in t and continuously differentiable with respect to \mathbf{x} , and

$$\dot{\mathbf{x}} = \mathbf{f}(t, \mathbf{x}), \quad \text{with } \mathbf{x}(t_0) = \mathbf{x}_0. \quad (3.4)$$

A continuously differentiable function $\mathbf{x} : \mathcal{I} \rightarrow \mathcal{D}$ is said to be a solution to (3.4) on the interval $\mathcal{I} \subseteq \mathbb{R}$ with initial condition $\mathbf{x}(0) = \mathbf{x}_0 \in \mathcal{D}$ if and only if $\mathbf{x}(t)$ satisfies (3.4) for all $t \in \mathcal{I}$. We denote the solution to the initial value problem (IVP) (3.4) by $\phi(\cdot, \mathbf{x}_0)$, so that the *flow* of the dynamical system (3.4) is given by the map $\phi : \mathcal{I} \times \mathcal{D} \rightarrow \mathcal{D}$ and is continuous and continuously differentiable in t .

3.1.1 Existence and Uniqueness of Solutions

For the mathematical model to predict the future state of the system from its current state, the IVP must have a unique solution. The unique existence of solutions of the IVP (3.4) can be ensured by imposing some constraints on the right-hand side function $\mathbf{f}(t, \mathbf{x})$. In fact, continuity of $\mathbf{f}(t, \mathbf{x})$ in its arguments ensures that there exist at least one solution, but, it is not sufficient to ensure the uniqueness of the solution. The key constraint

used to prove uniqueness is the Lipschitz condition, whereby $\mathbf{f}(t, \mathbf{x})$ satisfies the inequality

$$\|\mathbf{f}(t, \mathbf{x}) - \mathbf{f}(t, \mathbf{y})\| \leq L\|\mathbf{x} - \mathbf{y}\| \quad (3.5)$$

for all (t, \mathbf{x}) and (t, \mathbf{y}) in some neighborhood of (t_0, \mathbf{x}_0) .

For \mathbf{f} continuous in t and locally Lipschitz continuous in \mathbf{x} , according to the Theorem of *Picard Lindelöf* (see, e.g., [41]) it can be shown that there exist some $\delta > 0$, such that the IVP (3.4) has a unique solution over $[t, t + \delta]$. In fact, δ may be small so that local Lipschitz continuity cannot guarantee the existence and uniqueness of the solutions over a given time interval $[t_0, t_1]$. The interval of existence may be extended by repeated applications of the local *Picard Lindelöf* theorem, however, in general, it cannot be extended indefinitely. There is a maximum interval $[t_0, T)$ where the unique solution exists. In general, T may be less than t_1 , in which case as $t \rightarrow T$, the solution leaves any compact set over which \mathbf{f} is locally Lipschitz in \mathbf{x} .

The existence and uniqueness of the solution over the interval $[t_0, t_1]$, where t_1 may be arbitrarily large, can be proved by requiring \mathbf{f} to satisfy a global Lipschitz condition. That is, if \mathbf{f} satisfies the inequality (3.5) for all $\mathbf{x}, \mathbf{y} \in \mathbb{R}^n$ and is uniformly in t for all $t \in [t_0, t_1]$, then the IVP (3.4) has a unique solution over $[t_0, t_1]$.

Remark 1. Consider the linear system $\dot{\mathbf{x}} = A(t)\mathbf{x} + \mathbf{g}(t) = \mathbf{f}(t, \mathbf{x})$, where $A(t)$ and $\mathbf{g}(t)$ are continuous functions of t . Over any finite interval of time $[t_0, t_1]$, the elements of $A(t)$ are bounded and the conditions of the global existence and uniqueness are satisfied. Therefore, the linear system has a unique solution over $[t_0, t_1]$.

Remark 2. The Lipschitz property of a function is a stronger condition than continuity but weaker than continuous differentiability. Thus, for the case where \mathbf{f} is continuous differentiable, local Lipschitz continuity is implied, which ensures the local existence and uniqueness of the solution of the IVP (3.4). On the other hand, if $[\partial\mathbf{f}/\partial\mathbf{x}]$ is bounded by a constant k over the interval of interest, then \mathbf{f} is Lipschitz on the same interval with Lipschitz constant $L = k$, and a unique solution exists over the interval of interest.

Although for linear systems the global Lipschitz condition is a reasonable requirement, it is restrictive and models of many nonlinear systems may fail to satisfy it though they have unique global solutions. At the expense of having to know more about the solution of the system the following global existence and uniqueness theorem achieves, that requires the function \mathbf{f} to be only locally Lipschitz [51].

Theorem 3.1.1. *Let $\mathbf{f}(t, \mathbf{x})$ be continuous in t and locally Lipschitz in \mathbf{x} for all $t \geq t_0$ and all \mathbf{x} in a domain $\mathcal{D} \subset \mathbb{R}^n$. Let \mathcal{M} be a compact subset of \mathcal{D} , $\mathbf{x}_0 \in \mathcal{M}$, and suppose it is known that every solution of (3.4) lies entirely in \mathcal{M} . Then, there is a unique solution that is defined for all $t \geq t_0$.*

The trick in applying the Theorem 3.1.1 is to check the assumption that every solution lies in a compact set without actually solving the differential equation. Lyapunov's method for studying stability is very valuable in this respect.

3.1.2 Continuous Dependence on Initial Conditions and Parameters

An essential factor for the validity of any mathematical model is the continuous dependence of its solutions on the data (initial states and parameters) of the problem. The least we should expect is that arbitrarily small errors in the data will not result in large errors in the solutions obtained by the system.

The solution of the IVP (3.4) defined on a compact time interval depends continuously on its initial state if solutions starting at nearby points are defined on the same interval and remain close to each other on that interval. Continuous dependence on parameters is defined similarly. Let $\phi(t, \mathbf{x}_0, \mathbf{p}_0)$ be a solution of $\dot{\mathbf{x}} = \mathbf{f}(t, \mathbf{x}, \mathbf{p}_0)$ defined on $\mathcal{I} = [t_0, t_1]$, with $\phi(t_0, \mathbf{p}_0) = \mathbf{x}_0$. The solution is said to depend continuously on \mathbf{p} if for any $\varepsilon > 0$, there exists a $\delta > 0$ such that for all \mathbf{p} in the ball $\{\mathbf{p} \in \mathbb{R}^q \mid \|\mathbf{p} - \mathbf{p}_0\| < \delta\}$, the equation $\dot{\mathbf{x}} = \mathbf{f}(\mathbf{x}, \mathbf{p})$ has a unique solution $\phi(t, \mathbf{p})$ defined on \mathcal{I} , with $\phi(t_0, \mathbf{p}) = \mathbf{x}_0$, and satisfies $\|\phi(t, \mathbf{p}) - \phi(t, \mathbf{p}_0)\| < \varepsilon$ for all $t \in \mathcal{I}$.

The continuous dependence on initial conditions and parameters can be studied simultaneously as stated by the following theorem [51].

Theorem 3.1.2. *Let $\mathbf{f}(t, \mathbf{x}, \mathbf{p})$ be continuous in $(t, \mathbf{x}, \mathbf{p})$ and locally Lipschitz in \mathbf{x} (uniformly in t and \mathbf{p}) on $\mathcal{I} \times \mathcal{D} \times \{\|\mathbf{p} - \mathbf{p}_0\| \leq c\}$, where $\mathcal{D} \subset \mathbb{R}^n$ is an open connected set. Let $\phi(t, \mathbf{p}_0)$ be a solution of $\dot{\mathbf{x}} = \mathbf{f}(t, \mathbf{x}, \mathbf{p}_0)$ with $\phi(t_0, \mathbf{p}_0) = \mathbf{x}_0 \in \mathcal{D}$. Suppose $\phi(t, \mathbf{p}_0)$ is defined and belongs to \mathcal{D} for all $t \in [t_0, t_1]$. Then, given $\varepsilon > 0$, there is $\delta > 0$ such that if*

$$\|\mathbf{z}_0 - \mathbf{y}_0\| < \delta \quad \text{and} \quad \|\mathbf{p} - \mathbf{p}_0\| < \delta$$

then there exist a unique solution $\mathbf{z}(t, \mathbf{p})$ of $\dot{\mathbf{x}} = \mathbf{f}(t, \mathbf{x}, \mathbf{p})$ defined on $[t_0, t_1]$, with $\mathbf{z}(t_0, \mathbf{p}) = \mathbf{z}_0$, and $\mathbf{z}(t, \mathbf{p})$ satisfies

$$\|\mathbf{z}(t, \mathbf{p}) - \mathbf{y}(t, \mathbf{p}_0)\| < \varepsilon, \quad \forall t \in [t_0, t_1].$$

Remark 3. If \mathbf{f} is continuous in its arguments and has continuous first partial derivatives with respect to \mathbf{x} and \mathbf{p} , we know from Theorem 3.1.2 the local unique existence of solutions and continuous dependence of initial values and parameters. Thus, well-posedness property of the system results by showing the uniform boundedness of the Jacobian of \mathbf{f} with respect to \mathbf{x} over the interval of interest.

Remark 4. The continuous differentiability of \mathbf{f} with respect to \mathbf{x} and \mathbf{p} implies the additional property that the solution $\mathbf{x}(t, \mathbf{p})$ is differentiable with respect to \mathbf{p} near \mathbf{p}_0 . We use this property to calculate the sensitivity equations which provide first-order estimates of the effect of parameter variations on solutions.

3.1.3 Stability of Equilibrium Points

Stability of equilibrium points is usually characterized in the sense of Lyapunov. Consider the autonomous system

$$\dot{\mathbf{x}} = \mathbf{f}(\mathbf{x}) \quad (3.6)$$

where $\mathbf{f} : \mathcal{D} \rightarrow \mathbb{R}^n$ is locally Lipschitz. Assume that solutions of (3.6) are defined for all $t \geq 0$. Suppose $\mathbf{x}_e \in \mathcal{D}$ is an equilibrium point of (3.6); that is, $\mathbf{f}(\mathbf{x}_e) = \mathbf{0}$. For convenience, we consider the case when the equilibrium point is at the origin of \mathbb{R}^n ; i.e., $\mathbf{x}_e = \mathbf{0}$ and $\mathbf{f}(\mathbf{x})$ satisfies $\mathbf{f}(\mathbf{0}) = \mathbf{0}$ and we will study the stability of the origin $\mathbf{x} = \mathbf{0}$.

An equilibrium point is stable if all solutions starting at nearby points stay nearby; otherwise it is unstable. It is asymptotically stable if all solutions starting at nearby points not only stay nearby, but also tend to the equilibrium point as time approaches infinity. These notions are made precise in the next definition.

Definition 1. The equilibrium point $\mathbf{x} = \mathbf{0}$ of (3.6) is

- stable if, for each $\varepsilon > 0$, there exists a $\delta = \delta(\varepsilon) > 0$ such that

$$\|\mathbf{x}(0)\| < \delta \Rightarrow \|\mathbf{x}(t)\| < \varepsilon, \quad \forall t \geq 0,$$

- unstable if it is not stable,
- asymptotically stable if it is stable and δ can be chosen such that

$$\|\mathbf{x}(0)\| < \delta \Rightarrow \lim_{t \rightarrow \infty} \mathbf{x}(t) = \mathbf{0}.$$

Lyapunov stability theorems give sufficient conditions for stability and asymptotic stability.

Theorem 3.1.3. (*Lyapunov's Theorem*) Let $V : \mathcal{D} \rightarrow \mathbb{R}$ be a continuously differentiable function such that

$$V(\mathbf{0}) = 0 \text{ and } V(\mathbf{x}) > 0 \text{ in } \mathcal{D} - \{\mathbf{0}\}. \quad (3.7)$$

The derivative of V along the trajectories of (3.6), denoted by $\dot{V}(\mathbf{x})$, is given by

$$\dot{V} = \sum_{i=1}^n \frac{\partial V}{\partial \mathbf{x}_i} \dot{\mathbf{x}}_i = \sum_{i=1}^n \frac{\partial V}{\partial \mathbf{x}_i} \mathbf{f}_i(\mathbf{x}).$$

If

$$\dot{V}(\mathbf{x}) \leq 0 \text{ in } \mathcal{D}, \quad (3.8)$$

then the equilibrium solution $\mathbf{x}(t) \equiv \mathbf{0}$ is stable. Moreover, if

$$\dot{V} < 0 \text{ in } \mathcal{D} - \{\mathbf{0}\}, \quad (3.9)$$

then the equilibrium solution $\mathbf{x}(t) \equiv \mathbf{0}$ is asymptotically stable. Finally, if $\mathcal{D} = \mathbb{R}^n$ and $V(\cdot)$ is such that

$$V(\mathbf{x}) \rightarrow \infty \text{ as } \|\mathbf{x}\| \rightarrow \infty \quad (3.10)$$

then the equilibrium solution $\mathbf{x}(t) \equiv \mathbf{0}$ is globally asymptotically stable.

In cases where the Lyapunov function fails to satisfy the asymptotic stability condition of Theorem 3.1.3 because its derivative is only negative semidefinite, the Krasovskii-LaSalle invariance principle can be used to relax the strict negative-definiteness condition on the Lyapunov derivative while ensuring system asymptotic stability [37, 51]. First we introduce a few definitions.

Let $\mathbf{x}(t)$ be a solution of (3.6). A point p is said to be a *positive limit point* of $\mathbf{x}(t)$ if there exists a sequence $\{t_n\}$, with $t_n \rightarrow \infty$ as $n \rightarrow \infty$, such that $\mathbf{x}(t_n) \rightarrow p$ as $n \rightarrow \infty$. The set of all positive limit points of $\mathbf{x}(t)$ is called the *positive limit set* of $\mathbf{x}(t)$. A set \mathcal{D} is said to be an *invariant set* with respect to (3.6) if

$$\mathbf{x}(0) \in \mathcal{D} \Rightarrow \mathbf{x}(t) \in \mathcal{D}, \quad \forall t \in \mathbb{R}.$$

That means, if a solution belongs to \mathcal{D} at some time instant, then it belongs to \mathcal{D} for all future and past time. A set \mathcal{D} is said to be a *positively invariant set* if

$$\mathbf{x}(0) \in \mathcal{D} \Rightarrow \mathbf{x}(t) \in \mathcal{D}, \quad \forall t \geq 0.$$

We can now formulate the following theorem:

Theorem 3.1.4. (*Krasovskii-LaSalle's theorem*) Let $\mathcal{D}_c \subset \mathcal{D}$ be a compact set that is positively invariant with respect to (3.6). Let $V : \mathcal{D} \rightarrow \mathbb{R}$ be a continuously differentiable negative-semidefinite Lyapunov function in \mathcal{D}_c . Let \mathcal{E} be the set of all points in \mathcal{D}_c where $\dot{V}(\mathbf{x}) = \mathbf{0}$ and let \mathcal{R} be the largest invariant set in \mathcal{E} . Then, every solution starting in \mathcal{D}_c approaches \mathcal{R} as $t \rightarrow \infty$.

When our interest is to show that $\mathbf{x}(t) \rightarrow \mathbf{0}$ as $t \rightarrow \infty$, we need to establish that the largest invariant set in \mathcal{E} is the origin. This is done by showing that no solution other than the trivial solution $\mathbf{x}(t) \equiv \mathbf{0}$ can stay entirely in \mathcal{E} . Specializing Theorem 3.1.4 to this case and taking $V(\mathbf{x})$ to be positive definite, we obtain the following corollary:

Corollary 3.1.1. *Let $\mathbf{x} = \mathbf{0}$ be an equilibrium point for (3.6). Let $V : \mathcal{D} \rightarrow \mathbb{R}$ be a continuously differentiable positive definite function on \mathcal{D} containing the origin $\mathbf{x} = \mathbf{0}$, such that $\dot{V}(\mathbf{x}) \leq 0$ in \mathcal{D} . Let $\mathcal{N} = \{\mathbf{x} \in \mathcal{D} \mid \dot{V}(\mathbf{x}) = 0\}$ and suppose that no solution other than the trivial solution $\mathbf{x}(t) \equiv \mathbf{0}$ can stay entirely in \mathcal{N} . Then, the origin is asymptotically stable.*

Remark 5. The linear time-invariant (autonomous) system

$$\dot{\mathbf{x}} = A\mathbf{x} \quad (3.11)$$

has an equilibrium point at the origin. The equilibrium point is isolated if and only if $\det(A) \neq 0$ and the stability properties of the origin can be characterized by the locations of the eigenvalues of the matrix A . The equilibrium point $\mathbf{x} = \mathbf{0}$ is stable if and only if all eigenvalues of A satisfy $\operatorname{Re}\lambda_i \leq 0$ and for every eigenvalue with $\operatorname{Re}\lambda_i = 0$ and algebraic multiplicity $q_i \geq 2$, $\operatorname{rank}(A - \lambda_i I) = n - q_i$, where n is the dimension of \mathbf{x} . The equilibrium point $\mathbf{x} = \mathbf{0}$ is (globally) asymptotically stable if and only if A is *Hurwitz*; that is, all eigenvalues of A satisfy $\operatorname{Re}\lambda_i < 0$.

For nonlinear systems, the local asymptotical stability of equilibrium points of the system can be reduced to show the local asymptotical stability of the linearized system around the equilibrium point by using the theorem of *Lyapunov's indirect method* (see, e.g., [51]).

3.1.4 Compartmental Systems

In physiological compartment models with well-mixed compartments, the mass contained in the compartment is expressed by $x_i = v_i c_i$, where v_i is the strict positive constant compartment volume and c_i denote the concentration in compartment i . For an n compartment system the instantaneous mass balances for each compartment i are expressed by the following set of equations

$$\dot{x}_i = v_i \dot{c}_i = \sum_{j \neq i} f_{ji} - \sum_{k \neq i} f_{ik} - e_i + b_i, \quad i = 1, \dots, n, \quad (3.12)$$

where the mass transfers, called *flows* or *fluxes*, from compartment i to compartment j are denoted by f_{ij} . Additional inflows b_i and e_i represent the interactions of compartment i with its periphery. For each compartment i this equation expresses the fact that the rate of accumulation of the quantity x_i is just the difference between the inflows f_{ij} , b_i and the outflows f_{ik} , e_i . An example of a compartmental system is given in Figure 3.1. A detailed analysis of compartmental networks can be found in [15, 47], from where the below-mentioned results and designations are partly taken.

All flow functions are defined to be non-negative on the non-negative orthant, i.e., $f_{ij}, b_i, e_i \in \mathbb{R}_+$ for all t . The signs in (3.12) indicate the direction

of flow, and all flow functions for non-existing links do not appear in the equations. Generally, the inflows b_i are constant, while f_{ij} and e_i can be functions of the state variable \mathbf{c} and possibly t .

Since there cannot be negative concentrations, the quantities c_i must always be non-negative, i.e., $\mathbf{c} \in \mathbb{R}_+^n$ for all t . Moreover, it is clear that there cannot be a positive outflow from an empty compartment, i.e.,

$$c_i = 0 \Rightarrow f_{ij} = 0 \text{ and } e_i = 0. \quad (3.13)$$

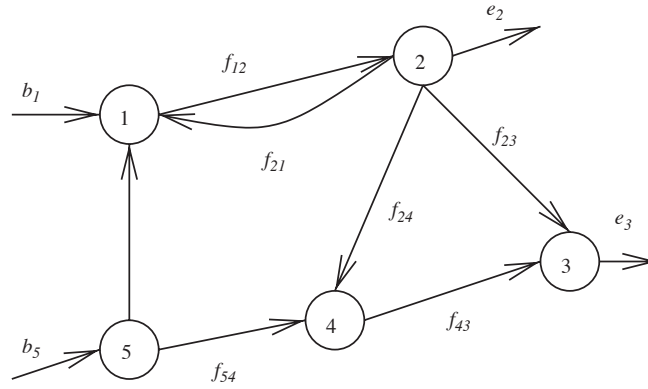


Figure 3.1 – Example of a compartmental system taken from Bastin [15].

Under the condition (3.13), if f_{ij} and e_i are k -times continuously differentiable, i.e., C^k , we can write them as

$$f_{ij} = r_{ij}c_i, \quad e_i = q_i c_i \quad (3.14)$$

for appropriate functions r_{ij} and q_i which are defined on \mathbb{R}_+^n , non-negative and at least C^{k-1} . These functions are called *fractional rates*.

In the scope of physiological compartment models considered in this thesis, we will assume that the fractional rates are smooth and strictly positive functions in their arguments. In other words, we assume that the flows r_{ij} and q_i vanish only if $c_i = 0$.

With these definitions and notations, the compartment system (3.12) is written as

$$v_i \dot{c}_i = \sum_{j \neq i} r_{ji} c_j - \sum_{k \neq i} r_{ik} c_i - q_i c_i + b_i \quad i = 1, \dots, n. \quad (3.15)$$

From this equation, we can easily obtain that, when $c_i = 0$, $c_i \geq 0$ for all t regardless of the values of c_j for $i \neq j$. Thus, the positive orthant \mathbb{R}_+^n is a forward invariant set for the system (3.15). That is; if $\mathbf{c} \in \mathbb{R}_+^n$ and $c_i = 0$,

then

$$\dot{c}_i = \frac{1}{v_i} \left(\sum_{j \neq i} r_{ji} c_j + b_i \right) \geq 0. \quad (3.16)$$

Moreover, by considering the total mass contained in the system $m := \sum_i v_i c_i$, we see that

$$\dot{m} = \sum_i v_i \dot{c}_i = \sum_i (b_i - q_i c_i) \quad \text{for } i = 1, \dots, n, \quad (3.17)$$

and thus the trajectories of the system remain bounded for bounded t intervals if b_i are bounded functions of time for all i .

The system (3.15) can be written in matrix form as

$$\dot{\mathbf{c}} = \mathbf{v} \mathbf{A} \mathbf{c} + \mathbf{v} \mathbf{b}, \quad (3.18)$$

where $\mathbf{v} = \text{diag}(\frac{1}{v_1}, \dots, \frac{1}{v_n})$, \mathbf{b} is the $n \times 1$ vector of functions b_i and A is known as *compartmental matrix* with the following properties:

- A has non-negative off-diagonal entries

$$a_{ij} = r_{ji} \geq 0 \quad \text{for } i \neq j. \quad (3.19)$$

Systems with this property are referred to *cooperative systems*. If the fractional transfer coefficients are constant, (3.19) represents a linear system with constant coefficients and A is called a *Metzler matrix*.

- A has non-positive diagonal entries

$$a_{ii} = -q_i - \sum_{j \neq i} r_{ij} \leq 0. \quad (3.20)$$

- A is diagonally dominant corresponding to its columns

$$|a_{ii}| \geq \sum_{j \neq i} a_{ji}. \quad (3.21)$$

By inserting the elements of A into (3.21) we see that

$$|a_{ii}| = | -q_i - \sum_{j \neq i} r_{ij} | \geq \sum_{j \neq i} |r_{ij}|, \quad (3.22)$$

and thus, the equality in the diagonal dominance of A expressed in (3.21) holds only for a compartment system which has no outflows, called *outflow closed system*. In this case, q_i 's disappear in (3.22) and each column of A sums to zero. This, in turn implies that A is always a singular matrix for outflow closed systems. Otherwise, if at least one of the compartments has

an outflow, the system is called *open* and the matrix A is a nonsingular, strict diagonally dominant matrix.

If A is a constant matrix, by considering the sign of the diagonal elements of A , we can conclude for open systems from the Theorem of Gershgorin (see, e.g., [93]), that all eigenvalues of A have negative real parts. This conclusion follows from the fact that every eigenvalue of A lies in a circle (called *Gershgorin disc*) centered at a_{ii} with radius sum of the norms of the other elements on the same row $\sum_{j \neq i} a_{ij}$. Since we know that the eigenvalues of A are the same as the eigenvalues of A^T , it follows that every eigenvalue of A must lie in a Gershgorin disc corresponding the columns of A . Because A is a diagonally dominant Metzler matrix with non-positive diagonal elements, A has only eigenvalues λ_i with $\text{Re}(\lambda_i) \leq 0$, and for $q_i \neq 0$, all eigenvalues of A satisfy $\text{Re}(\lambda_i) < 0$.

Showing that the eigenvalues of the system matrix $\mathbf{v}A$ have the same property is equivalent to show that $\mathbf{v}A$ is similar to a diagonally dominant Metzler matrix C with non-positive diagonal entries, since we know that similar matrices share the same eigenvalues.

Thus, we must prove that there exists a nonsingular matrix T with $C = T(\mathbf{v}A)T^{-1}$. By choosing $T = \text{diag}(v_1, \dots, v_n)$ it can be shown that

$$C = T(\mathbf{v}A)T^{-1} = (a_{ij}/v_j)_{i,j=1,\dots,n}, \quad (3.23)$$

which is also a Metzler matrix with non-positive diagonal elements. It is obvious that the diagonal dominance of C results from the diagonal dominance of A since

$$c_{ii} + \sum_{j \neq i} c_{ji} = \frac{1}{v_i} \left(a_{ii} + \sum_{j \neq i} a_{ji} \right) \leq 0 \quad (3.24)$$

for $v_i > 0$. According to the argumentation from above, the real parts of the eigenvalues of C , and consequently of $\mathbf{v}A$, are non-positive and are strictly negative for open systems.

Furthermore, for constant A and constant inflows b_i , the total mass m fulfills the requirements of a Lyapunov function, since m satisfies

$$m(\mathbf{0}) = 0, \quad m(\mathbf{c}) > 0 \quad \text{for } \mathbf{c} \neq \mathbf{0} \quad \text{and} \quad (3.25)$$

$$\dot{m}(\mathbf{c}) = \sum_i -q_i c_i \leq 0 \quad \text{for } \mathbf{c} \neq \mathbf{0}. \quad (3.26)$$

Although the concentrations of outflow closed compartments do not appear in the right-hand side of (3.26), from equations (3.15) it is obvious that the system can maintain the $\dot{m}(\mathbf{c})$ condition only at the origin. Therefore $m(\mathbf{c})$ must decrease toward $\mathbf{0}$ and consequently $\mathbf{c}(t) \rightarrow \mathbf{0}$ as $t \rightarrow \infty$. To summarize, for constant A , the homogenous system is asymptotically stable and also the inhomogeneous system with constant inputs will have the same

property.

For nonlinear systems, the local asymptotical stability of equilibrium points of the system can be reduced to showing the local asymptotical stability of linearized system about the equilibrium point by using *Lyapunov's indirect method* (see e.g. [51]).

For nonlinear compartmental systems with constant transfer coefficients which have a unique equilibrium point, even the global asymptotic stability of the equilibrium point can be shown by means of the theorem given by Leenheer [61]. A well-known result on systems of this type asserts that the associated semiflow $\phi : \mathbb{R}_+ \times \mathbb{R}_+^n \rightarrow \mathbb{R}_+^n$, $(t, \mathbf{c}_0) \mapsto \phi(t, \mathbf{c}_0) := \mathbf{c}(t)$ is monotone with respect to the natural (componentwise) partial order on \mathbb{R}_+^n given by

$$\mathbf{c} \leq \mathbf{z} \quad \text{if and only if} \quad c_i \leq z_i, \quad i \in \{1, \dots, n\}. \quad (3.27)$$

That is, ϕ preserves the order of the initial conditions (see [104], Prop. 3.1.1), i.e., for $\mathbf{c}_0, \bar{\mathbf{c}}_0 \in \mathbb{R}_+^n$ the condition $\mathbf{c}_0 \leq \bar{\mathbf{c}}_0$ implies that $\phi_t(\mathbf{c}_0) \leq \phi_t(\bar{\mathbf{c}}_0)$ for $t \in [0, \infty)$. As a third requirement, since all trajectories are bounded and the system evolves within a closed state space $\mathcal{D} \subset \mathbb{R}_+^n$ it follows that for every $\mathbf{c} \in \mathcal{D}$ the corresponding semi-orbit $O(\mathbf{c}) := \{\phi_t(\mathbf{c}), t \geq 0\}$ has compact closure. In summary, we are now in position to apply Theorem 5 of Leenheer et al. [61], which asserts that the aforementioned properties are sufficient for the unique equilibrium point in \mathcal{D} to be globally attractive [55].

3.2 Optimization and Parameter Identifiability

One of the fundamental questions of parameter identification is whether or not the parameters in the present system can be uniquely estimated from a given set of experimental observation. In this context *observability/identifiability* of a constrained model structure are defined as the possibility to reconstruct the state of the system and to uniquely determine the unknown constant parameters of the system from observing its input-output behavior, respectively. Because the unknown parameters can be considered as additional system states with time derivative zero, identifiability can be seen as a special case of observability. Intuitively, the ability to distinguish between each state variable from its neighboring points on the basis of observations is constitutive to ensure (local) observability, and observability problem concerns with finding such a criteria. The time evolution of the system (3.1) for a given \mathbf{u} is fixed once the initial conditions \mathbf{x}_0 are known. Thus (local) observability/identifiability analysis of the system results in studying the (local) injectivity of the output function y with respect to the parameters.

3.2.1 A Priori Observability/Identifiability

Under the ideal conditions of error-free model structure and noise-free data, a priori observability/identifiability analysis is a theoretical framework to answer the question, whether the planned measurements will contain enough information for the estimation of unknown parameters. This analysis takes place before the estimation process and it is essential that the input and measurement times can be chosen at will, and thus are structural properties. A property is said to be *structural (or generic)* if it is true for *almost any* value of parameters except a thin set of zero measure.

In the following, we consider the case where the inputs \mathbf{u} are constant and hence can be interpreted as additional parameters of the system

$$\dot{\mathbf{x}}(t) = \mathbf{f}(\mathbf{x}(t)), \quad \text{with } \mathbf{x}(t_0) = \mathbf{x}_0 \quad (3.28)$$

$$y(t) = h(\mathbf{x}(t)). \quad (3.29)$$

Here, it is assumed that $\mathbf{f} : \mathcal{D} \rightarrow \mathbb{R}^n$ and $h : \mathcal{D} \rightarrow \mathbb{R}$ are real analytic functions, and the output $y = y(t, \mathbf{x}_0)$ is viewed as a function of the initial condition \mathbf{x}_0 . Systems of the form (3.28)-(3.29) are a valid description for many biological processes under constant measurement conditions and represent a sufficient framework for the type of models and experiments considered in this thesis.

The most natural definition of observability is the following.

Definition 2. Let $\mathcal{U} \subseteq \mathcal{D}$. Assume that for any initial conditions $\mathbf{x}_0, \mathbf{x}_1 \in \mathcal{U}$ the corresponding solutions $\mathbf{x}_0(t), \mathbf{x}_1(t)$ for $t \in [t_0, t_1], t_1 > t_0$ both lie in \mathcal{U} . Then, if

$$h(\mathbf{x}_0(t)) \neq h(\mathbf{x}_1(t))$$

for some $t \in [t_0, t_1]$, then $\mathbf{x}_0, \mathbf{x}_1$ are said to be \mathcal{U} -distinguishable.

We denote by $\mathcal{I}(\mathbf{x}_0, \mathcal{U})$ all points in \mathcal{U} that are not \mathcal{U} -distinguishable from \mathbf{x}_0 . The system (3.28)-(3.29) is said to be locally observable at $\mathbf{x}_0 \in \mathcal{D}$ if for every open neighborhood \mathcal{U} of \mathbf{x}_0 , $\mathcal{I}(\mathbf{x}_0, \mathcal{U}) = \mathbf{x}_0$.

If \mathcal{U} is equal to \mathcal{D} , the system is said to be *observable* at $\mathbf{x}_0 \in \mathcal{D}$. Notice, however, if (3.28)-(3.29) has the observability property, it is still possible that there is an arbitrary large interval of time in which two points of \mathcal{D} can not be distinguished from each other. The concept of *local observability* sets a limit on time interval and thus is a stronger property than *observability*. In practice, however, it is often sufficient to distinguish between neighboring points. Therefore a weakened concept of local observability can be defined as follows.

Definition 3. The system (3.28)-(3.29) is locally weakly observable at \mathbf{x}_0 if for every open neighborhood \mathcal{U} of \mathbf{x}_0 there exist an open neighborhood \mathcal{V} of \mathbf{x}_0 contained in \mathcal{U} , such that $\mathcal{I}(\mathbf{x}_0, \mathcal{U}) \cap \mathcal{V} = \mathbf{x}_0$.

Intuitively, the referred system is *locally weakly observable*, if one can instantaneously distinguish each point $\mathbf{x}_0 \in \mathcal{D}$ from its neighbors.

Recall $h : \mathcal{D} \rightarrow \mathbb{R}$ and $\mathbf{f} : \mathcal{D} \rightarrow \mathbb{R}^n$ are real analytic functions, the latter is called a vector field on \mathcal{D} . Differentiation of h along the trajectories of the system $\dot{\mathbf{x}}(t) = \mathbf{f}(\mathbf{x}(t))$ is formally done by Lie differentiation. The derivative \dot{y} is given by

$$\dot{y} = \frac{\partial h}{\partial \mathbf{x}}[\mathbf{f}(x)] := L_{\mathbf{f}}h(x), \quad (3.30)$$

where $L_{\mathbf{f}}h$ is called the *Lie derivative* of h along \mathbf{f} . By definition $L_{\mathbf{f}}^0 = h$ and higher order (iterated) Lie derivatives are defined by

$$L_{\mathbf{f}}^2 = L_{\mathbf{f}} \cdot L_{\mathbf{f}}h(x), \dots, L_{\mathbf{f}}^k = L_{\mathbf{f}} \cdot L_{\mathbf{f}}^{k-1}h(x).$$

Definition 4. The linear space over \mathbb{R} of all iterated Lie derivatives at any fixed \mathbf{x}_0

$$\mathcal{O}(\mathbf{x}_0) = \text{span}_{\mathbb{R}}\{L_{\mathbf{f}}^k h(\mathbf{x}_0), k \geq 0\}$$

is called the *observation space*. The dimension of the observation space may vary with $\mathbf{x}_0 \in \mathcal{D}$, but if the iterated Lie derivatives $L_{\mathbf{f}}^k h(\mathbf{x}_0)$, for $k \geq 0$, are linearly independent for all $\mathbf{x}_0 \in \mathcal{D}$, then $\dim(\mathcal{O}(\mathbf{x}_0)) = k$ for all $\mathbf{x}_0 \in \mathcal{D}$.

Let $d\mathcal{O} = \{d\mathcal{H}, \mathcal{H} \in \mathcal{O}\}$ denote the linear space spanned by the gradients of the Lie derivatives. It is the dimension of $d\mathcal{O}$ which defines the locally weak observability [40].

Theorem 3.2.1. *The system (3.28)-(3.29) is locally weak observable for all \mathbf{x} in an open dense set of \mathcal{D} if and only if*

$$\dim_{\mathbb{R}, \mathbf{x}} d\mathcal{O} = n. \quad (3.31)$$

As it is shown in [11] it is enough to calculate the first $n-1$ Lie derivatives of the output function.

Theorem 3.2.2. *Condition (3.31) is equivalent to the algebraic rank criterion*

$$\text{rank } J(x) := \text{rank}(dL_{\mathbf{f}}^0 h(\mathbf{x}_0)^T, \dots, dL_{\mathbf{f}}^{n-1} h(\mathbf{x}_0)^T) = n. \quad (3.32)$$

The structural identifiability methods based on the differential algebraic framework as described above exploit the characteristic set of the differential ideal associated to the dynamic equations of the system. The construction of this characteristic set ignores the algebraic set containing the steady state initial states of the system (which is contained in the "thin set", where the generic properties do not hold) and furthermore some of the structural relationships among the initial states and the other parameters. It has been shown, however, when started at this "special" initial conditions, the characteristic set of the ideal generated by the polynomials of the system

may change, which leads to a failure of the identifiability test, unless a new characteristic set is calculated to be taken as the basis [94].

In biological/physiological problems, however, identification experiments are often performed on systems started from equilibrium initial conditions, which may provide valuable information about some components of the initial condition vector and some constraints among the unknown constant parameters. The physiological models considered in this thesis also fall into this scope. In such a framework, one is usually concerned with testing hypotheses and need to focus on parameter values which are physiologically meaningful, whereas the rest need not necessarily be identifiable [46].

Furthermore, the unique identifiability of the unknown parameters is only a necessary condition for estimating them, but, it by no means guarantees that such a solution can actually be found using real data. Thus some form of a priori uniqueness analysis of the model may be an essential early step in the design of parameter estimation problem [21].

Reid [88] has defined the term *sensitivity identifiability*, which is motivated by the fundamental association between system output parameter sensitivities and system identification capability, and thus provides an additional tool to test *a posteriori* numerical identifiability, from which we want to make use here.

First, we will briefly summarize the mathematical framework of nonlinear local optimization techniques and then we will introduce the methods for sensitivity identifiability.

3.2.2 Nonlinear Least Squares Optimization

So far, we have focused exclusively on the ideal concept of error-free measurements. In practical applications, however, the observations may be corrupted by some measurement noise.

We consider the general nonlinear dynamical system (3.1) with a discrete time observation process. Assume that the observations $\{Y_i\}_{i=1}^N$ are affected by random deviations, which leads to a statistical model for the observation process

$$Y_i = h(\mathbf{x}(t_i), \mathbf{p}) + \sigma_i \epsilon_i \quad \text{for } i = 1, \dots, N, \quad (3.33)$$

where the fitted data $\{y_i\}_{i=1}^N$ are interpreted as the realizations of the observed data $\{Y_i\}_{i=1}^N$. The sample points of N longitudinal measured process output t_i are ordered such that $t_0 \leq t_1 < t_2 < \dots < t_N < t_{max}$ and the observation function $h(\cdot)$ is again continuously differentiable in both variables \mathbf{x} and \mathbf{p} . Here, we consider the case that all the experimental uncertainty can be attributed to the dependent variables Y_i and there are enough data points to provide a good sampling of the experimental uncertainties (i.e., $N > q + n$). Further, the errors ϵ_i are assumed to be random variables

which can be described by a Gaussian distribution with zero mean and constant variance $\sigma_0^2 < \infty$, i.e.,

$$\epsilon_i \sim \mathcal{N}(0, \sigma_0^2) \quad (3.34)$$

and are uncorrelated (i.e., $\text{cov}(\epsilon_i, \epsilon_j) = 0$ whenever $i \neq j$).

For the estimation of unknown parameters, we use the ordinary least squares method (OLS), which requires to minimize the weighted sum of the squared errors loss function,

$$J(\mathbf{x}_0, \mathbf{p}) = \sum_{i=0}^N \left(\frac{Y_i - h(\mathbf{x}(t_i), \mathbf{p})}{\sigma_0} \right)^2 = \sum_{i=0}^N \epsilon_i^2 \quad (3.35)$$

with respect to initial conditions \mathbf{x}_0 and parameters \mathbf{p} . Hence the errors are Gaussian distributed according to (3.34), the probability density function (pdf) of the error ϵ_i is given by

$$p(\epsilon_i) = \frac{1}{\sigma_0 \sqrt{2\pi}} \exp \left(-\frac{1}{2} \left(\frac{\epsilon_i}{\sigma_0} \right)^2 \right). \quad (3.36)$$

Because the errors ϵ_i are assumed to be independent, the maximum likelihood function is equal to the product of the pdfs of each sample

$$\prod_{i=0}^N p(\epsilon_i), \quad (3.37)$$

which has to be maximized to obtain parameters of being correct with the highest probability. This is accomplished when $J(\mathbf{x}_0, \mathbf{p})$ in Equation (3.35) is minimized.

In most applications, the assumption of a normal distribution for the errors is very reasonable and often at least approximatively valid in practice. The central limit theorem states that the pdf of a sum of arbitrary distributed random variables approaches a Gaussian distribution as the number of random variables increases. Thus the assumption of a Gaussian distributed error can be justified and under these assumptions the least squares estimate

$$\operatorname{argmin}_{\mathbf{x}_0, \mathbf{p}} \sum_{i=1}^N (Y_i - h(\mathbf{x}(t_i), \mathbf{p}))^2 \quad (3.38)$$

and the maximum likelihood estimate are equivalent [48, 80]. Since the gradient of the loss function $J(\boldsymbol{\vartheta})$ is nonlinear in the parameters $\boldsymbol{\vartheta} = (\mathbf{x}_0, \mathbf{p})$, a nonlinear optimization technique has to be applied to search for the optimal parameters $\boldsymbol{\vartheta}_{opt}$.

In local optimization techniques an iterative algorithm is required. The iterative search is started at one initial point and only the neighborhood of

this point is examined. For nonlinear optimization problems, usually many local optima exist and with local optimization algorithms one of them closest to the initial point is found. A search of global character can be constructed by restarting a local method from many different initial points and finally choosing the best local solution. It is obvious that a good guess of the initial parameters will lead to fast convergence of the algorithm and a high probability of converge to the best solution. In physiological modeling the parameters usually represent physical variables or other interpretable quantities for which enough prior knowledge is available to chose a reasonable initial guess.

A natural procedure to find a minimum of a given loss function with respect to the parameters is to evaluate this function and possibly its derivatives for different parameter values $\boldsymbol{\vartheta}^{(k)}$. At each iteration k , a new parameter value can be computed from the past parameter values, the previous loss function values, and possibly its derivatives

$$\boldsymbol{\vartheta}^{(k)} = f \left(\boldsymbol{\vartheta}^{(j)}, J(\boldsymbol{\vartheta}^{(j)}), \frac{\partial}{\partial \boldsymbol{\vartheta}^{(j)}} J(\boldsymbol{\vartheta}^{(j)}) \right) \quad \text{with } j = k - 1, k - 2, \dots, 0. \quad (3.39)$$

Consequently, at each iteration the loss function and possibly its derivatives have to be evaluated. If the whole data set is large, it is divided into representative subsets to successively apply the optimization process (3.39).

In direct search algorithms, only the evaluation of the loss function is used and no derivatives are required. Even if such methods are easy to implement, they are not reasonable to apply if the derivatives are available, since they usually show slow convergence. Even if the derivatives are unavailable, a powerful alternative method to direct search algorithms for the generation of search directions is to apply a gradient-based method in connection with finite difference techniques to compute the gradient numerically.

3.2.3 General Gradient Based Algorithms

In the following, we assume that the gradient $\underline{\mathbf{g}} = \frac{\partial J(\boldsymbol{\vartheta})}{\partial \boldsymbol{\vartheta}}$ of the loss function $J(\boldsymbol{\vartheta})$ with respect to the parameter vector $\boldsymbol{\vartheta}$ can either be calculated analytically or is approximated by finite difference techniques (see below).

The principle of all gradient-based algorithms is to modify the search direction according to

$$\boldsymbol{\vartheta}^{(k)} = \boldsymbol{\vartheta}^{(k-1)} - \mu^{(k-1)} \underline{\mathbf{p}}^{(k-1)} \quad \text{with } \underline{\mathbf{p}}^{(k-1)} = \underline{\mathbf{R}}^{(k-1)} \underline{\mathbf{g}}^{(k-1)}. \quad (3.40)$$

Here, the gradient direction $\underline{\mathbf{g}}^{(k-1)}$ is modified by some direction matrix $\underline{\mathbf{R}}^{(k-1)}$, $\underline{\mathbf{p}}^{(k-1)}$ is the modified gradient direction and $\mu^{(k-1)}$ is the step size.

The goal of the optimization is to obtain a decrease in the loss function value in each iteration step, i.e., $J(\boldsymbol{\vartheta}^{(k)}) < J(\boldsymbol{\vartheta}^{(k-1)})$. This is the case for positive definite direction matrices $\underline{R}^{(k-1)}$. Different choices of the direction matrix and step size distinguish between existing algorithms such as steepest descent, Newton, quasi-Newton, and conjugate gradient methods.

Finite Difference Techniques

If the derivation of an analytical expression for the gradient is not possible or it is computationally too expensive to evaluate, finite difference techniques can be used for numerical calculation of the gradient.

The gradient component i at point $\boldsymbol{\vartheta}$ can be approximated by the difference quotient

$$\underline{g}_i(\boldsymbol{\vartheta}) \approx \frac{J(\boldsymbol{\vartheta} + \Delta\boldsymbol{\vartheta}_i) - J(\boldsymbol{\vartheta})}{\Delta\boldsymbol{\vartheta}_i}, \quad (3.41)$$

where $\Delta\boldsymbol{\vartheta}_i$ is a "small step" into the i th coordinate axis direction. This means that for approximation of the full gradient \underline{g} at point $\boldsymbol{\vartheta}$ the expression (3.41) has to be evaluated for all search space directions and thus the computational effort required for gradient determination is equal to the number of parameters $q + n$.

In principle, it is also possible to approximate the Hessian by applying finite difference techniques to the gradient. The i th column \underline{h}_i of the Hessian \underline{H} can be calculated by

$$\underline{h}_i \approx \frac{\underline{g}(\boldsymbol{\vartheta} + \Delta\boldsymbol{\vartheta}_i) - \underline{g}(\boldsymbol{\vartheta})}{\Delta\boldsymbol{\vartheta}_i}. \quad (3.42)$$

For this calculation, however, the gradients have to be available analytically.

Quasi-Newton Methods

In Newton's method the direction matrix \underline{R} in (3.40) is chosen as the inverse of the Hessian $(\underline{H}^{(k-1)})^{-1}$ of the loss function at the point $\boldsymbol{\vartheta}^{(k-1)}$,

$$\boldsymbol{\vartheta}^{(k)} = \boldsymbol{\vartheta}^{(k-1)} - \mu^{(k-1)} (\underline{H}^{(k-1)})^{-1} \underline{g}^{(k-1)}. \quad (3.43)$$

Hence, to apply the Newton's method all second order derivatives of the loss function have to be known analytically or estimated by finite difference techniques, which requires $\mathcal{O}(q + n)$ gradient calculations. The decrease in the loss function value can only be achieved for a positive definite Hessian $\underline{H}^{(k-1)}$. In the neighborhood of the optimum this condition is always fulfilled, however, it cannot be necessarily expected to hold for the initial point $\boldsymbol{\vartheta}^{(0)}$ and the first iterations.

To avoid this problem a modified Newton method is often applied in which the Hessian is approximated by a matrix $\hat{H}^{(k-1)}$ that is guaranteed to be positive definite but is close to $\underline{H}^{(k-1)}$. The approach of approximating the inverse Hessian has the advantage that no matrix inversion has to be performed in (3.43). The approximation of the Hessian is usually started in the opposite gradient direction and is defined for further iteration steps as

$$\hat{H}^{(k)} = \hat{H}^{(k-1)} + \underline{Q}^{(k-1)}, \quad (3.44)$$

where all quasi-Newton methods differ by the kind of formula for \underline{Q} [80]. The Gauss-Newton method is the nonlinear least squares version of the general Newton method in (3.43).

3.2.4 Constrained Nonlinear Optimization

Constraints emerge from available knowledge or restrictions about the parameters. A general constrained nonlinear optimization problem may include inequality and equality constraints or constraints regarding the bounded parameters by their minimum and maximum value. Thus, in the framework of a nonlinear least squares problem the estimation problem (3.38) is subject to the constraints

$$g_i(\boldsymbol{\vartheta}) \leq 0, \quad i = 1, \dots, m, \quad (3.45)$$

$$h_j(\boldsymbol{\vartheta}) = 0, \quad j = 1, \dots, l. \quad (3.46)$$

This leads to the following Lagrangian, which is defined as the sum of the unconstrained loss function and the weighted constraints:

$$L(\boldsymbol{\vartheta}, \boldsymbol{\lambda}) = J(\boldsymbol{\vartheta}) + \sum_{i=1}^m \lambda_i g_i(\boldsymbol{\vartheta}) + \sum_{j=1}^l \lambda_{j+m} h_j(\boldsymbol{\vartheta}). \quad (3.47)$$

The *Kuhn-Tucker* equations give the following necessary (and for convex problems also sufficient) conditions for the optimality [112]

$$\boldsymbol{\vartheta}_{opt} \text{ is feasible, i.e., it meets the constraints,} \quad (3.48)$$

$$\lambda_i g_i(\boldsymbol{\vartheta}_{opt}) = 0, \quad i = 1, \dots, m \quad \lambda_i \geq 0, \quad (3.49)$$

$$\frac{\partial J(\boldsymbol{\vartheta}_{opt})}{\partial \boldsymbol{\vartheta}} + \sum_{i=1}^m \lambda_i \frac{\partial g_i(\boldsymbol{\vartheta}_{opt})}{\partial \boldsymbol{\vartheta}} + \sum_{j=1}^l \lambda_{j+m} \frac{\partial h_j(\boldsymbol{\vartheta}_{opt})}{\partial \boldsymbol{\vartheta}} = \mathbf{0}. \quad (3.50)$$

The equation (3.49) describes the canceling of the gradients between the loss function and the active constraints at the solution point. For the gradients to be canceled, *Lagrange multipliers* (λ_i , $i = 1, \dots, m$) are necessary to balance the deviations in magnitude of the loss function and constraint gradients. Only active constraints are included in this canceling operation, thus, the Lagrange multipliers of those inequality constraints with $g_i(\boldsymbol{\vartheta}_{opt}) < 0$ are zero. The Equation (3.50) requires the first order derivative of the Lagrangian to be equal to zero.

Constrained quasi-Newton methods guarantee superlinear convergence by accumulating second order information regarding the Kuhn-Tucker equations using a quasi-Newton updating procedure. These methods are commonly referred to as *Sequential Quadratic Programming (SQP)* methods and are included in many optimization packages.

We used the *Matlab* routine *fmincon* to solve the constrained nonlinear optimization problem [70]. The function *fmincon* uses a Sequential Quadratic Programming method to solve the subproblem at each iteration. At the begin of each iteration the gradient of the objective function at the current point is evaluated (using finite difference equations), and also an estimate of the Hessian of the Lagrangian is updated to choose a new location to start the next iteration. The successive improvement of the estimates, which is subject to a specialized tolerance, leads to the optimization result after a number of iterations. The simulation of the system trajectory is done by the ODE solver *ode15s*.

3.2.5 A Posteriori Identifiability

To test *a posteriori* the local identifiability of parameters $\boldsymbol{\vartheta} = (\boldsymbol{x}_0, \boldsymbol{p})$ in the following the concept of *sensitivity identifiability* is outlined. For this, we denote by $\hat{\boldsymbol{\vartheta}} = \boldsymbol{\vartheta}_{opt}$ the vector of estimated parameter, obtained by minimizing the nonlinear least squares functional

$$J(\boldsymbol{\vartheta}) = \|Y - h(\boldsymbol{\vartheta})\|^2 \quad (3.51)$$

as described above. To obtain a local minima, the following two conditions have to be satisfied. First

$$\nabla_{\boldsymbol{\vartheta}} J(\boldsymbol{\vartheta}) \big|_{\boldsymbol{\vartheta}=\hat{\boldsymbol{\vartheta}}} = -2\chi^n(\hat{\boldsymbol{\vartheta}})^T (Y - h(\hat{\boldsymbol{\vartheta}})) = 0, \quad (3.52)$$

where $\chi^N(\hat{\boldsymbol{\vartheta}})$ is called the *output sensitivity matrix* of the system and its i -th row is equal to $\nabla_{\boldsymbol{\vartheta}} h(t_i, \hat{\boldsymbol{\vartheta}})$, i.e.,

$$\chi_{ij}^N(\boldsymbol{\vartheta}_0) = \frac{\partial h(t_i, \boldsymbol{\vartheta})}{\partial \boldsymbol{\vartheta}_j} \big|_{\boldsymbol{\vartheta}=\boldsymbol{\vartheta}_0} \quad 1 \leq i \leq N, \quad 1 \leq j \leq q + n. \quad (3.53)$$

And second, the Hessian

$$\nabla^2 J(\boldsymbol{\vartheta}) \big|_{\boldsymbol{\vartheta}=\hat{\boldsymbol{\vartheta}}} = 2\chi^N(\hat{\boldsymbol{\vartheta}})^T \chi^N(\hat{\boldsymbol{\vartheta}}) - G(\hat{\boldsymbol{\vartheta}}) \quad (3.54)$$

with

$$G(\hat{\boldsymbol{\vartheta}}) = 2 \sum_{i=1}^N \left(Y_i - h(t_i, \hat{\boldsymbol{\vartheta}}) \right) \nabla_{\boldsymbol{\vartheta}}^2 h(t_i, \boldsymbol{\vartheta}) \big|_{\boldsymbol{\vartheta}=\hat{\boldsymbol{\vartheta}}} \quad (3.55)$$

is positive definite. Suppose the model output h is well approximated by its linear Taylor expansion around $\hat{\boldsymbol{\vartheta}}$, i.e.,

$$\Delta h \approx \chi^N(\hat{\boldsymbol{\vartheta}}) \Delta \boldsymbol{\vartheta}, \quad (3.56)$$

with $\Delta h = h(\boldsymbol{\vartheta}) - h(\hat{\boldsymbol{\vartheta}})$ and $\Delta \boldsymbol{\vartheta} = \boldsymbol{\vartheta} - \hat{\boldsymbol{\vartheta}}$. To obtain a unique solution of (3.56) for $\Delta \boldsymbol{\vartheta}$, nonsingularity of the sensitivity matrix $\chi^N(\hat{\boldsymbol{\vartheta}})$ is required. This lead us to the following necessary and sufficient condition for sensitivity identifiability of the structured system [21, 46].

Corollary 3.2.1. *A structure is called sensitivity identifiable, if a uniquely local solution of Equation (3.56) for $\Delta \boldsymbol{\vartheta}$ can be obtained. This is the case if and only if the matrix $\chi^N(\hat{\boldsymbol{\vartheta}})$ has full rank.*

In this linearized case, $G(\hat{\boldsymbol{\vartheta}}) = 0$ in Equation (3.54), $\chi^N(\hat{\boldsymbol{\vartheta}})^T \chi^N(\hat{\boldsymbol{\vartheta}})$ is positive definite and hence invertible. Thus an equivalent condition to Corollary (3.2.1) can be formulated.

Corollary 3.2.2. *A uniquely local solution of Equation (3.56) for $\Delta \boldsymbol{\vartheta}$ can be obtained if and only if the matrix $\chi^N(\hat{\boldsymbol{\vartheta}})^T \chi^N(\hat{\boldsymbol{\vartheta}})$ is invertible, i.e.,*

$$\det \left(\chi^N(\hat{\boldsymbol{\vartheta}})^T \chi^N(\hat{\boldsymbol{\vartheta}}) \right) \neq 0. \quad (3.57)$$

For a given $\boldsymbol{\vartheta} = \hat{\boldsymbol{\vartheta}}$, the sensitivity functions are defined by

$$S_{\mathbf{p}_k}(t) = \frac{\partial \mathbf{x}}{\partial \mathbf{p}_k}, \quad k = 1, \dots, q \quad (3.58)$$

$$K_{\mathbf{x}_{0l}}(t) = \frac{\partial \mathbf{x}}{\partial \mathbf{x}_{0l}}, \quad l = 1, \dots, n, \quad (3.59)$$

where \mathbf{x}_{0l} is the l th component of the initial condition \mathbf{x}_0 . The vector functions $S = (S_{\mathbf{p}_1}, \dots, S_{\mathbf{p}_q})$ and $K = (K_{\mathbf{x}_{01}}, \dots, K_{\mathbf{x}_{0n}})$ can be obtained by simultaneously solving the following system of sensitivity differential equations

$$\dot{S}(t) = \frac{\partial \mathbf{f}}{\partial \mathbf{x}} S(t) + \frac{\partial \mathbf{f}}{\partial \mathbf{p}}, \quad \text{with } S(t_0) = O_{n \times q}, \quad (3.60)$$

$$\dot{K}(t) = \frac{\partial \mathbf{f}}{\partial \mathbf{x}} K(t), \quad \text{with } K(t_0) = I_{n \times n}, \quad (3.61)$$

where O and I denote the zero and identity matrices, $\frac{\partial \mathbf{f}}{\partial \mathbf{x}}$ and $\frac{\partial \mathbf{f}}{\partial \mathbf{p}}$ are the Jacobians with respect to \mathbf{x} and \mathbf{p} , respectively.

Because the parameters \mathbf{p} may have different units, it is convenient to use the so called *normalized* sensitivity coefficients $\frac{\mathbf{p}}{\mathbf{x}} \frac{\partial \mathbf{x}}{\partial \mathbf{p}}$ to make them comparable [109].

By investigating the sensitivity function matrix for observations $\{Y_i\}_{i=1}^N$, the $N \times (q+n)$ output sensitivity matrix $\chi^N(\hat{\boldsymbol{\vartheta}})$ consists of the corresponding columns containing only the time derivatives of the output function with respect to parameter \mathbf{p} and initial conditions \mathbf{x}_0

$$\chi^N(\hat{\boldsymbol{\vartheta}}) = \begin{bmatrix} \frac{\partial h(t_1)}{\partial \mathbf{p}_1} & \dots & \frac{\partial h(t_1)}{\partial \mathbf{p}_q} & \frac{\partial h(t_1)}{\partial \mathbf{x}_{01}} & \dots & \frac{\partial h(t_1)}{\partial \mathbf{x}_{0n}} \\ \vdots & \ddots & \vdots & \vdots & \ddots & \vdots \\ \frac{\partial h(t_N)}{\partial \mathbf{p}_1} & \dots & \frac{\partial h(t_N)}{\partial \mathbf{p}_q} & \frac{\partial h(t_N)}{\partial \mathbf{x}_{01}} & \dots & \frac{\partial h(t_N)}{\partial \mathbf{x}_{0n}} \end{bmatrix}. \quad (3.62)$$

Remark 6. To allow for equality constraints in the sensitivity analysis, the sensitivity matrix χ^N is extended by the Jacobian Z associated with the equality constraints in (3.3). Assuming a number of M equality constraints, the extended $(N+M) \times (q+n)$ sensitivity matrix reads

$$\Omega^N(\hat{\boldsymbol{\vartheta}}) := (\chi^N \ Z). \quad (3.63)$$

Remark 7. Notice that distinguishability underlies also the concept of sensitivity identifiability. If a parameter does not influence the observations, it can also not be distinguished from any other parameter by observing the output process and the sensitivities of the output to that parameter is zero. Also, if there is a linear dependence between any of the parameters, there will be also one between the sensitivities of the output to these parameters. In both of these cases, the sensitivity matrix will be rank deficient, meaning that the parameter are not uniquely local identifiable.

3.2.6 Qualitative Analysis of Parameter Estimates

We make the standard statistical assumption that there exists a "true" value $\boldsymbol{\vartheta}_0$ of the parameter vector $\boldsymbol{\vartheta}$. Thus, the estimated parameter values $\hat{\boldsymbol{\vartheta}}$ can be interpreted as realizations of this random variable $\boldsymbol{\vartheta}_0$ and the accuracy of the parameter estimates ultimately depends on the statistical properties of $\boldsymbol{\vartheta}_0$. In order to qualitatively analyze the estimates, we use a standard error approach [13, 19]. From the asymptotic theory of statistical analysis, it can be shown that as $N \rightarrow \infty$, $\hat{\boldsymbol{\vartheta}}$ is approximately distributed according to a multivariate normal distribution, i.e.,

$$\hat{\boldsymbol{\vartheta}} \sim \mathcal{N}_{n+q}(\boldsymbol{\vartheta}_0, \Sigma_0), \quad (3.64)$$

where the covariance matrix Σ_0 is given by

$$\Sigma_0 = \sigma_0^2 (\chi^N(\boldsymbol{\vartheta}_0)^T \chi^N(\boldsymbol{\vartheta}_0))^{-1}. \quad (3.65)$$

The covariance matrix Σ_0 is used to formulate the standard errors for the estimates $\hat{\boldsymbol{\vartheta}}$. These are given by

$$SE_k(\boldsymbol{\vartheta}_0) = \sqrt{\sigma_0^2 (\chi^N(\boldsymbol{\vartheta}_0)^T \chi^N(\boldsymbol{\vartheta}_0))_{kk}^{-1}}, \quad k = 1, \dots, q+n. \quad (3.66)$$

Because $\boldsymbol{\vartheta}_0$ is unknown, it is replaced by $\hat{\boldsymbol{\vartheta}}$ when calculating approximations for (3.66). Moreover, the unknown constant error variance σ_0^2 is approximated by $\hat{\sigma}_0^2$ which is calculated as

$$\hat{\sigma}_0^2 = \frac{1}{N - (q+n)} |Y - h(\hat{\boldsymbol{\vartheta}})|^2. \quad (3.67)$$

This lead us to the approximated covariance matrix

$$\hat{\Sigma}_0 = \hat{\sigma}_0^2 (\chi^N(\hat{\boldsymbol{\vartheta}})^T \chi^N(\hat{\boldsymbol{\vartheta}}))^{-1}, \quad (3.68)$$

and standard errors

$$SE_k(\hat{\boldsymbol{\vartheta}}) = \sqrt{(\hat{\Sigma}_0)_{kk}}, \quad k = 1, \dots, q+n, \quad (3.69)$$

which are used to quantify uncertainty in the estimation.

For $\hat{\boldsymbol{\vartheta}}$ we define a vector of *coefficients of variation* $v(\hat{\boldsymbol{\vartheta}}) \in \mathbb{R}^{q+n}$ such that for each $k = 1, \dots, q+n$,

$$v_k(\hat{\boldsymbol{\vartheta}}) = \frac{\sqrt{(\hat{\Sigma}_0)_{kk}}}{\hat{\boldsymbol{\vartheta}}_k}. \quad (3.70)$$

The components of the vector $v(\hat{\boldsymbol{\vartheta}})$ are the dimensionless ratios of each standard error for a parameter to the corresponding nominal parameter value.

Next, we define

$$\alpha(\hat{\boldsymbol{\vartheta}}) = |v(\hat{\boldsymbol{\vartheta}})|, \quad (3.71)$$

which is called the *parameter selection score*, and note that $\alpha(\hat{\boldsymbol{\vartheta}})$ near zero indicates lower uncertainty possibilities in the estimation while large values of $\alpha(\hat{\boldsymbol{\vartheta}})$ suggest that one could expect to find a wide uncertainty in at least some of the estimates [19].

Furthermore, a set of parameters may be identifiable but the relevant matrix $\chi^T \chi$ may be near singular, which results in a poor estimability. The correlation coefficients between the components of $\hat{\boldsymbol{\vartheta}}$ reveals direct information on our ability to estimate each parameter and on the effect of parametrization of the model.

The correlation coefficients between two components of $\hat{\boldsymbol{\vartheta}}$ is given by

$$\text{corr}(\hat{\boldsymbol{\vartheta}}_k, \hat{\boldsymbol{\vartheta}}_l) = \frac{\text{cov}(\hat{\boldsymbol{\vartheta}}_k, \hat{\boldsymbol{\vartheta}}_l)}{\sigma_{\boldsymbol{\vartheta}_k} \sigma_{\boldsymbol{\vartheta}_l}}. \quad (3.72)$$

Using the definition of covariance matrix, we have that $\text{cov}(\hat{\boldsymbol{\vartheta}}_k, \hat{\boldsymbol{\vartheta}}_l)$ is simply the (k, l) -th element of $\hat{\Sigma}_0$ and the standard derivations $\sigma_{\boldsymbol{\vartheta}_k}$ and $\sigma_{\boldsymbol{\vartheta}_l}$ are the square roots of the (k, k) -th and (l, l) -th diagonal entries.

Chapter 4

Modeling Isoprene

Isoprene is one of the most abundant endogenous volatile organic compounds (VOCs) contained in human breath and is considered to be a potentially useful biomarker for diagnostic and monitoring purposes as described in Section 1.2. However, neither the exact biochemical origin of isoprene nor its physiological role are understood in sufficient depth, thus hindering the validation of breath isoprene tests in clinical routine.

Exhaled isoprene concentrations are reported to change under different clinical and physiological conditions, especially in response to enhanced cardiovascular and respiratory activity. Physiologically, this effect could be attributed to functional changes in the lung such as redistribution of ventilation and/or perfusion, recruitment and distension of pulmonary capillaries or changes in mixed venous concentration due to depletion of an isoprene buffer tissue. Investigating isoprene exhalation kinetics under dynamical exercise helps to gather the relevant experimental information for understanding the gas exchange phenomena associated with this important VOC.

In the following we will investigate several models concerning isoprene exchange mechanism under physical exercise starting with a five compartment model developed by Filser et al. [30]. The modeling focus in the present work lies in the global dynamics of the averaged compartmental concentrations, therefore, no attention has been paid to any transport delays between tissues, heart and lung. Such effects can be taken into account by considering delay differential equations. The interested reader may refer to Batzel et al. [16] for modeling examples of cardiovascular and respiratory systems with time delay and to Haddad et al. [37] for a qualitative analysis of such compartmental dynamical systems.

The following basic assumptions apply to the models considered in the scope of this thesis.

- Uptake occurs only via inhalation whereas excretion occurs via exhalation and metabolic elimination.

- The lung compartment is assumed to be ventilated by a continuous unidirectional stream of gas. Ventilation is tidal in nature and concentrations of gases in exhaled breath are subject to fluctuations throughout the breathing cycle. The dynamics of gases in inhalation and exhalation phase can be captured by considering two separate mass balance systems for each of them (see, e.g., [68]). Such a formulation may be indispensable to describe processes which take place within one respiratory circle. We are interested in mid- to long term kinetics of compounds and extract the end-tidal breathing volume for analysis though. Additionally, the analysis delay of approx. 10 s entails the mixture of about three subsequent end-tidal breath phases in the sample line during normal breathing. Thus, we study the averaged breath concentrations and consider the assumption of continuous and unidirectional ventilation to be appropriate for our purposes.

We also assume that the left and right cardiac output are equal and continuous.

- Diffusion between blood in the capillaries and air in the alveoli is thought to be a very rapid process. Therefore, an instantaneous equilibration between alveolar air and end-capillary (arterial) blood is assumed. Due to its low affinity for blood and its small molecular size, this instantaneous diffusion equilibrium is a reasonable assumption for isoprene. It is likely to hold also under moderate, sub-anaerobic exercise conditions [115]. Additionally, since isoprene does not form chemical bindings with blood, Henry's Law (A.9) applies. Consequently, the proportional relationship between arterial concentration C_a and mixed alveolar concentration C_A is expressed by

$$C_a = \lambda_{b:air} C_A. \quad (4.1)$$

Here, $\lambda_{b:air}$ denotes the isoprene-specific blood:gas partition coefficient as introduced in Section 1.2.

- Venous equilibrium as described in Section 2.3 is assumed. Accordingly, the relationship between the single compartment concentration (C_i) and effluent venous blood ($C_{i,v}$) is described by

$$C_{i,v} = \lambda_{b:i} C_i, \quad (4.2)$$

where $\lambda_{b:i}$ is the partition coefficient between blood and compartment.

- In metabolic active compartments, the rate of production is assumed to be constant, whereas metabolic elimination is described either by *Michaelis-Menten* kinetics or by linear kinetics as described in Section

2.3. For experiments carried out using a closed exposure system, a saturable Michaelis-Menten kinetics may be appropriate to describe the metabolic elimination. For normal conditions with low or negligible concentrations of isoprene in the atmosphere, however, saturable kinetics can be approximated by linear kinetics since it has been shown that up to 30 ppm (parts per million) of isoprene in the atmosphere the metabolic rate is proportional to this concentration [30].

4.1 A Five Compartment Physiological Toxicokinetic Model

The toxicologic effect of inhaled isoprene has thrilled the first investigations of its exchange mechanisms. Filser et al. [30] have derived a physiological five compartment model, which includes the lung, fat, muscle compartments, liver and richly perfused tissue (RPT) compartment (containing brain, intestines, kidney and spleen). Inhalation studies have been carried out to investigate the carcinogenic effects of isoprene and to estimate its tissue and organ concentrations, ultimate reactive metabolites, and, metabolically produced epoxides. Liver and RPT compartment are specified as sites of metabolism based on the knowledge described in Section 1.2 and on in vivo gas exchange experiments in a closed exposure system performed in [30]. A sketch of the model structure is given in Figure 4.1.

In the mentioned article besides the in vivo determination of the metabolic parameters for isoprene (given in Table 4.1), in vitro studies were performed using a headspace technique to determine blood:tissue and blood:air partition coefficients (given in Table B.1). Additionally, the constant production rate k_{pr}^{liv} was estimated from the isoprene concentrations in the headspace of the closed exposure system.

Metabolic parameters	Abbreviation	Man	Unit
Maximum metabolic rate in liver	V_{max}^{liv}	1690	($\mu\text{mol/h}$)/indiv.
Maximum metabolic rate in RPT	V_{max}^{rpt}	188	($\mu\text{mol/h}$)/indiv.
Michaelis Menten constant	K_m	2	$\mu\text{mol/l}$

Table 4.1 – Metabolic parameters of isoprene obtained in mice and rats, extrapolated to humans based on body weight to a power of 3/4. V_{max} is splitted assigning 90% to the liver and 10% to the richly perfused tissue group. The Michaelis constant (K_m) is assumed to be identical in rats and humans and the same value for K_m is given in both compartments [30].

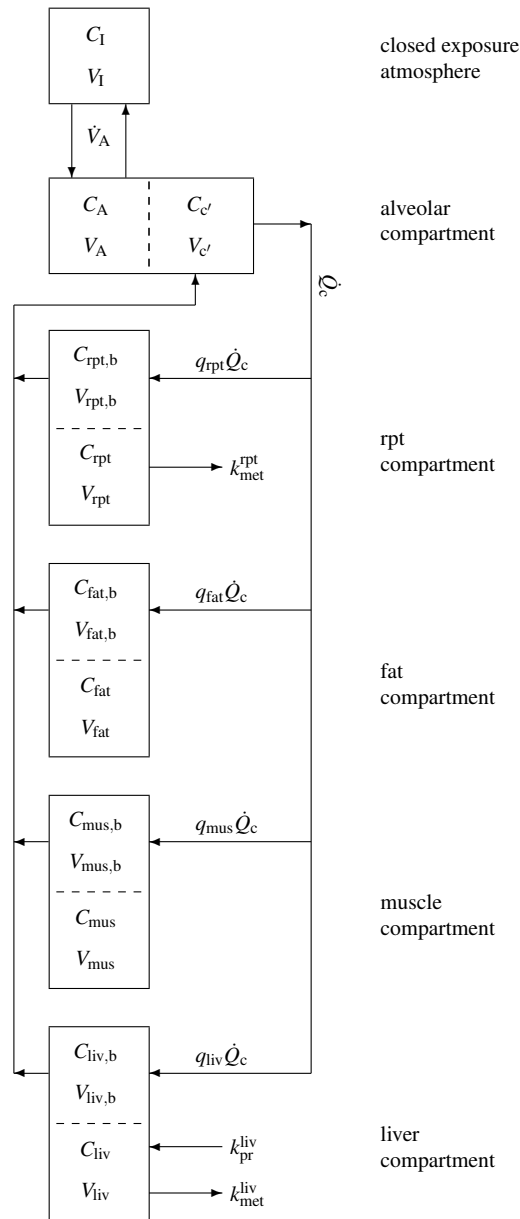


Figure 4.1 – The model sketch of the five compartment model developed by Filser et al. [30]. The body is subdivided into five distinct functional units: alveolar/end-capillary compartment (gas exchange), RPT (metabolic elimination) includes brain, intestine, kidney, spleen and other organs, fat compartment (storage), muscle compartment (storage), and liver compartment (production and metabolic elimination). Dashed borders indicate diffusion equilibrium. A closed exposure atmosphere was used to determine the metabolic parameters.

The lung was assumed to be a single homogeneous compartment with a diffusion equilibrium between alveolar gas and end-capillary blood. Under these assumptions the model is described by the following set of differential equations.

Alveolar compartment,

$$\tilde{V}_A \frac{dC_A(t)}{dt} = \dot{V}_A(t) (C_I - C_A(t)) + \dot{Q}_c(t) (C_{\bar{v}}(t) - C_A(t) \lambda_{b:air}) , \quad (4.3)$$

RPT compartment,

$$\begin{aligned} \tilde{V}_{\text{rpt}} \frac{dC_{\text{rpt}}(t)}{dt} &= q_{\text{rpt}}(t) \dot{Q}_c(t) (C_a(t) - \lambda_{b:\text{rpt}} C_{\text{rpt}}(t)) \\ &- k_{\text{met}}^{\text{rpt}} \lambda_{b:\text{rpt}} C_{\text{rpt}}(t) , \end{aligned} \quad (4.4)$$

fat compartment,

$$\tilde{V}_{\text{fat}} \frac{dC_{\text{fat}}(t)}{dt} = q_{\text{fat}}(t) \dot{Q}_c(t) (C_a(t) - \lambda_{b:\text{fat}} C_{\text{fat}}(t)) , \quad (4.5)$$

muscle compartment,

$$\tilde{V}_{\text{mus}} \frac{dC_{\text{mus}}(t)}{dt} = q_{\text{mus}}(t) \dot{Q}_c(t) (C_a(t) - \lambda_{b:\text{mus}} C_{\text{mus}}(t)) , \quad (4.6)$$

and, liver compartment,

$$\begin{aligned} \tilde{V}_{\text{liv}} \frac{dC_{\text{liv}}(t)}{dt} &= q_{\text{liv}}(t) \dot{Q}_c(t) (C_a(t) - \lambda_{b:\text{liv}} C_{\text{liv}}(t)) \\ &+ k_{\text{pr}}^{\text{liv}} - k_{\text{met}}^{\text{liv}} \lambda_{b:\text{liv}} C_{\text{liv}}(t) . \end{aligned} \quad (4.7)$$

In view of the diffusion equilibria, the compartment capacities are governed by the effective volumes

$$\begin{aligned} \tilde{V}_A &:= V_A + V_{c'} \lambda_{b:air} , \\ \tilde{V}_{\text{rpt}} &:= V_{\text{rpt}} + V_{\text{rpt},b} \lambda_{b:\text{rpt}} , \\ \tilde{V}_{\text{fat}} &:= V_{\text{fat}} + V_{\text{fat},b} \lambda_{b:\text{fat}} , \\ \tilde{V}_{\text{mus}} &:= V_{\text{mus}} + V_{\text{mus},b} \lambda_{b:\text{mus}} , \\ \tilde{V}_{\text{liv}} &:= V_{\text{liv}} + V_{\text{liv},b} \lambda_{b:\text{liv}} . \end{aligned}$$

The mixed venous concentration is given by the following algebraic equation as the weighted average of the compartmental venous concentrations

$$\begin{aligned} C_{\bar{v}}(t) &:= q_{\text{rpt}}(t) \lambda_{b:\text{rpt}} C_{\text{rpt}}(t) + q_{\text{fat}}(t) \lambda_{b:\text{fat}} C_{\text{fat}}(t) \\ &+ q_{\text{mus}}(t) \lambda_{b:\text{mus}} C_{\text{mus}}(t) + q_{\text{liv}}(t) \lambda_{b:\text{liv}} C_{\text{liv}}(t) . \end{aligned} \quad (4.8)$$

The above five compartment model was only investigated for steady state conditions, where the constant blood flow fractions to the systemic compartments were determined proportional to the cardiac output. To capture the redistribution of the systemic perfusion during ergometer exercise, we approximate the fractional blood flows through the systemic compartments by the following equations.

$$\begin{aligned} q_{\text{rpt}}(\dot{Q}_c) &:= q_{\text{rpt}}^{\text{rest}} - (q_{\text{rpt}}^{\text{rest}} - q_{\text{rpt}}^{\text{min}}) \times \left(1 - \exp\left(-\tau_{\text{rpt}} \max\left\{0, \frac{\dot{Q}_c - \dot{Q}_c^{\text{rest}}}{\dot{Q}_c^{\text{rest}}}\right\}\right)\right), \\ q_{\text{liv}}(\dot{Q}_c) &:= q_{\text{liv}}^{\text{rest}} + (q_{\text{liv}}^{\text{rest}} - q_{\text{liv}}^{\text{min}}) \times \left(1 - \exp\left(-\tau_{\text{liv}} \max\left\{0, \frac{\dot{Q}_c - \dot{Q}_c^{\text{rest}}}{\dot{Q}_c^{\text{rest}}}\right\}\right)\right), \\ q_{\text{fat}}(\dot{Q}_c) &:= \text{constant}, \\ q_{\text{mus}}(\dot{Q}_c) &:= 1 - \left(q_{\text{rpt}}(\dot{Q}_c) + q_{\text{fat}}(\dot{Q}_c) + q_{\text{liv}}(\dot{Q}_c)\right). \end{aligned}$$

Here, $q_i \in (0, 1)$ designates the fractional blood flow to the compartment i and $\tau_{\text{rpt}}, \tau_{\text{liv}}$ are positive constants. These relationships are justified by exponential fitting of the perfusion data given in [77], and, $\tau_{\text{rpt}}, \tau_{\text{liv}}$ are estimated to be 1.18 and 1.08 respectively. Reference values for the indicated fractional blood flows can be found in Table B.2, where fractional blood flows for rest conditions q_i^{rest} and for maximal workload ($q_{\text{rpt}}^{\text{min}}, q_{\text{liv}}^{\text{min}}$) correspond the values for 0 W and 150 W, respectively.

When investigating the exhalation dynamics of isoprene under ergometer workloads, we are interested in effects of physiological and metabolic parameters on exhaled concentrations. The five compartment model described above fails to capture the observed isoprene time courses during ergometer experiments described in Section 1.3.

As it has been mentioned previously, physical activity causes distinctive changes in exhaled isoprene profile. End-tidal isoprene abruptly increases at the onset of exercise, e.g., at 75 W, usually by a factor of about 3 – 4 compared with steady state value during rest (compare Figure 1.3). This phase is followed by a gradual decline and the development of a new steady state after about 15 min of pedaling [53]. This abrupt peak shaped response of isoprene has assumed to be a result of changes in hemodynamics or in pulmonary function rather than comparatively slow mechanisms of endogenous synthesis. Indeed, a constant source of isoprene has been suggested during sleep and during exercise [50].

Isoprene has a small blood:gas partition coefficient which implies its low affinity for blood and makes the human body an inefficient source for isoprene. According to the basic model of inert gas exchange in the lung (cf. Equation (1.4)), low soluble gases react highly sensitive even to small changes in ventilation or pulmonary perfusion. More specifically, Farhi's equation (1.4) predicts that, other factors being equal, increasing/decreasing

alveolar ventilation will result in decreased/increased exhaled breath concentrations, whereas the relationship between breath concentrations and cardiac output is monotonic and reflects the dependence on supply. Based on similar reasoning, Karl et al. [50] suggested a physiological two compartment model describing the breath isoprene time courses during exercise on an ergometer. We start by investigating this model as it seems to explain the observed concentration courses of isoprene during exercise on an ergometer and thus is widely accepted as "standard model".

4.2 A Serial Model of the Lung

The aforementioned physiological model consists of two compartments. The first compartment contains the blood-lung circuit where the source of isoprene is situated without precise specification of its exact location. The production rate of isoprene is assumed to be constant. The second compartment contains the breath air-lung circuit where isoprene exchange occurs between the environment and alveolar air. The lung is assumed to consist of adjacent segments of lung volume, so that blood passes several alveoli in series with concentration declining from the venous to arterial side. In each differential volume of the lung gas exchange between capillary blood and arterial air is by passive diffusion. The model sketch from the original work of Karl et al [50] is given below.

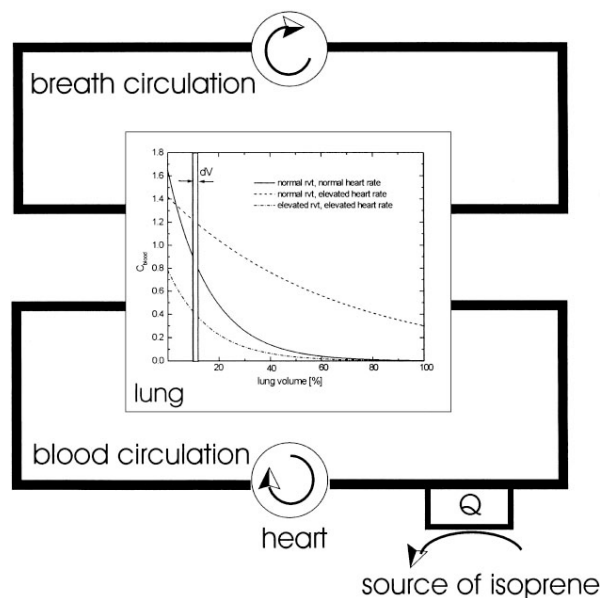


Figure 4.2 – The model sketch of the two compartment model developed by Karl et. al. [50].

Recall that the gas exchange in one alveolus is described by Equation (2.6). In steady state (independent of time), the Equation (2.6) reduces to the first-order, linear ordinary differential equation

$$\frac{d}{dv}C_b(v) = \frac{\dot{V}_A}{\dot{Q}_c V'_D} \left(C_I - \frac{C_b(v)}{\lambda_{b:\text{air}}} \right). \quad (4.9)$$

We suppose that the blood concentration at the inflow is fixed at $C_b(0)$. In steady state, the concentration at each position v is given by the solution of the Equation (4.9)

$$C_b(v) = C_I \lambda_{b:\text{air}} + \exp\left(-\frac{v}{\lambda_{b:\text{air}}} \cdot \frac{\dot{V}_A}{\dot{Q}_c V'_D}\right) (C_b(0) - C_I \lambda_{b:\text{air}}). \quad (4.10)$$

(Compare [50] Equation (3) for $C_I = 0$).

Now we take account of the assumption that the lung consists of several alveoli connected in series. Let V_L denote the whole lung volume. If the inspired concentration of the substance equals zero ($C_I = 0$), Equation (4.10) extended to the whole lung volume (i.e., evaluated at V_L) yields

$$C_a = C_{\bar{v}} \exp\left(-\frac{1}{\lambda_{b:\text{air}}} \cdot \frac{\dot{V}_A}{\dot{Q}_c}\right), \quad (4.11)$$

where the blood entering the lung has the mixed venous concentration $C_{\bar{v}}$ and the blood leaving the lungs has the arterial concentration C_a . (Compare [50] Equation (4)).

To get the blood concentration in the lung, we average the blood concentrations in each alveolus over the lung volumina V_L with respect to v :

$$\bar{C}_b = \frac{1}{V_L} \int_0^{V_L} C_b(v) dv = C_{\bar{v}} \lambda_{b:\text{air}} \frac{\dot{Q}_c}{\dot{V}_A} \left(1 - \exp\left(-\frac{1}{\lambda_{b:\text{air}}} \cdot \frac{\dot{V}_A}{\dot{Q}_c}\right) \right). \quad (4.12)$$

(Compare [50] Equation (5)).

Because of the large alveolar surface area compared to alveolar volume equilibrium between capillary blood and alveolar gas in each partial lung volume is assumed. Over the whole lung volume, the correlation between the average blood isoprene concentration and the average breath isoprene concentration is expressed by the following equation according to Henry's Law (A.9).

$$C_A = \frac{\bar{C}_b}{\lambda_{b:\text{air}}}. \quad (4.13)$$

By considering a single homogenous body compartment with a constant production rate the mass balance equation for the blood-lung compartment is given by

$$\frac{d}{dt}C_{\text{body}}(t)\tilde{V}_{\text{body}} = \dot{Q}_c(t)(C_a(t) - C_{\bar{v}}(t)) + k_{\text{pr}}. \quad (4.14)$$

We take the venous equilibrium assumption into account and state that the mixed venous blood concentration and the concentration in the tissue compartment are proportional with proportionality constant $\lambda_{\text{b:body}}$, which denotes the blood:body partition coefficient, i.e.,

$$C_{\bar{v}} = \lambda_{\text{b:body}}C_{\text{body}}. \quad (4.15)$$

Finally, substituting Equations (4.15) and (4.11) into Equation (4.14) yields

$$\frac{d}{dt}C_{\bar{v}}(t) = \frac{\lambda_{\text{b:body}}}{\tilde{V}_{\text{body}}} \left(\dot{Q}_c(t)C_{\bar{v}}(t) \left(\exp \left(-\frac{\dot{V}_A(t)}{\lambda_{\text{b:air}}\dot{Q}_c(t)} \right) - 1 \right) + k_{\text{pr}} \right). \quad (4.16)$$

For steady state conditions, and when C_A is known, the production rate can be derived from the model equations (4.11)-(4.14). Simulation results for exercise conditions performed with real-time measurements of physiological data show that the volume of the body compartment and its blood:tissue partition coefficient do not affect the height of the initial peak in exhaled concentration, but the following decrease to a new steady state.

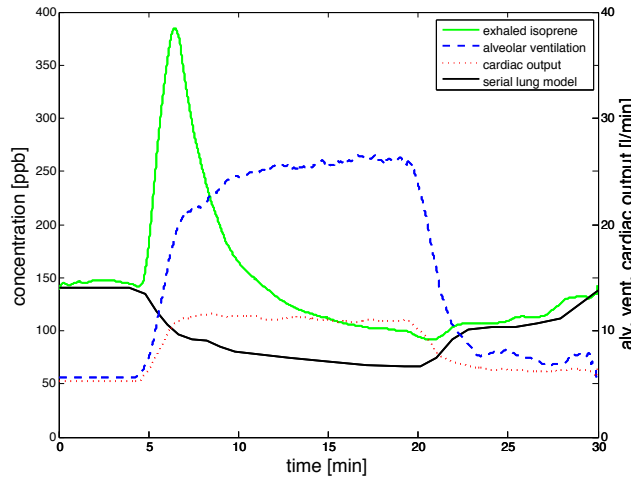


Figure 4.3 – Isoprene exhalation profile during one step exercise: 5 min resting - 15 min exercise (75 W) - 10 min resting (green line) compared to the serial model described above with the same data (black). For the simulation $\tilde{V}_A = 5$ l, $\tilde{V}_{\text{body}} = 51.55$ l and $\lambda_{\text{b:body}} = 0.11$ are assumed.

According to this model, the initial peak shaped behavior of exhaled isoprene at the onset of exercise can only be explained by markedly delayed increase in alveolar ventilation with respect to the pulmonary blood flow. According to the explanation in [50] as soon as exercise starts the pulmonary blood flow increases (which is proportional to the heartbeat frequency) resulting in a higher breath isoprene concentration because during this initial period of exercise the breathing rate has not yet changed. As the source of isoprene stays constant, the enhanced rate of evaporation leads to a decline in the blood isoprene concentration and thus of the evaporation rate. A few minutes after the start of exercise, the breath rate increases, leading to an enhanced dilution of isoprene, again resulting in a decline in the breath isoprene concentration to a new, lower steady-state level. This effects are reversed at the end of the exercise where breath rate and heart rate again reach values similar to those before the start of exercise, and therefore also the concentration of isoprene in the breath becomes similar to that before the start of experiment. The breath rate during the experiment has not been measured continuously. In fact, as stated in Section 1.2 the assumption of a delayed response of alveolar ventilation to dynamical exercise with respect to pulmonary blood flow is physiologically not justified and it also contradicts experimental evidence (see e.g., [53]). Figure 4.3 shows real-time data obtained during a one-step exercise at 75 W compared to the model output with the same data.

Moreover, the assumption of alveoli connected in series is questionable. A more common view of the actual geometry of the lung is that alveoli are connected in parallel [43, 114, 118]. The blood leaving the right heart is subdivided many times by the branching pulmonary arterial tree before it reaches the alveoli. After passing through the alveoli, it is collected by the pulmonary veins. The alveolar capillaries are therefore connected in parallel in the sense that the pulmonary blood flow is the sum of the blood flows of the individual alveoli. In a similar way, air entering the trachea is subdivided many times by the bronchial tree before it reaches the alveoli, and the total alveolar ventilation is the sum of the individual alveolar ventilations [43]. However, due to several normal factors, there exist regional differences in gas exchange down the normal lung causing an uneven distribution of ventilation-perfusion (\dot{V}_A/\dot{Q}_c) ratios (see Section 1.4). The influence of \dot{V}_A/\dot{Q}_c distribution on the gas exchange between alveolar air and arterial blood can be described by a multi compartment model having a range of \dot{V}_A/\dot{Q}_c values from zero to infinity. In such a model shunt is represented by not ventilated alveoli ($\dot{V}_A/\dot{Q}_c = 0$) and alveolar dead space is represented by not perfused alveoli ($\dot{V}_A/\dot{Q}_c \approx \infty$). As \dot{V}_A/\dot{Q}_c -ratios increase from zero and decrease from infinity, gas exchange efficiency increases until the optimum ratio of about 0.86 is reached. In real life, there is a spread of \dot{V}_A/\dot{Q}_c values throughout the lung around this "ideal" value. The larger the spread, the greater is the inefficiency of gas exchange.

In the following we will consider a three compartment lung model, with compartments representing homogenous groups of alveoli that are connected in parallel.

4.3 A Parallel Model of the Lung

We consider each alveolus as a homogenous well-mixed compartment and that as blood passes through the alveolus, it achieves equilibrium with alveolar air. If we number the alveoli using an index i , $i = 1, \dots, n$, and denote the mean alveolar concentration in alveolus i by $C_{A,i}$, the mass balance equation derived from Equation 2.7 for each alveolus reads

$$\begin{aligned} \tilde{V}_{A,i} \frac{d}{dt} C_{A,i}(t) &= q_i \dot{Q}_c(t) (C_{\bar{v}}(t) - C_{A,i}(t) \lambda_{b:\text{air}}) \\ &+ v_i \dot{V}_A(t) (C_I(t) - C_{A,i}(t)). \end{aligned} \quad (4.17)$$

Here fractional blood and air flows to compartment i are denoted by q_i and v_i , respectively. The effective volume of alveoli i again is defined by $\tilde{V}_{A,i} := V_{A,i} + V_{i,b} \lambda_{b:\text{air}}$, where $V_{A,i}$ is the volume of gaseous phase, and $V_{i,b}$ is the capillary blood volume. In steady state the solution of (4.17) are

$$C_{A,i} = \frac{r_i C_I + C_{\bar{v}}}{r_i + \lambda_{b:\text{air}}}, \quad C_{a,i} = \lambda_{b:\text{air}} \frac{r_i C_I + C_{\bar{v}}}{r_i + \lambda_{b:\text{air}}}, \quad (4.18)$$

where $r_i = v_i/q_i$ and $C_{a,i}$ is the arterial concentration.

We take into account that alveolar capillaries are connected in parallel, so that the composition of the mixed venous blood and of the inspired air is the same for different alveoli. Furthermore, the pulmonary blood flow is the sum of the blood flows of the individual alveoli and the alveolar ventilation is the sum of the individual alveolar ventilations, so we get

$$\dot{V}_A = \sum_i v_i \dot{V}_A, \quad \dot{Q}_c = \sum_i q_i \dot{Q}_c. \quad (4.19)$$

The mixed alveolar air is a mixture of air samples from different alveoli and is calculated by the ventilation-weighted average of the gas coming from each compartment. Similarly, the systemic arterial blood is a mixture of arterial blood flowing through the pulmonary capillaries of the various alveoli and thus is the perfusion-weighted mean of the blood coming from each compartment. The mean alveolar concentration (C_A) and the mean arterial concentration (C_a) are given by

$$C_A = \sum_i v_i C_{A,i} \quad C_a = \sum_i q_i C_{a,i}. \quad (4.20)$$

Even though in each individual alveolus diffusion equilibrium between end-capillary blood and alveolar air holds, no such equilibrium is required between the mean arterial and mean alveolar concentrations. Under steady state conditions as described in Equation (4.18), it can be shown that mean arterial and mean alveolar concentrations are in equilibrium only if the ventilation-perfusion ratio is uniform throughout the lung (see [43]). This means that if we denote the ventilation-perfusion ratio for the lung as a whole by r_0 , $r_i = r_0$ holds for all i .

To sum up, assuming that each parallel lung compartment is in steady state at every time instant and that the ventilation-perfusion ratios r_i are uniform throughout the lung, it can be concluded that mean arterial and mean alveolar concentrations are in equilibrium according to Henry's Law ($C_a = \lambda_{\text{b:air}} C_A$) and the mass-balance equation of the homogeneous lung corresponds to the basic model equation (1.2) described in Section 1.4.

In the following we only make use of the assumption that in each sub-compartment of the lung a diffusion equilibrium between end-capillary blood and alveolar air holds ($C_{A,i} = \lambda_{\text{b:air}} C_{a,i}$), and so we construct a three compartment lung model. A sketch of this model is given in Figure 4.4.

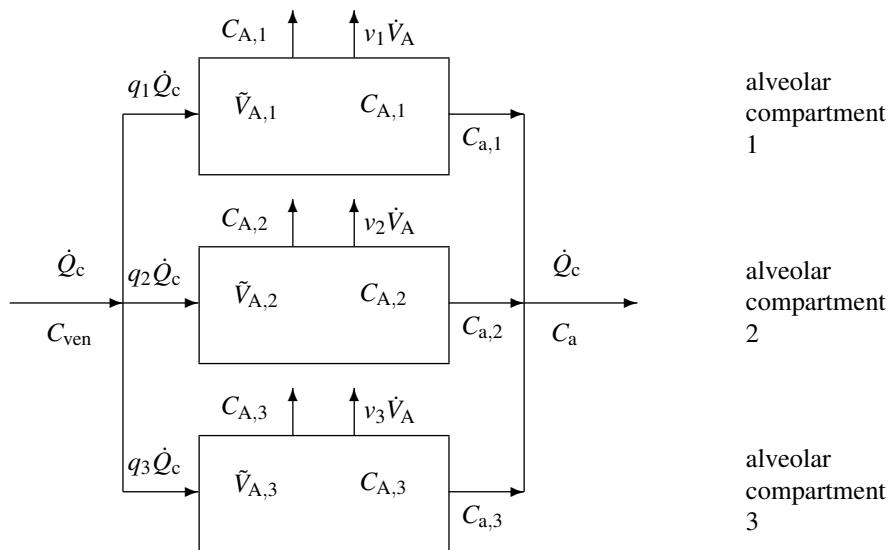


Figure 4.4 – Sketch of the 3 compartment lung model. Compartments are connected in parallel.

The mass-balance equations for the alveolar compartments read

$$\tilde{V}_{A,1} \frac{d}{dt} C_{A,1}(t) = q_1 \dot{Q}_c(t) (C_{\bar{v}}(t) - C_{A,1}(t) \lambda_{b:air}) - v_1 \dot{V}_A(t) C_{A,1}(t), \quad (4.21)$$

$$\tilde{V}_{A,2} \frac{d}{dt} C_{A,2}(t) = q_2 \dot{Q}_c(t) (C_{\bar{v}}(t) - C_{A,2}(t) \lambda_{b:air}) - v_2 \dot{V}_A(t) C_{A,2}(t), \quad (4.22)$$

$$\tilde{V}_{A,3} \frac{d}{dt} C_{A,3}(t) = q_3 \dot{Q}_c(t) (C_{\bar{v}}(t) - C_{A,3}(t) \lambda_{b:air}) - v_3 \dot{V}_A(t) C_{A,3}(t). \quad (4.23)$$

Multicompartment lung models with severe \dot{V}_A/\dot{Q}_c heterogeneity have been suggested by several investigators [45, 89], mostly consisting of a non-ventilated compartment ($\dot{V}_A/\dot{Q}_c = 0$), a non-perfused compartment ($\dot{V}_A/\dot{Q}_c \approx \infty$), and a "perfect" compartment ($\dot{V}_A/\dot{Q}_c \approx 1$). However, we prefer to make use of the quantitatively more realistic example suggested by Hlastala [42] of the three compartment representation of the normal lung given in Table 4.2. This lung model has a low \dot{V}_A/\dot{Q}_c compartment representing the shunt, a normal compartment, and a high \dot{V}_A/\dot{Q}_c compartment representing the dead space.

	fractional ventilation (v_i)	fractional perfusion (q_i)
Compartment 1	0.1	0.2
Compartment 2	0.75	0.76
Compartment 3	0.15	0.04

Table 4.2 – Three compartment lung with shunt and dead space as suggested in [42].

In normal subjects, the more uniform topographical distribution of blood flow during exercise results in a much more uniform matching of ventilation and perfusion throughout the lung, and the whole lung ventilation-perfusion ratio increases to a range of 2 to 4 with an average of 2.5 [62, 118]. For this reason we assume that the fractional flows are uniformly distributed with the start of exercise and approximate them by piecewise linear functions. If we replace this three compartment representation of the lung with the homogenous lung of the five compartment model described in Section 4.1, we see that the combined model is still lacking to explain the observed concentrations of isoprene under workload. Since the only source of isoprene

is situated in the liver compartment and workload causes a decrease of the fractional blood flow through the liver compartment, an increase in the exhaled concentration can not be achieved in response to exercise.

With respect to the model assumptions about the sources and sinks of isoprene, it can be concluded that the three compartment representation of the lung is capable to explain the peak shaped isoprene profile only if an extreme distribution of the fractional flows q_i and v_i are assumed. This distribution needs to allow a high concentrated accumulation of isoprene in the lung under steady state conditions. This means that in steady state, the most perfused lung compartment must get the least ventilation to lead to an enhanced isoprene excretion when the ventilation-perfusion distribution becomes much more uniform at the start of the exercise. Compared to a shunt perfusion of about 3% and a dead space ventilation of about 25% in normal lung [42], this values are physiologically not realistic and they lead to an extremely high mixed venous concentration in steady state which is in contraction to the values of about 9 nmol/l given in the literature [74].

An example of the above description is given in Figure 4.5. Thereby, the lung is treated as consisting of a pure dead space compartment, an ideal compartment, and a pure shunt compartment. A lumped well-mixed homogenous body compartment with a constant production rate and a linear metabolic elimination is considered.

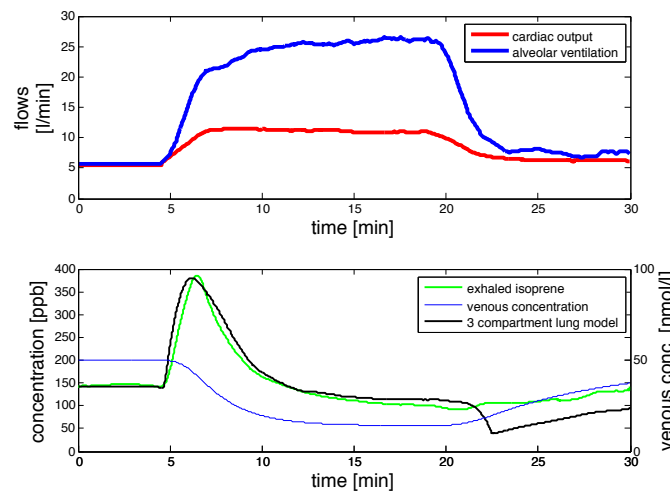


Figure 4.5 – Simulation result of the exhaled isoprene behavior during ergometer exercise at 75 W (the three compartment lung model combined with a lumped body compartment).

The mass-balance for the body compartment is governed by the following differential equation

$$\begin{aligned} \tilde{V}_{\text{body}} \frac{dC_{\text{body}}(t)}{dt} &= \dot{Q}_c(t) (C_a(t) - C_{\text{body}}(t)\lambda_{\text{b:body}}) \\ &+ k_{\text{pr}} - k_{\text{met}} C_{\text{body}}(t)\lambda_{\text{b:body}}. \end{aligned} \quad (4.24)$$

Parameters for this simplified model are given in Table B.3.

4.4 Stratified Inhomogeneity

Stratified inhomogeneity refers to the regional inhomogeneities in the lung in terms of a diffusion conductance term as described in Section 1.4. The theory is developed by Scheid et al. [97]. In this suggested series model, the lung is assumed to consist of a proximal compartment and a distal compartment. The proximal lung compartment is not perfused, but continuously ventilated, and it exchanges gas by diffusion with the distal compartment. The distal compartment is not ventilated but perfused with a continuous blood flow and exchanges gas by diffusion with both the proximal compartment and capillary blood. A perfect diffusion equilibration between the blood in the capillary and the alveolar air contained in the distal lung compartment is assumed. So the storage capacity of the combined distal compartment is governed by the effective volume $\tilde{V}_{A,2} := V_{A,2} + V_c\lambda_{\text{b:air}}$, where $V_{A,2}$ and V_c denote the gaseous volume of the distal compartment and the volume of the blood contained in the capillaries, respectively. Diffusion across the alveolar membrane between both lung compartments is assumed to be rate-limiting and quantified by the substance-specific diffusion conductance D . A sketch of the model structure is given in Figure 4.6.

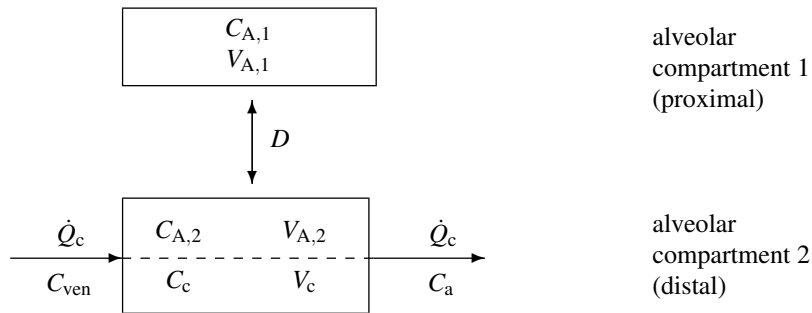


Figure 4.6 – Sketch of the stratified lung model.

For simulation purposes under exercise conditions, we model the diffusion conductance D as a function of time being linear dependent on the alveolar ventilation \dot{V}_A as

$$D(t) = D_{\text{rest}} + \tau \left(\dot{V}_A(t) - \dot{V}_A^{\text{rest}} \right), \quad \tau > 0. \quad (4.25)$$

We have chosen the constant τ to be 0.85, which has the following influence on the gas exchange mechanism of the lung. During steady state, the small conductance term D_{rest} reduces the gas exchange efficiency by causing a diffusion limitation between the proximal and distal lung compartments. As ventilation increases with the start of exercise, due to more efficient mixing of the gases resident in both lung compartments, the diffusion conductance increases and the lung becomes more efficient.

The model is described by the following differential equations.

Proximal compartment

$$V_{A,1} \frac{dC_{A,1}(t)}{dt} = -C_{A,1}(t)\dot{V}_A(t) + D(C_{A,2}(t) - C_{A,1}(t)), \quad (4.26)$$

and distal compartment

$$\tilde{V}_{A,2} \frac{dC_{A,2}(t)}{dt} = \dot{Q}_c(t) (C_{\bar{v}}(t) - C_{A,2}(t)\lambda_{b:\text{air}}(t)) - D(C_{A,2}(t) - C_{A,1}(t)). \quad (4.27)$$

A single body compartment presented as before is introduced and the mass balance in this compartment is described by

$$\begin{aligned} \tilde{V}_{\text{body}} \frac{dC_{\text{body}}(t)}{dt} &= \dot{Q}_c(t) (C_{A,2}(t)\lambda_{b:\text{air}} - C_{\text{body}}\lambda_{b:\text{body}}) \\ &+ k_{\text{pr}} - k_{\text{met}}C_{\text{body}}(t)\lambda_{b:\text{body}}. \end{aligned} \quad (4.28)$$

Similar to the arguments for the three compartment lung model, also for the stratified inhomogeneous lung, the mixed venous concentration has to be very high for exhaled isoprene to result in a 3 – 4 fold increase over the steady state levels. An example leading to the initial peak is shown in Figure 4.7 and the corresponding parameters are listed in Table B.4.

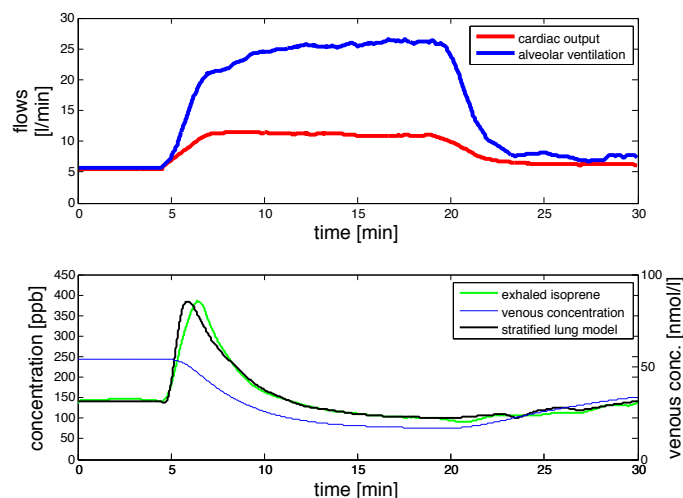


Figure 4.7 – Simulation result of the exhaled isoprene behavior during ergometer exercise at 75 W (the stratified lung model is combined with a lumped body compartment).

4.5 Discussion to the Aforecited Models

The lipophilic behavior of isoprene (as expressed by a small blood:air partition coefficient) advises us to consider the effects regarding the functional changes in the lung. However, a physiologically relevant description of its exhalation dynamics under exercise conditions could not be achieved by the discussed lung models which take into account regional inhomogeneities throughout the lung. With the assumption of a constant production rate in the liver compartment, where exercise leads to a decreased fractional blood flow, an initial increase of exhaled isoprene concentration can only be achieved by allowing a high concentrated accumulation in the lung under steady state conditions. This, in turn, requires very high mixed venous concentrations, which contradicts earlier findings.

We mentioned that in normal subjects, the more uniform topographical distribution of pulmonary blood flow during exercise results in a relatively uniform matching of ventilation and perfusion throughout the lung [62,118]. Since during exercise ventilation increases more than perfusion, the overall ventilation-perfusion ratio increases from a value of about 1 at rest to a range of 2 to 4 when the intensity of the exercise is increased from moderate to severe [62]. Other factors remaining unchanged, this effect would cause a decrease in the exhaled breath concentrations of low soluble VOCs according to Farhi's equation (1.4). Interestingly, exhaled isoprene profiles during workload challenges drastically depart from this predicted trend, see Figure 4.9. In contrast, exhaled breath profiles of butane (also a blood-borne

endogenous VOC) under dynamical exercise obey the qualitative behavior anticipated from Farhi's equation (1.4) [54], even though both compounds are comparable in terms of their physico-chemical properties. In particular, both butane and isoprene have similar molecular weights and similar blood:gas partition coefficients and therefore the diffusing capacity of the lung for both gases should be similar according to *Graham's law* (see A.7). This discrepancy suggests that some compound-specific (release) mechanism needs to be taken into account for clarifying the physiological behavior of isoprene.

Regarding the lung, an alternative isoprene source might comprise the pulmonary surfactant, which is a complex mixture of lipids and specific proteins lining the epithelial surface of the lung. Within the alveoli, its main function is to reduce surface tension at the air-liquid interface and ensure alveolar stability during respiratory motion [63].

A storage function of the pulmonary surfactant for isoprene and a release mechanism due to the hyperinflation of the lung [117] is conceivable, however, there is little evidence to pursue this hypothesis. On the other hand, experimental evidence suggests a systemic source of isoprene as will be presented in the next section.

4.6 Revealing Information from Experiments

The experimental data presented in the following are taken from the study cohort in [52] and [53], where five (age 27-34 years, 4 male, 1 female) and eight (age 25-30, 5 male, 3 female) normal healthy volunteers have been investigated, respectively. Figure 4.9 shows representative experimental results for one single volunteer (27 years, male).

All protocols started with an initial resting phase without workload. Then for the first two protocols the test subject was challenged to pedal at constant speed between 70-80 $r \text{ min}^{-1}$ on the ergometer, which was set up for constant workload resistance according to each protocol. In protocol 3 exercise carried out with two subsequent phases of arm-crank exercise followed by pedaling. Exercise protocols are given in Figure 4.8.

Breath isoprene concentrations are assessed by means of a real-time setup designed for synchronized measurements of exhaled breath VOCs (using PTR-MS) as well as a variety of respiratory and hemodynamic parameters as described in Section 1.3.

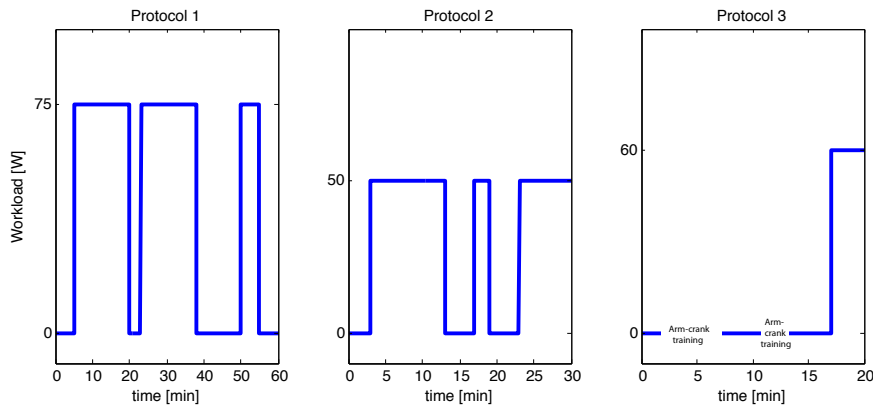


Figure 4.8 – Protocols of the three workload scenarios corresponding to the data presented in Figure 4.9.

(First column): Two legged ergometer experiment. Protocol: 5 min resting - 15 min exercise (75 W) - 3 min resting - 15 min exercise (75 W) - 12 min resting - 5 min exercise (75 W) - 5 min resting.

(Second column): One legged ergometer experiment. Protocol: 3 min resting - 10 min left leg (50 W) - 4 min resting - 2 min left leg (50 W) - 4 min resting - 7 min right leg (50 W).

(Third column): Arm/two-legged ergometer experiment. Protocol: 2 min resting - 5 min arm-crank training (2.5 kg/arm) - 4 min resting - 2 min arm-crank training (2.5 kg/arm) - 4 min resting - 3 min two-legged exercise (60 W).

The first column of Figure 4.9 presents measurement results during a 2-legged ergometer exercise with three subsequent workload phases at 75 W, and pauses of 3 min and 12 min, respectively. The breath isoprene concentration profiles during these three workload phases display similar shape. Nevertheless, the height of the characteristic exercise peak is significantly higher during the first phase of workload, despite an almost identical behavior of cardiac output and alveolar ventilation throughout all exercise segments. This indicates the existence of a buffer tissue compartment for isoprene. The concentration peak observed during the first workload phase is restored if the pauses between workload phases are extended: Approximately one hour of rest is necessary to achieve a complete recovery of the initial peak height [53].

The second column of Figure 4.9 shows representative results in response to one-legged ergometer exercise at 50 W. After 10 minutes of pedaling with the left leg, breath isoprene profiles closely resemble the two-legged case and a clear washout effect emerges, yielding a lower peak height when continuing the exercise with the same leg. However, if the working limb is switched to the right leg after a short break of the same length as before, an immediate

recovery of the initial peak size can be observed. The observation that the rise in cardiac output and alveolar ventilation is of comparable order in all three phases of exercise appears to exclude functional changes of the lung (redistribution of ventilation-perfusion ratio, distension of pulmonary capillaries) as the main cause for the peak-shaped isoprene profile at the onset of exercise and strongly supports the hypothesis of a peripheral source affecting breath isoprene output.

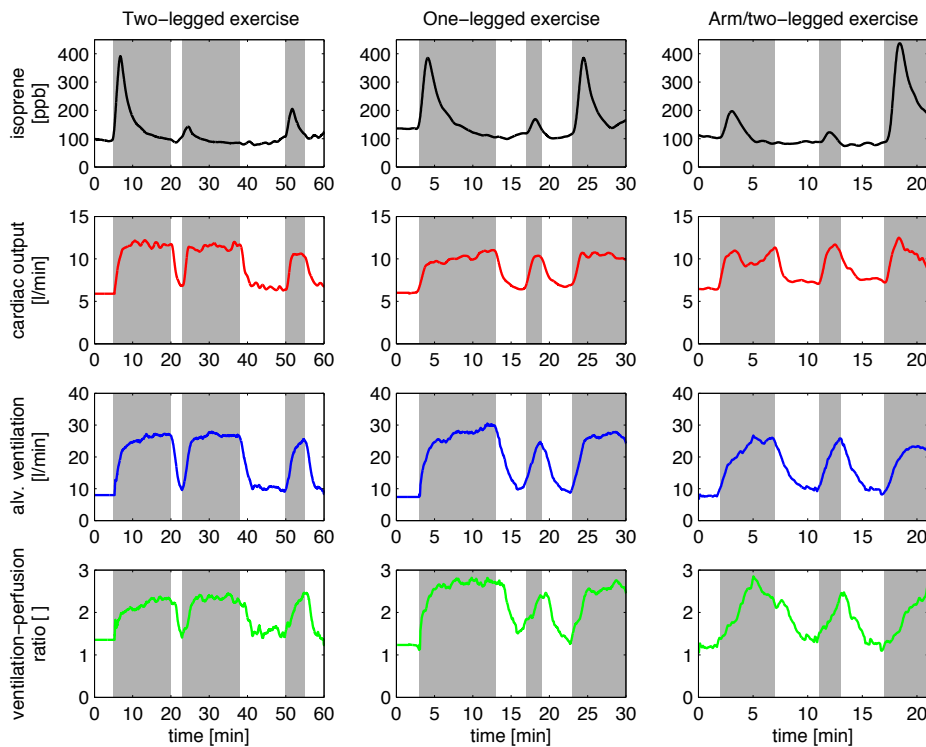


Figure 4.9 – Typical smoothed profiles of end-exhaled isoprene concentrations and physiological parameters in response to predefined workload scenarios of one single volunteer (27 years, male).

The experiment presented in the third column of Figure 4.9 allows for a more precise specification of the location of the above-mentioned tentative isoprene buffer, namely skeletal muscles, by stimulating single muscle groups with distinct masses. While repeated dynamic arm-crank exercises with an intermediate pause of 4 minutes yield the same washout effect as described above, subsequent two-legged ergometer exercise at 60 W yields a much higher peak compared to arm-crank exercise, despite a similar behavior of the ventilation-perfusion ratio within all three workload segments. We attribute this effect to the smaller mass of arm musculature as well as to the smaller fractional perfusion of the arm muscle group as compared to leg mus-

culature. This experiment proposes that a major part of isoprene variability during exercise conditions can be ascribed to an increased fractional perfusion of the working locomotor muscles, eventually leading to higher isoprene concentrations in mixed venous blood at the onset of physical activity.

This rationale is in accordance with the predominant physiological role of working muscle during exercise. Collectively, the skeletal muscles constitute up to 40-45% of body weight, which is more than any other single organ. At rest, about 10–15% of cardiac output is distributed to skeletal muscle, while during strenuous exercise skeletal muscle may receive more than 80% of total blood flow, thus rendering it as one of the major factors in overall cardiovascular hemodynamics [76].

4.6.1 A first three compartment model for isoprene

In the light of the experiments outlined above the mathematical model of isoprene distribution presented here is based on the assumption of a peripheral source of isoprene in the body. The lung is considered to be a homogenous single compartment with a fixed storage volume V_A . An instantaneous equilibrium between end-capillary blood (corresponding to arterial blood) and alveolar air is assumed, leading to a directly proportional relationship (Henry's law (A.9)) between the arterial blood concentration C_a and the alveolar air concentration C_A , viz.,

$$C_a = \lambda_{b:air} C_A. \quad (4.29)$$

Here, $\lambda_{b:air}$ is the dimensionless substance specific partition coefficient between blood and air. In view of this diffusion equilibrium, the alveolar compartment capacity is governed by the effective storage volume $\tilde{V}_A := V_A + \lambda_{b:air} V_{c'}$, where $V_{c'}$ represents the capillary blood volume. Thus, the mass-balance equation for the lung reads according to (2.7)

$$\tilde{V}_A \frac{dC_A}{dt} = \dot{Q}_c (C_{\bar{v}} - C_a) + \dot{V}_A (C_I - C_A), \quad (4.30)$$

where $C_{\bar{v}}$ and C_I are the concentrations in mixed venous blood and inhaled air, respectively. Cardiac output is denoted by \dot{Q}_c , while \dot{V}_A denotes the alveolar ventilation.

The body is subdivided into two homogenous functional units: a richly perfused tissue compartment (including intestines, liver, brain, connective muscles and skin) and a peripheral tissue compartment. The model structure is sketched in Figure 4.10. While production and metabolic elimination of isoprene occurs in both compartments, the peripheral tissue compartment takes the role of an isoprene buffer and is postulated to contain the working muscle compartment, which receives a disproportionately high fraction of the systemic blood flow as soon as exercise starts.

The venous blood concentration leaving the compartment is considered to be in equilibrium with the respective tissue concentration at every instant t (venous equilibrium). Based on this assumption, the storage capacities in richly perfused and peripheral tissue can again be expressed as effective volumes $\tilde{V}_{\text{rpt}} := V_{\text{rpt}} + \lambda_{\text{b:rpt}} V_{\text{rpt,b}}$ and $\tilde{V}_{\text{per}} := V_{\text{per}} + \lambda_{\text{b:per}} V_{\text{per,b}}$, respectively. Here, V_{\star} and $V_{\star,\text{b}}$ denote the volumes of intracellular space and vascular blood, respectively, while $\lambda_{\text{b:\star}}$ is the blood:tissue partition coefficient of the corresponding compartment ¹. Mass balance equations read

$$\tilde{V}_{\text{rpt}} \frac{dC_{\text{rpt}}}{dt} = (1 - q_{\text{per}}) \dot{Q}_{\text{c}} (C_{\text{a}} - \lambda_{\text{b:rpt}} C_{\text{rpt}}) + k_{\text{pr}}^{\text{rpt}} - k_{\text{met}}^{\text{rpt}} \lambda_{\text{b:rpt}} C_{\text{rpt}}, \quad (4.31)$$

for richly perfused tissue and

$$\tilde{V}_{\text{per}} \frac{dC_{\text{per}}}{dt} = q_{\text{per}} \dot{Q}_{\text{c}} (C_{\text{a}} - \lambda_{\text{b:per}} C_{\text{per}}) + k_{\text{pr}}^{\text{per}} - k_{\text{met}}^{\text{per}} \lambda_{\text{b:per}} C_{\text{per}}, \quad (4.32)$$

for peripheral tissue, with the kinetic rate constants k_{pr}^{\star} and k_{met}^{\star} describing production and metabolic elimination, respectively, and q_{\star} denoting a fractional blood flow.

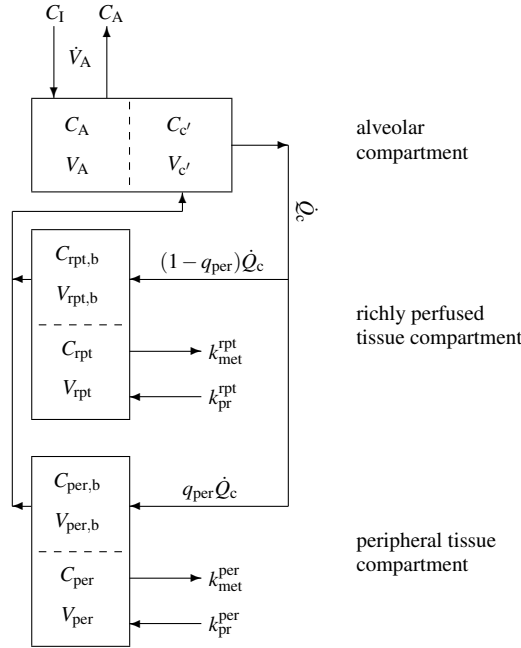


Figure 4.10 – Sketch of the model structure. The body is divided into three distinct functional units: alveolar/end-capillary compartment (gas exchange), richly perfused tissue (metabolism and production) and peripheral tissue (storage, metabolism and production). Dashed boundaries indicate a diffusion equilibrium. Abbreviations connote as in Table 4.3.

In order to capture the redistribution of the systemic perfusion during ergometer exercise, the fractional blood flow $q_{\text{per}} \in (0, 1)$ to peripheral tissue is assumed to resemble the fractional blood flow to both legs, which is approximated to increase with cardiac output according to

$$q_{\text{per}}(\dot{Q}_c) := q_{\text{per}}^{\text{rest}} + (q_{\text{per}}^{\text{max}} - q_{\text{per}}^{\text{rest}}) \times \left(1 - \exp\left(-\tau \max\left\{0, \frac{\dot{Q}_c - \dot{Q}_c^{\text{rest}}}{\dot{Q}_c^{\text{rest}}}\right\}\right)\right), \quad (4.33)$$

where $\tau > 0$ is a constant. The associated concentrations in mixed venous and arterial blood are given by

$$C_{\bar{v}} := (1 - q_{\text{per}})\lambda_{\text{b:rpt}}C_{\text{rpt}} + q_{\text{per}}\lambda_{\text{b:per}}C_{\text{per}} \quad (4.34)$$

and Equation (4.29), respectively. Moreover, we state that the measured (end-tidal) isoprene concentration equals the alveolar level, i.e.,

$$C_{\text{meas}} = C_A. \quad (4.35)$$

Discussion to this model

During rest, the peripheral compartment is characterized by high isoprene concentrations resulting from extrahepatic production with a constant rate. However, due to the minute fractional blood flow to these tissues, mixed venous concentrations are mainly governed by the lower isoprene content in venous blood returning from the richly perfused tissue group. At the start of exercise, the fractional perfusion in the periphery increases and the mixed venous concentrations become dominated by peripheral venous return. The isoprene concentration peak visible in breath hence is considered as a consequence of the corresponding increase in the underlying mixed venous concentration.

While the cause and effect relationships proposed above remain speculative, the presented modeling study (see also [52] and [56]) certainly yields new interesting perspectives on previous experimental findings. Several experiments have been summarized here demonstrating that the peak-shaped behavior of end-tidal isoprene during exercise is most probably associated with the increased activity and perfusion of the skeletal muscle group.

The simulation result given in Figure 4.11 shows a perfect match between observed data and model output by means of the three compartment model. For a detailed description of model validation and estimation we refer to [52].

To make a more precise description of the peripheral origin of isoprene in the following we will formulate a five compartment model similar to that given by Filser et al. [30] with some adaptations based on the experimental findings described above. Attention will be paid to the original compartmental segmentation. A further requirement is the description of the exhaled isoprene profiles of the one-legged exercise (as presented in Figure 4.9) by means of the extended model.

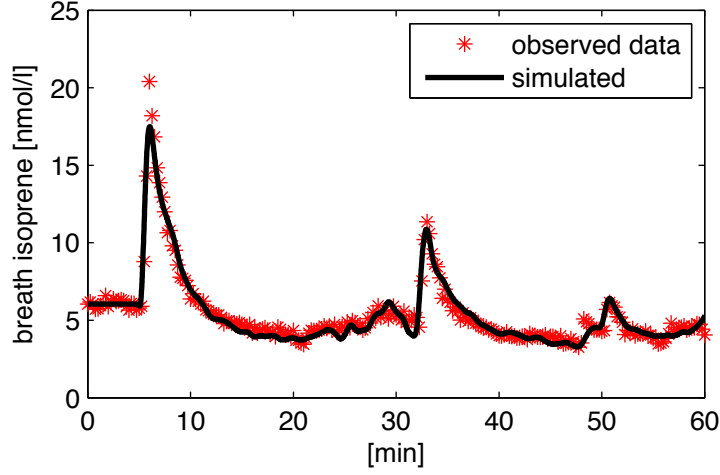


Figure 4.11 – Simulation result of the three compartment peripherie model taken from [52].

4.7 A Five Compartment Model

The following five compartment model maintains the compartmental segmentation of the toxicokinetic physiological five compartment model introduced by Filser [30]. Only the muscle compartment will be understood now as working muscle compartment containing skeletal muscles, whereas resting muscles and skin are included in the RPT compartment. In the muscle compartment, we assume a metabolic activity concerning isoprene expressed by a constant production rate and by a linear kinetic for metabolic elimination. A sketch of the model structure is given in Figure 4.12. The mass balance equations are derived in the same way as before and listed below.

The mass balance equations for the alveolar compartment reads

$$\tilde{V}_A \frac{dC_A(t)}{dt} = \dot{V}_A(t) (C_I - C_A(t)) + \dot{Q}_c(t) (C_{\bar{v}}(t) - C_a(t)), \quad (4.36)$$

while for the RPT, liver and working muscle compartments we find that

$$\begin{aligned} \tilde{V}_{\text{rpt}} \frac{dC_{\text{rpt}}(t)}{dt} &= q_{\text{rpt}}(t) \dot{Q}_c(t) (C_a(t) - \lambda_{\text{b:rpt}} C_{\text{rpt}}(t)) \\ &- k_{\text{met}}^{\text{rpt}} \lambda_{\text{b:rpt}} C_{\text{rpt}}(t), \end{aligned} \quad (4.37)$$

$$\begin{aligned} \tilde{V}_{\text{liv}} \frac{dC_{\text{liv}}(t)}{dt} &= q_{\text{liv}}(t) \dot{Q}_c(t) (C_a(t) - \lambda_{\text{b:liv}} C_{\text{liv}}(t)) \\ &+ k_{\text{pr}}^{\text{liv}} - k_{\text{met}}^{\text{liv}} \lambda_{\text{b:liv}} C_{\text{liv}}(t), \end{aligned} \quad (4.38)$$

and

$$\begin{aligned} \tilde{V}_{\text{mus}} \frac{dC_{\text{mus}}(t)}{dt} &= q_{\text{mus}}(t) \dot{Q}_c(t) (C_a(t) - \lambda_{\text{b:mus}} C_{\text{mus}}(t)) \\ &+ k_{\text{pr}}^{\text{mus}} - k_{\text{met}}^{\text{mus}} \lambda_{\text{b:mus}} C_{\text{mus}}(t) \end{aligned} \quad (4.39)$$

respectively. Finally, for the fat compartment we have

$$\tilde{V}_{\text{fat}} \frac{dC_{\text{fat}}(t)}{dt} = q_{\text{fat}}(t) \dot{Q}_c(t) (C_a(t) - \lambda_{\text{b:fat}} C_{\text{fat}}(t)) . \quad (4.40)$$

The mixed venous concentration is given as the weighted average of the compartmental venous concentrations

$$\begin{aligned} C_{\bar{v}}(t) &:= q_{\text{rpt}}(t) \lambda_{\text{b:rpt}} C_{\text{rpt}}(t) + q_{\text{fat}}(t) \lambda_{\text{b:fat}} C_{\text{fat}}(t) \\ &+ q_{\text{mus}}(t) \lambda_{\text{b:mus}} C_{\text{mus}}(t) + q_{\text{liv}}(t) \lambda_{\text{b:liv}} C_{\text{liv}}(t) . \end{aligned} \quad (4.41)$$

The alveolar concentration is assumed to be proportional to the arterial concentration

$$C_a(t) = \lambda_{\text{b:air}} C_A(t) , \quad (4.42)$$

and again, we state that the measured (end-tidal) isoprene concentration equals the alveolar level, i.e.,

$$y := C_{\text{meas}} = C_A . \quad (4.43)$$

The redistribution of the systemic perfusion during ergometer exercise is described by the following equations.

$$\begin{aligned} q_{\text{rpt}}(\dot{Q}_c) &:= q_{\text{rpt}}^{\text{rest}} - (q_{\text{rpt}}^{\text{rest}} - q_{\text{rpt}}^{\text{min}}) \times \left(1 - \exp\left(-\tau_{\text{rpt}} \max\left\{0, \frac{\dot{Q}_c - \dot{Q}_c^{\text{rest}}}{\dot{Q}_c^{\text{rest}}}\right\}\right)\right), \\ q_{\text{fat}}(\dot{Q}_c) &:= \text{constant}, \\ q_{\text{mus}}(\dot{Q}_c) &:= q_{\text{mus}}^{\text{rest}} + (q_{\text{mus}}^{\text{max}} - q_{\text{mus}}^{\text{rest}}) \times \left(1 - \exp\left(-\tau_{\text{mus}} \max\left\{0, \frac{\dot{Q}_c - \dot{Q}_c^{\text{rest}}}{\dot{Q}_c^{\text{rest}}}\right\}\right)\right), \\ q_{\text{liv}}(\dot{Q}_c) &:= 1 - \left(q_{\text{rpt}}(\dot{Q}_c) + q_{\text{fat}}(\dot{Q}_c) + q_{\text{mus}}(\dot{Q}_c)\right) . \end{aligned}$$

Here, $q_i \in (0, 1)$ designates the fractional blood flow to the compartment i and $\tau_{\text{rpt}}, \tau_{\text{mus}}$ are positive constants.

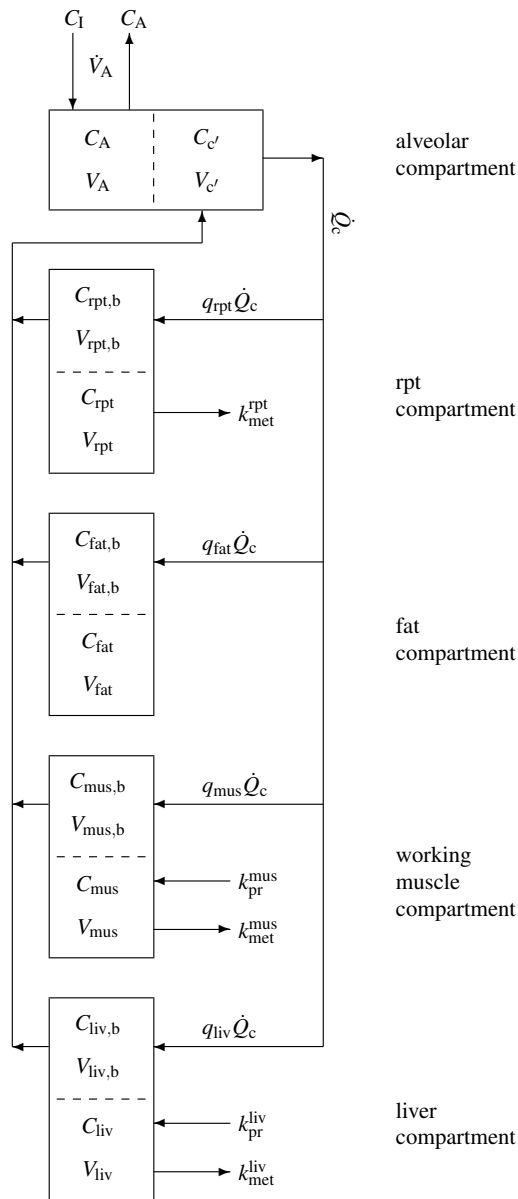


Figure 4.12 – Sketch of the model structure. The body is divided into five distinct functional units: alveolar/end-capillary compartment (gas exchange), richly perfused tissue (metabolic elimination) includes resting muscle, skin, intestines, brain, kidney, spleen and other organs), fat compartment (storage), working muscle compartment (metabolic elimination and production), and liver compartment (metabolic elimination and production). Dashed boundaries indicate a diffusion equilibrium.

As before, the compartment capacities are defined as

$$\begin{aligned}\tilde{V}_A &:= V_A + V_{c'} \lambda_{b:\text{air}}, \\ \tilde{V}_{\text{rpt}} &:= V_{\text{rpt}} + V_{\text{rpt},b} \lambda_{b:\text{rpt}}, \\ \tilde{V}_{\text{fat}} &:= V_{\text{fat}} + V_{\text{fat},b} \lambda_{b:\text{fat}}, \\ \tilde{V}_{\text{mus}} &:= V_{\text{mus}} + V_{\text{mus},b} \lambda_{b:\text{mus}}, \\ \tilde{V}_{\text{liv}} &:= V_{\text{liv}} + V_{\text{liv},b} \lambda_{b:\text{liv}}.\end{aligned}$$

For later purposes, we note that a model accommodating the experimental situation during exhalation and inhalation to and from a fixed volume exposure atmosphere can simply be derived by augmenting Equations (4.36)-(4.38) with an additional compartment obeying

$$\tilde{V}_I \frac{dC_I(t)}{dt} = \dot{V}_A(t) (C_A(t) - C_I(t)). \quad (4.44)$$

This typically describes closed system (rebreathing) setups such as in Filser et al. [30]. The external measurable inputs are denoted by $\mathbf{u} := (\dot{V}_A, \dot{Q}_c, C_I)$ and $\mathbf{p} := (k_{\text{pr}}^{\text{mus}}, k_{\text{pr}}^{\text{liv}}, k_{\text{met}}^{\text{rpt}}, k_{\text{met}}^{\text{mus}}, k_{\text{met}}^{\text{liv}}, \tilde{V}_{\text{mus}}, \tau_{\text{mus}})$ represents the constant vector of parameters to be estimated from measured breath concentrations y .

In the following, we will discuss some qualitative properties of the underlying system. Note first that Equations (4.36)-(4.38) can be written as a time-varying inhomogenous linear system

$$\dot{\mathbf{c}} = A(\mathbf{u}, \mathbf{p})\mathbf{c} + \mathbf{b}(\mathbf{u}, \mathbf{p}) =: \mathbf{f}(\mathbf{u}, \mathbf{p}, \mathbf{c}). \quad (4.45)$$

As the system is linear, for any given initial condition $\mathbf{c}(0)$ there is a unique global solution. According to the Remark 3.1.4 in Section 3.1 we know that the positive orthant \mathbb{R}_+^n is a forward invariant set for our system. That means, the components of the state variable $\mathbf{c} = (C_A, C_{\text{rpt}}, C_{\text{fat}}, C_{\text{mus}}, C_{\text{liv}})^T$ remain non-negative for all t . Moreover, by considering the total mass of substance contained in the system we postulate that the trajectories of the system remain bounded for bounded rates of production and metabolic elimination. Indeed, if we define m as a continuously differentiable function

$$m := \sum_i \tilde{V}_i C_i \geq 0, \quad (4.46)$$

we obtain

$$\begin{aligned}\dot{m} &= \dot{V}_A(C_I - C_A) - k_{\text{met}}^{\text{rpt}} C_{\text{rpt}} \lambda_{b:\text{rpt}} \\ &+ k_{\text{pr}}^{\text{mus}} - k_{\text{met}}^{\text{mus}} C_{\text{mus}} \lambda_{b:\text{mus}} + k_{\text{pr}}^{\text{liv}} - k_{\text{met}}^{\text{liv}} C_{\text{liv}} \lambda_{b:\text{liv}}.\end{aligned} \quad (4.47)$$

By considering the positivity of all involved parameters, it can readily be verified that the trajectories remain bounded. Moreover, for constant \mathbf{u} (which corresponds to rest or constant workload conditions) the compartmental concentrations have been shown to approach a globally asymptotically stable equilibrium (compare (3.26)), since for this case we achieve that

$$\dot{m} = -C_A \dot{V}_A - k_{\text{met}}^{\text{rpt}} C_{\text{rpt}} \lambda_{\text{b:rpt}} - k_{\text{met}}^{\text{mus}} C_{\text{mus}} \lambda_{\text{b:mus}} - k_{\text{met}}^{\text{liv}} C_{\text{liv}} \lambda_{\text{b:liv}} \leq 0. \quad (4.48)$$

Thus, m is a Lyapunov function of the homogenous system and the trajectories approach the asymptotically stable equilibrium point $\mathbf{c}^e(\mathbf{u}) := -A^{-1}\mathbf{b}$ according to the argumentation in Remark 3.1.4.

Based on the isoprene profiles observed during moderate ergometer challenges of one representative single test subject our aim is now to (at least partially) determine the *subject-dependent* parameter vector

$$\mathbf{p} = (k_{\text{pr}}^{\text{mus}}, k_{\text{pr}}^{\text{liv}}, k_{\text{met}}^{\text{rpt}}, k_{\text{met}}^{\text{mus}}, k_{\text{met}}^{\text{liv}}, \tilde{V}_{\text{mus}}, \tau_{\text{mus}})$$

as well as the nominal endogenous steady state levels $\mathbf{c}_0 = \mathbf{c}(t_0)$ by solving the OLS problem

$$\operatorname{argmin}_{\mathbf{c}_0, \mathbf{p}} \sum_{i=0}^n (y_i - C_A(t_i))^2. \quad (4.49)$$

Here $y_i = C_{\text{meas},i}$ is the measured end-tidal isoprene concentration at time instant t_i ($t_0 = 0$). The optimization problem is subject to the constraints

$$\begin{cases} \mathbf{g}(\mathbf{u}_0, \mathbf{p}, \mathbf{c}_0) = \mathbf{0} & \text{(steady state)} \\ \mathbf{p}, \mathbf{c}_0 \geq \mathbf{0} & \text{(positivity)} \\ \underline{\mathbf{c}}_6^e(\mathbf{u}_0, \mathbf{p}) = 25 \text{ nmol/l} & \text{(exposure steady state)}. \end{cases} \quad (4.50)$$

The vector function \mathbf{g} is the right-hand side of the ODE system (4.36)-(4.38) and the last constraint complies the inhalation studies provided by Filser et al. [30]. This has been introduced to account for additional information regarding the biotransformation of isoprene. The solution point will be denoted by $(\hat{\mathbf{p}}, \hat{\mathbf{c}}_0)$.

Under normal conditions (apart from inhalation studies) the atmosphere is assumed to be free of isoprene since ambient air isoprene concentrations are generally less than 10 ppb [81] and thus are considered as negligible. For simulations purposes the measured physiological functions \dot{V}_A and \dot{Q}_c were converted to input function handles \mathbf{u} by applying a local smoothing procedure to the associated data and interpolating the resulting profiles with sum of sine functions. Tissue volumes and partition coefficients are as in Table B.1. Parameters corresponding to the fractional blood flows are given below.

Parameter	Symbol	Nominal value (units)
<i>Fractional blood flows</i>		
Fat	q_{fat}	0.03
RPT	$q_{\text{rpt}}^{\text{rest}}, q_{\text{rpt}}^{\text{min}}$	0.55, 0.22
Muscle	$q_{\text{mus}}^{\text{rest}}, q_{\text{mus}}^{\text{max}}$	0.1, 0.7
Constant	τ_{mus}	1.22

Table 4.3 – Reference values for model parameters. Compare also Table B.1.

The above minimization problem has been solved by using the *Matlab* routine *fmincon* (see Section 3.2.4). Fitted parameter values and initial conditions are given in Table 4.4 and Figure 4.14 shows the simulation result.

Local identifiability of the estimated parameters in Table 4.4 was investigated by checking the non-singularity of the information matrix $Q := S^T S$ according to the sensitivity identifiability as described in Section 3.2.5. Thereby, the sensitivity the i th row of the sensitivity function matrix S is given by

$$S_{i,-} := \left(\frac{\partial y(t_{i-1}, \hat{\mathbf{p}}, \hat{\mathbf{c}}_0)}{\partial \mathbf{p}} \frac{\partial y(t_{i-1}, \hat{\mathbf{p}}, \hat{\mathbf{c}}_0)}{\partial \mathbf{c}_0} \right). \quad (4.51)$$

Normalized sensitivities are obtained by multiplying each term of the sensitivity function matrix S by the ratio of the parameter over the observation y as discussed in Section 3.2.5. To take into account the noise in the measurements and the numerical accuracy, we adopted the standard numerical rank criterion

$$\text{rank } Q = \max\{k; \sigma_k > \varepsilon \|Q\|_{\infty}\}, \quad (4.52)$$

where $\sigma_1 \geq \sigma_2 \geq \dots \geq 0$ are the singular values of Q and $\varepsilon = 10^{-8}$ denotes the maximum relative error of the calculated sensitivities [36]. We find that the information matrix Q has full rank suggesting that all estimated parameters are practically identifiable.

However, some degree of ill-conditioning is present as can be concluded from calculating the approximate posterior correlation matrix R defined by

$$R_{i,j} := Q_{i,j}^{-1} \left(Q_{i,i}^{-1} Q_{j,j}^{-1} \right)^{1/2} \in [-1, 1]. \quad (4.53)$$

The entry $R_{i,j}$ quantifies the degree of interplay between the i th and j th elements of the parameter vector $(\hat{\mathbf{p}}, \hat{\mathbf{c}}_0)$. A value of $R_{i,j}$ near +1 or -1 indicates that it may be difficult to estimate both parameters separately, as changes in the model output caused by perturbing one of these parameters can nearly be compensated by an appropriate perturbation of the other [46, 92].

High correlations are achieved between the elements of the parameter vector $(k_{\text{met}}^{\text{mus}}, k_{\text{pr}}^{\text{mus}}, C_{\text{mus}}(0), \tilde{V}_{\text{mus}})$ and for the pair $(k_{\text{met}}^{\text{rpt}}, C_{\text{rpt}}(0))$ in a range

of absolute values between 0.9541 and 0.9944. This indicates a poor estimability of the above-mentioned parameter pairs if only the breath isoprene dynamics in Figure 4.14 are taken into account. However, the constraints in (4.50) provide additional information on these parameters that will prove sufficient for guaranteeing the extraction of reliable estimates.

Parameter	Symbol	Nominal value (units)	CV
Metabolism rate RPT	$k_{\text{met}}^{\text{rpt}}$	1.22 (1/min)	2.86
Production muscle	$k_{\text{pr}}^{\text{mus}}$	97.31 (nmol/min)	0.31
Metabolism rate muscle	$k_{\text{met}}^{\text{mus}}$	0.9 (1/min)	0.66
Production liver	$k_{\text{pr}}^{\text{liv}}$	8.5 (nmol/min)	3.14
Metabolism rate liver	$k_{\text{met}}^{\text{liv}}$	2.06 (1/min)	3.92
Initial concentration alveoli	$C_A(0)$	5.5 (nmol/l)	0.03
Initial concentration rpt	$C_{\text{rpt}}(0)$	7.08 (nmol/l)	0.86
Initial concentration fat	$C_{\text{fat}}(0)$	412.5 (nmol/l)	17.42
Initial concentration muscle	$C_{\text{mus}}(0)$	136.46 (nmol/l)	0.11
Initial concentration liver	$C_{\text{fat}}(0)$	10.57 (nmol/l)	0.11
Volume muscle	\tilde{V}_{mus}	11.34 (l)	0.09
Constant muscle comp.	τ_{mus}	1.95	0.04

Table 4.4 – Decisive model parameters resulting from the fit in Fig. 4.14. The corresponding coefficients of variation (CV, in %) were obtained by the use of traditional sensitivities according to the standard error approach.

To determine the parameter and initial concentrations to which the model solution is most sensitive, we use the information obtained from the semi-relative sensitivities over the observation interval $[t_0, t_n]$ and calculate the L_2 -norm in time to get an overall measure thereof, viz.,

$$\zeta(\mathbf{p}_j) := \int_{t_0}^{t_n} \left(\frac{\partial y(t, \hat{\mathbf{p}}, \hat{\mathbf{c}}_0)}{\partial \mathbf{p}_j} \frac{\partial \hat{\mathbf{p}}_j}{\max_s |y(s)|} \right)^2 dt, \quad (4.54)$$

and similarly for the components of \mathbf{c}_0 . From the graphical comparison of these sensitivity indices we can conclude that the output is mostly influenced by $k_{\text{pr}}^{\text{mus}}$, $C_{\text{mus}}(0)$, \tilde{V}_{mus} , and τ_{mus} .

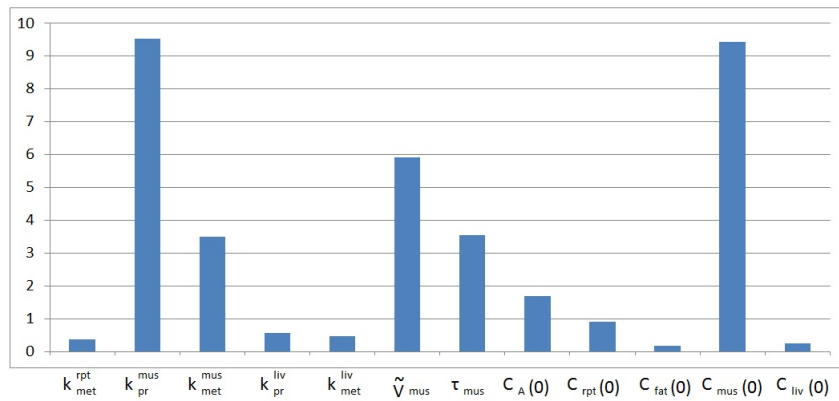


Figure 4.13 – Squared L_2 -norm of the semi-relative sensitivities (cf. Eq. (4.54)) with respect to the fitted parameters in Table 4.4.

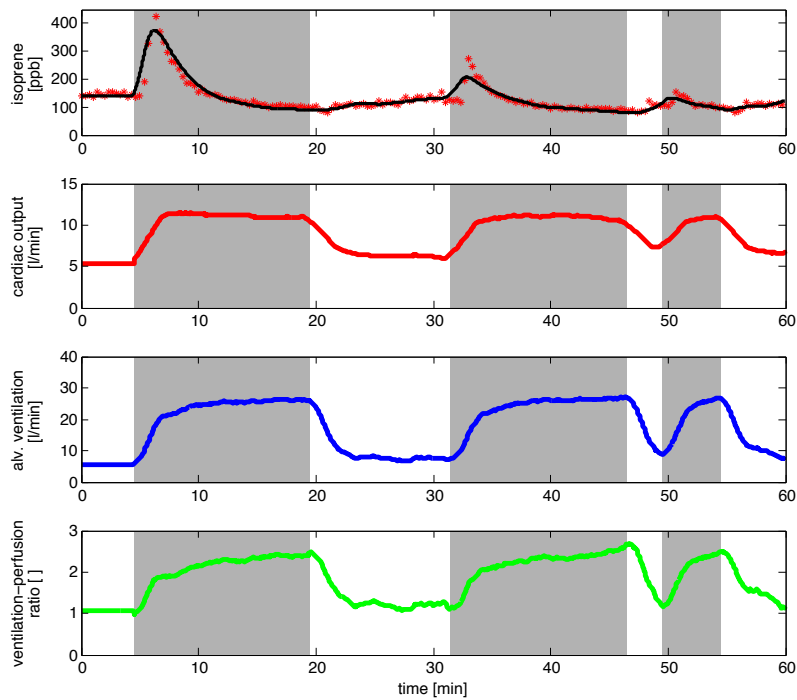


Figure 4.14 – Two-legged ergometer exercise at 75 W with intermediate pauses of varying lengths. First row shows observed (in red) versus simulated (in black) isoprene profiles.

Protocol: 5 min resting - 15 min exercise (75 W) - 12 min resting - 15 min exercise (75 W) - 3 min resting - 5 min exercise (75 W) - 5 min resting.

The interpretation of the model output with respect to exercise is the same as in three compartment model, but the presented five compartment model has verified the assumption of a muscle compartment to be the main source of exhaled isoprene. The leg contraction experiment presented in Figure 4.7 also confirms that a release mechanism resulting from an increased venous return from the contracting muscles plays an important role in the observed peak in breath isoprene concentration.

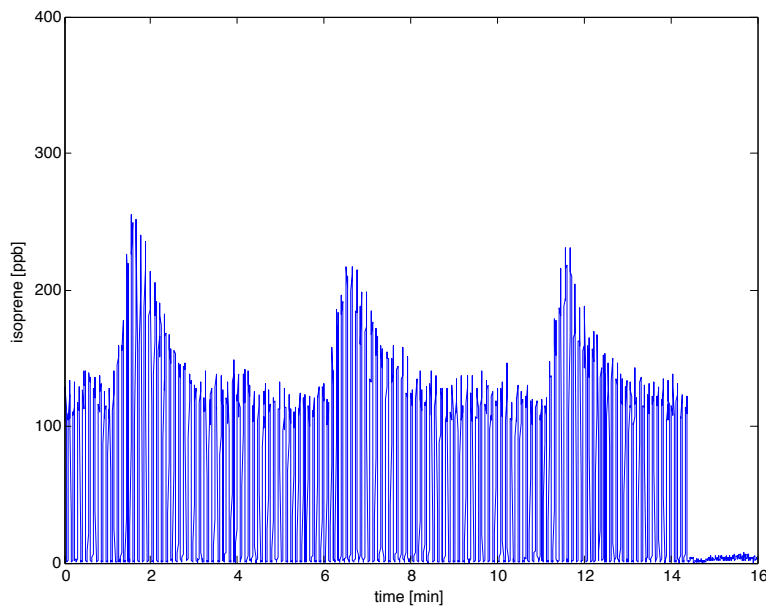


Figure 4.15 – Leg contraction at minutes 1, 6, and 11.

The estimated parameters in both models are of comparable order. Moreover, arterial and mixed venous concentrations at the start of the experiment are in line with data available from the literature.

The estimated arterial concentration $C_a(0) = 4.12$ nmol/l and mixed venous concentration $C_{\bar{v}}(0) = 10$ nmol/l are in direct accordance with available data from the literature [74]. Total endogenous production is approximately 111.96 nmol/min, which is comparable to previous predictions ranging from 2.5 to 5.7 nmol/min/kg bodyweight [30, 38]. Moreover, the estimated value for \tilde{V}_{mus} lies in the range (7.5 - 12 l) of experimentally measured thigh muscle volumes in [108].

Recall the effect of the one-legged exercise from Figure 4.9 where switching the working limb caused an immediate recovery of the initial peak size. Figure 4.16 shows simulation results of the one-legged exercise by the means of a six compartment model, adapted by dividing the muscle compartment into two parts representing each leg. Blood flows through the limbs are defined such that the resting limb gets half of the steady state blood flow

whereas the working limb gets the rest. The parameter values are listed in Table 4.5.

The one-legged exercise was performed by the same test subject at a different time with a steady state breath concentration of $C_A = 5.34$ nmol/l. Consequently, other compartmental initial concentrations were also changed as they can be calculated from the model equations (4.36)-(4.38) for steady state conditions. If the metabolic parameters $k_{\text{met}}^{\text{rpt}}$, $k_{\text{pr}}^{\text{liv}}$, and $k_{\text{met}}^{\text{liv}}$ are kept constant, the observed isoprene profile is approximated by the simulated profile, only by modified parameters of the working muscle compartment. (The parameter values are listed in Table 4.5).

First, the increase in fractional blood flow from rest to work is faster compared to the two-legged exercise. A greater relative perfusion of the single leg has been suggested by Davies and Sargeant [23] to explain why one-leg peak oxygen uptake is greater than 50 % of the two-leg value during unilateral compared to bilateral cycling. Additionally, a physiological phenomenon known as *bilateral deficit* (BD) may be responsible for this effect. Bilateral deficit states that during a movement that requires simultaneous activation of both limbs total force exerted by two limbs is less than the sum of the force produced by the left and right limbs acting alone. Thus, an increased activation of the musculature is conceivable when switching to one-legged cycling.

In general, the evidence of BD is suggested only during isokinetic bilateral activations of homogenous muscle groups. In isokinetic contractions, the muscle contracts and shortens at constant speed. A specialized apparatus that provides variable resistance is needed to keep the speed constant irrespective of how much effort is exerted. In our laboratory exercise tests are carried out on a medical ergometer operating at constant levels of power, independent of pedal speed. Thus the influence of the aforementioned mechanism of BD is questionable in this case. However, it has been shown by Dunstheimer et al. [25] by unilateral versus bilateral cycling experiments that BD also exists for more complex, alternating movements, e.g., short-term and high intensity cycling. Although the underlying exact mechanisms are not understood in sufficient deep, yet, compared to with unilateral cycling, a decreased activation of the muscles involved during bilateral cycling of the legs may explain the observed BD [25]. More specifically, it has been suggested that during cycling, the BD might be attributed to a larger total muscle mass involved in the unilateral cycling tasks compared to the bilateral test. If the foot of the working leg is fixed during unilateral cycling, the involved leg has to actively pull up and push down. In contrast, during the bilateral cycling the test subject has only to push down on the pedal, thereby not using the entire leg musculature. This argumentation is in accordance with the estimated enhanced production rate $k_{\text{pr}}^{\text{mus}}$ and the muscle volume \tilde{V}_{mus} .

Parameter	Symbol	Nominal value (units)
Initial concentration alveoli	$C_A(0)$	5.34 (nmol/l)
Initial concentration rpt	$C_{\text{rpt}}(0)$	7.13 (nmol/l)
Initial concentration fat	$C_{\text{fat}}(0)$	401 (nmol/l)
Initial concentration muscle (each leg)	$C_{\text{mus}}(0)$	148.44 (nmol/l)
Initial concentration liver	$C_{\text{fat}}(0)$	10.43 (nmol/l)
Constant	τ_{rpt}	2.7
Constant	τ_{mus}	3.6
Production muscle	$k_{\text{pr}}^{\text{mus}}$	195 (nmol/min)
Metabolism rate muscle	$k_{\text{met}}^{\text{mus}}$	1.98 (l/min)
Volume muscle	\tilde{V}_{mus}	13.6 (l)

Table 4.5 – Decisive model parameters resulting from the fit in Fig. 4.16.

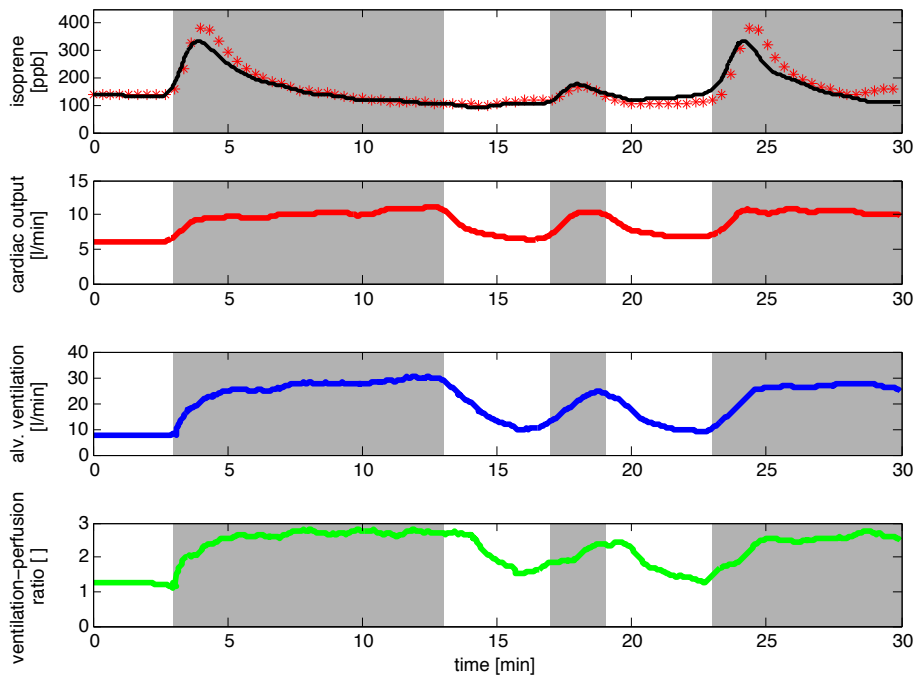


Figure 4.16 – Ergometer exercise at 50 W with intermediate pauses of varying lengths.

Protocol: 3 min resting - 10 min exercise left leg (50 W) - 4 min resting - 2 min exercise left leg (50 W) - 4 min resting - 7 min exercise right leg (50 W)

4.8 Discussion and Conclusions

The interplay between mathematical modeling and theory-driven experimentation has finally led us to a mathematical description of isoprene kinetics which respects all current data and which furthermore allows for new predictions that can be tested by adequate experiments.

The origin of endogenous isoprene in humans is mainly attributed to the mevalonate pathway of cholesterol biosynthesis [24, 50, 105]. The synthesis of mevalonate is inhibited by statins, which are used in the treatment and prevention of cardiovascular diseases by lowering serum cholesterol levels. The primary mechanism of action exerted by statin therapy is to competitively inhibit the activity of HMG-CoA reductase, which is the rate limiting enzyme in cholesterol synthesis [29]. Correspondingly, it has been reported that the administration of specific statins (such as lovastatin and atorvastatin) causes a proportional decline in breath isoprene concentrations and serum cholesterol levels [50, 105]. On the other hand, several studies have pointed out myotoxic effects to be a major adverse reaction of statin therapy, leading to the inhibition of skeletal muscle activity [27, 29, 116].

The extent to which the mevalonate pathway accounts for isoprene formation under physiological conditions is still a matter of debate [73, 107]. In particular, the above-mentioned pathway rests on the acid-catalyzed solvolysis of dimethylallyl-diphosphate in the liver which may be insignificant at physiological pH [100, 101]. In many plants, the formation of isoprene is enzyme-catalyzed, and isoprene seems to play a role in the heat protection of leaves [102]. Moreover, some indications of an isoprene synthase in bovine liver have been put forward in [100]. Hence, it cannot be excluded that an isoprene synthase is present in human tissues. However that may be, we suggest an additional peripheral origin of isoprene through the same basic biochemical pathway. Specifically, by adopting the assumption of a muscular source of isoprene, statin-induced lowering of isoprene concentration in the muscles may turn out as the main cause for the reduction of endogenous isoprene formation and the subsequent decrease of breath isoprene concentrations. An analogous argument might also give further insights into the surprising lack of statistically significant correlations between breath isoprene levels and blood cholesterol levels [59, 100].

Similarly, the proposed mechanisms may explain the age dependency of breath isoprene levels by correlating the latter to changes in the individual muscle mass. The characteristic median breath isoprene concentration in adults under resting conditions is about 100 ppb [59], whereas young children have demonstrably lower isoprene levels [65, 103, 107]. Breath isoprene concentrations have been reported to be non-detectable in the breath of neonates, while steadily increasing in teenagers and reaching a plateau level in the middle age [90, 103]. Moreover, isoprene levels in older people appear to decrease [59, 90].

Former investigations with respect to the age dependency of isoprene output and its reduction under statin therapy nicely fit into this rationale. Moreover, the present work suggests that the major part of physiologically formed isoprene stems from the skeletal musculature rather than hepatic production.

Appendix A

Physical Preliminaries

A.1 The Ideal Gas Law

The intuitive concepts concerning the behavior of gases with relation to changing conditions are the basis for the ideal gas law. A gas consists of free molecules in a state of random motion and its molecules fill any container in which they are enclosed. The ideal gas law expresses the relationship between pressure (P), volume (V), absolute temperature (T), the number of moles of gas (n) and the gas constant (R)

$$PV = nRT. \tag{A.1}$$

In respiratory physiology, P is usually measured in millimeters of mercury (mmHg), V in liters (l), and T in Kelvin (K). One mole is per definition the amount of substance which consists of $6.023 \cdot 10^{23}$ gas particles. The constant $R = 62.36 \text{ l} \cdot \text{mmHg} \cdot \text{mole}^{-1} \cdot \text{K}^{-1}$ is called the general gas constant ¹.

Three empirical gas laws can be derived from the ideal gas law. It says that for a constant absolute temperature and number of gas molecules, the pressure and volume are reciprocally related one to the other (Boyle-Mariottes Law). Also, at a constant pressure and number of gas molecules, the volume occupied by a gas is directly proportional to the absolute temperature (Gay-Lussacs law). Finally, under constant external conditions with regard to pressure and temperature, equal volumina of different ideal gases contain equal amounts of molecules (Avogadros law).

Gases obeying the ideal gas law are called *ideal gases*, which include beside oxygen and carbon dioxide all VOCs. The concept of an ideal gas is a model which only applies when the total pressure is low. This means specifically that the individual gas molecules can be treated as isolated points in space, having negligible molecular volume and exerting no intermolecular forces other than those resulting from perfectly elastic collisions between

¹Alternatively one can write $PV = NkT$, where N is the number of particles and k is Boltzmann's constant.

molecules. This is a reasonable assumption at the low pressures normally encountered in respiratory physiology because, under these conditions, the average intermolecular distance is about ten times the average molecular size. The ideal gas law, therefore, reasonably describes the behavior of respiratory gases [42].

If the equation (A.1) holds for any ideal gas, then it is also valid for mixtures of ideal gases. The partial pressure of a single gas specie i in a gas mixture is defined by

$$P_i = \frac{n_i RT}{V}. \quad (\text{A.2})$$

Specifically, for a mixture of N different gas species we may write

$$PV = (n_1 + \dots + n_N)RT. \quad (\text{A.3})$$

Relations (A.2) and (A.3) imply *Dalton's Law*

$$P = P_1 + P_2 + \dots + P_N, \quad (\text{A.4})$$

which expresses the fact that the total pressure P of a gas mixture equals to the sum of the partial pressures of its individual components.

Furthermore, it is useful to relate the partial pressure of a gas to its concentration (i.e., the number of molecules per unit volume). The required formula is easily obtained by substituting $C_{i,gas} = n_i/V$ into (A.2)

$$P_i = C_{i,gas}RT, \quad (\text{A.5})$$

where $C_{i,gas}$ is the concentration of the species i in the gas phase.

A.2 Diffusion and Solubility of Gases

The concept of partial pressures can be extended to gases in solution which is an important item for understanding of blood-gas transport mechanisms. Consider the situation where a liquid and a gas are in contact across the surface of the liquid. Molecules of the gas can enter the liquid and wander for a time among its molecules. They are then said to be dissolved in the liquid, forming a solution. Molecules in solution can also leave the liquid at its surface and become part of the gas again. A prototypic example for this situation in the present context is the alveolar-capillary membrane separating the respiratory microvasculature from the alveoli.

The diffusive flux J of gases through a barrier separating two regions characterized by distinct partial pressures P_j , $j = 1, 2$ is governed by *Fick's first law* of diffusion

$$J = \frac{\beta D A}{\ell} (P_1 - P_2). \quad (\text{A.6})$$

While moving between the alveolar space and capillary blood, each gas is subject to the same anatomically related limitations (cross sectional area \mathcal{A} and thickness of the membrane ℓ). Each gas, however, has a different solubility β and diffusivity \mathcal{D} in the membrane barrier.

Generally, all anatomically and gas related parameters in Equation (A.6) are lumped together under the term *diffusing capacity of the lung* (D_L)². At the alveolar-capillary interface Equation (A.6) hence simplifies to

$$J = D_L(P_A - P_b), \quad (\text{A.8})$$

where P_A and P_b are the partial pressures in alveolar air and capillary blood, respectively.

After a sufficient long time under constant conditions, the rate at which gas molecules enter the solution will become equal to the rate at which they leave. When this is the case for all of the gases present, the system is said to be at equilibrium, i.e., $J = 0$. If the gas molecules move independently of each other and do not form chemical combinations with some component of the solvent, the concentration of the gas in solution is proportional to its partial pressure in the gas. Solutions that obey this law are called *simple solutions*. For such solutions, we have

$$C_{i,liquid} = \alpha_i P_i, \quad (\text{Henry's Law}) \quad (\text{A.9})$$

where $C_{i,liquid}$ is the concentration of the species i in the solution and α_i is the solubility coefficient (also partition coefficient or Henry's Law constant) of that species³.

At diffusion equilibrium, using (A.5) and (A.9) the partition coefficient can be expressed as the dimensionless ratio between the concentration of the species in the solution and its concentration in the gas phase:

$$\lambda_{liquid:gas} = \frac{C_{i,liquid}}{C_{i,gas}} = \alpha_i RT. \quad (\text{A.10})$$

The partition coefficient is a measure of the solubility of a gas in a solvent at equilibrium. In our example $\lambda_{b:air}$ describes the solubility of the gas specie in blood.

²*Graham's law* states that the diffusivity of a gas is inversely proportional to the square root of its molecular weight MW. Therefore, from (A.6) the relative diffusing capacities of the lung for two distinct gases can be estimated via

$$\frac{D_{L_{gas,1}}}{D_{L_{gas,2}}} = \frac{\beta_{gas,1}}{\beta_{gas,2}} \times \frac{\sqrt{MW_{gas,2}}}{\sqrt{MW_{gas,1}}}. \quad (\text{A.7})$$

³The solubility coefficient is dependent on both solute and solvent, and is inversely related to temperature.

A.3 Unit Conversion Factors for Concentrations

For the following conversion factors, consider that temperature (T) is given in Kelvin (K). Partial pressure is given either in atmospheric pressure (atm) with gas constant $R = 0.08205 \text{ l} \cdot \text{atm} \cdot \text{mol}^{-1} \cdot \text{K}^{-1}$, or in millimeter of mercury (mmHg) with gas constant $R = 62.32 \text{ l} \cdot \text{mmHg} \cdot \text{mol}^{-1} \cdot \text{K}^{-1}$.

Conversion between Mole Basis (ppb) and Molar Concentration

Molar concentration is the concentration of a substance expressed in terms of molarity (denoted by M or mol/l). Using the ideal gas law (A.1), the amount of moles of an ideal gas in one liter mixture can be expressed by

$$\frac{n}{V} = \frac{P}{RT} \quad (\text{mol/l}). \quad (\text{A.11})$$

The concentration of 1 ppb (parts per billion; 1 mole part per one billion total moles) equals $1 \cdot 10^{-9}$ in decimal form. Thus the amount of moles of 1 ppb ideal gas in one liter mixture is

$$\frac{P}{RT} 1 \cdot 10^{-9} \quad (\text{mol/l}). \quad (\text{A.12})$$

Thus, the general formula for the conversion factor from mole basis to molar concentration is

$$C_{\text{mol/l}} = C_{\text{ppb}} \cdot 10^{-9} \frac{P}{RT}. \quad (\text{A.13})$$

Conversion between Molar Concentration and Mass Concentration

Mass concentration is the mass of a constituent substance divided by the volume of the mixture, a frequently used unit for mass concentration is grams per liter (g/l). In order to convert between molar concentration and mass concentration we need to know the molecular weight (MW) of the substance given in g/mol. The conversion formula between molar concentration and mass concentration is given by

$$C_{\text{g/l}} = C_{\text{mol/l}} \cdot MW_{\text{g/mol}}. \quad (\text{A.14})$$

Appendix B

Parameter Values

B.1 Physiological Parameters

Parameter	Symbol	Value
Compartment Volume^a [l]		
Arterial blood	V_a	2.85
Alveolar volume	V_A	4.1
Richly perfused tissue (RPT)	V_{rpt}	0.83
Fat tissue	V_{fat}	12.78
Resting muscle and skin	V_{rmus}	18.21
Working muscle	V_{mus}	18.21
Liver	V_{liv}	1.51
Compartmental blood volume^b (% of tissue volume)		
Richly perfused tissue (RPT)	$V_{rpt,b}$	10.8
Fat tissue	$V_{fat,b}$	3.80
Resting muscle and skin	$V_{rmus,b}$	7.98
Working muscle	$V_{mus,b}$	2.61
Liver	$V_{liv,b}$	37.2
Partition coefficient^c		
blood:air	$\lambda_{b:air}$	0.75
blood:rpt	$\lambda_{b:rpt}$	0.41
blood:fat	$\lambda_{b:fat}$	0.01
blood:muscle	$\lambda_{b:mus}$	0.51
blood:liver	$\lambda_{b:liv}$	0.39
Effective compartment volume [l]		
Alveolar	\tilde{V}_A	6.24
RPT (incl. resting muscle and skin)	\tilde{V}_{rpt}	19.81
Fat tissue	\tilde{V}_{fat}	12.78
Working muscle	\tilde{V}_{mus}	18.46
Liver	\tilde{V}_{liv}	1.73

Table B.1 – Physiological parameters and reference values: ^a Mörk et al [77] (according to the scaling for 70 kg body weight and 180 cm height), ^b Ottesen et al [83] (according to table 8.2), ^c Filser [30].

Parameter	Workload			
	0 W	50 W	100 W	150 W
Tissue blood flow (% of cardiac output)				
RPT (incl. resting muscle and skin)	0.545	0.34	0.25	0.22
Fat tissue	0.03	0.05	0.05	0.03
Working muscle	0.105	0.45	0.61	0.70
Liver	0.32	0.16	0.09	0.05

Table B.2 – Workload dependent fractional tissue blood flows according to Mörk et al [77].

B.2 Model Parameters

Parameter	Symbol	Nominal value (units)
<i>Three Compartment</i>		
<i>Parallel Lung Model</i>		
steady state and exercise blood flows (% of cardiac output)	$q_i = q_i/\dot{Q}_c$	
compartment 1		0 (steady state), 0.3 (exercise)
compartment 2		0.2 (steady state), 0.3 (exercise)
compartment 3		0.8 (steady state), 0.4 (exercise)
steady state and exercise air flows (% of alveolar ventilation)	$v_i = v_i/\dot{V}_A$	
compartment 1		0.8 (steady state), 0.4 (exercise)
compartment 2		0.2 (steady state), 0.3 (exercise)
compartment 3		0 (steady state), 0.3 (exercise)
compartment volumina	$\tilde{V}_{A,i}$	
compartment 1		0.5 [l]
compartment 2		5 [l]
compartment 3		0.5 [l]
body compartment	\tilde{V}_{body}	12 [l]
production rate	k_{pr}	150 [nmol/min]
elimination rate	k_{met}	2.4 [l/min]
body:blood partition coeff.	$\lambda_{\text{b:body}}$	0.55

Table B.3 – Model parameters and nominal values

Parameter	Symbol	Nominal value (units)
<i>Stratified Lung Model</i>		
production rate	k_{pr}	133.2 [nmol/min]
metabolism rate	k_{met}	1.86 [l/min]
proximal alveolar volume	$V_{\text{A},1}$	3 [l]
distal alveolar volume	$V_{\text{A},2}$	3 [l]
volume body	\tilde{V}_{body}	9 [l]
body:blood partition coeff.	$\lambda_{\text{body:b}}$	0.44

Table B.4 – Model parameters and nominal values

Appendix C

Symbols and Abbreviations

Primary symbols denoting physical quantities

C	concentration	nmol/l
P	partial pressure	mmHg
V	compartment volume	l
\tilde{V}	effective compartment volume	l
\dot{V}_A	alveolar ventilation	l/min
\dot{Q}_c	blood flow	l/min
q	fractional blood flow	dimensionless
r	ventilation-perfusion ratio	
$\lambda_{b:air}$	partition coefficient blood:air	dimensionless
$\lambda_{b:x}$	partition coefficient blood: compartment x	dimensionless
k_{pr}	endogenous production rate	nmol/min
k_{met}	metabolic elimination rate	l/min
K_m	Michaelis-Menten constant	$\mu\text{mol/l}$
V_{max}^x	maximum metabolic rate in compartment x	$\mu\text{mol/min}$

Secondary symbols denoting location of quantity

<i>in gas phase</i>	<i>in blood</i>	<i>compartments</i>
I inspired gas	a arterial blood	rpt richly perfused tissue
A alveolar gas	c capillary	fat fat compartment
E expired gas	v venous blood	mus muscle compartment
\bar{E} mixed expired gas	\bar{v} mixed venous blood	liv liver compartment

Bibliography

- [1] A Amann, J King, A Kupferthaler, K Unterkofler, H Koc, S Teschl, and H Hinterhuber. Exhaled breath analysis-quantifying the storage of lipophilic compounds in the human body. *Proceedings of Ecopole*, 3:9–13, 2009.
- [2] A Amann, W Miekisch, J Pleil, T Risby, and J Schubert. Methodological issues of sample collection and analysis of exhaled breath. In *European Respiratory Society Monograph 49*, pages 96–114. European Respiratory Society, Lausanne, 2010.
- [3] A Amann, G Poupart, S Telser, M Ledochowski, A Schmid, and S Mechtcheriakov. Applications of breath gas analysis in medicine. *Int J Mass Spectrom*, 239:227–33, 2004.
- [4] A Amann and D Smith, editors. *Breath gas analysis for clinical diagnosis and therapeutic monitoring*. World Scientific, Singapore, 2005.
- [5] A Amann, P Spaněl, and D Smith. Breath analysis: the approach towards clinical applications. *Mini Rev Med Chem*, 7:115–29, 2007.
- [6] A Amann, S Telser, L Hofer, A Schmid, and H Hinterhuber. Exhaled breath gas as a biochemical probe during sleep. In *Breath Analysis for Clinical Diagnosis and Therapeutic Monitoring*, pages 305–16. World Scientific, Singapore, 2005.
- [7] L C A Amorim and Z de L Cardeal. Breath air analysis and its use as a biomarker in biological monitoring of occupational and environmental exposure to chemical agents. *J Chromatogr B*, 853:1–9, 2007.
- [8] M E Andersen. Physiological modelling of organic compounds. *Ann Occup Hyg*, 35:309–21, 1991.
- [9] J C Anderson, A L Babb, and M P Hlastala. Modeling soluble gas exchange in the airways and alveoli. *Ann Biomed Eng*, 31:1402–22, 2003.

- [10] J C Anderson, W J E Lamm, and M P Hlastala. Measuring airway exchange of endogenous acetone using a single-exhalation breathing maneuver. *J Appl Physiol*, 100:880–9, 2006.
- [11] M Anguelova. *Observability and identifiability of nonlinear systems with applications in biology*. PhD thesis, Chalmers University of Technology and Göteborg University, 2007.
- [12] A Bajtarevic, C Ager, M Pienz, M Klieber, K Schwarz, M Ligor, T Ligor, W Filipiak, H Denz, M Fiegl, W Hilbe, W Weiss, P Lukas, H Jamnig, M Hackl, A Haidenberger, B Buszewski, W Miekisch, J Schubert, and A Amann. Noninvasive detection of lung cancer by analysis of exhaled breath. *BMC Cancer*, 9:348, 2009.
- [13] H T Banks, S Dediu, and S L Ernstberger. Sensitivity functions and their uses in inverse problems. *J Inv Ill-Posed Probl*, 15:1–26, 2007.
- [14] P J Barnes. Nitric oxide and airway disease. *Ann Med*, 27:389–93, 1995.
- [15] G Bastin and V Guffens. Congestion control in compartmental network systems. *Syst Control Lett*, 55:689–96, 2006.
- [16] J J Batzel, F Kappel, D Schneditz, and H T Tran. *Cardiovascular and Respiratory Systems: Modeling, Analysis, and Control*. SIAM, Philadelphia, 2007.
- [17] A Cailleux and P Allain. Isoprene and sleep. *Life Sci*, 44(24):1877–80, 1989.
- [18] W Cao and Y Duan. Current status of methods and techniques for breath analysis. *Critical Reviews in Analytical Chemistry*, 37:3–13, 2007.
- [19] A Cintrón-Arias, H T Banks, A Capaldi, and A L Lloyd. A sensitivity matrix based methodology for inverse problem formulation. *J Inv Ill-Posed Probl*, 17:545–64, 2009.
- [20] H J Clewell, 3rd, P R Gentry, J M Gearhart, T R Covington, M I Banton, and M E Andersen. Development of a physiologically based pharmacokinetic model of isopropanol and its metabolite acetone. *Toxicol Sci*, 63(2):160–72, Oct 2001.
- [21] C Cobelli and J J DiStefano III. Parameter and structural identifiability concepts and ambiguities: a critical review and analysis. *Am J Physiol*, 239:R7–24, 1980.

- [22] K A Cope, M T Watson, W M Foster, S S Sehnert, and T H Risby. Effects of ventilation on the collection of exhaled breath in humans. *J Appl Physiol*, 96:1371–9, 2004.
- [23] C T M Davies and A J Sargeant. Physiological responses to one- and two-legged exercise breathing air and 45 *J Appl Physiol*, 36:142–8, 1974.
- [24] E S Deneris, R A Stein, and J F Mead. Acid catalyzed formation of isoprene from a mevalonate-derived product using a rat liver cytosolic fraction. *J Biol Chem*, 260:1382–5, 1985.
- [25] D Dunstheimer, H Hebestreit, B Staschen, H M Strassburg, and R Jeschke. Bilateral deficit during short-term, high-intensity cycle ergometry in girls and boys. *Eur J Appl Physiol*, 84:557–61, 2001.
- [26] R A Dweik and A Amann. Exhaled breath analysis: the new frontier in medical testing. *J Breath Res*, 2:030301, 2008.
- [27] M Evans and A Rees. The myotoxicity of statins. *Curr Opin Lipidol*, 13:415–20, 2002.
- [28] L E Farhi. Elimination of inert gas by the lung. *Respir Physiol*, 3:1–11, 1967.
- [29] J Farmer. Statins and myotoxicity. *Curr Atheroscler Rep*, 5:96–100, 2003.
- [30] J G Filser, G A Csanády, B Denk, M Hartmann, A Kauffmann, W Kessler, P E Kreuzer, C Pütz, J H Shen, and P Stei. Toxicokinetics of isoprene in rodents and humans. *Toxicology*, 113:278–87, 1996.
- [31] R E Forster. Exchange of gases between alveolar air and pulmonary capillary blood: pulmonary diffusing capacity. *Physiol Rev*, 37(391-452), 1957.
- [32] G Freund and R L Weinsier. Standardized ketosis in man following medium chain triglyceride ingestion. *Metabolism*, 15:980–91, 1966.
- [33] P R Galassetti, B Novak, D Nemet, C Rose-Gottron, D M Cooper, S Meinardi, Robert Newcomb, F Zaldivar, and D R Blake. Breath ethanol and acetone as indicators of serum glucose levels: an initial report. *Diabetes Technol Ther*, 7:115–23, 2005.
- [34] D Gelmont, R A Stein, and J F Mead. Isoprene-the main hydrocarbon in human breath. *Biochem Biophys Res Commun*, 99(4):1456–60, 1981.

- [35] L E Gerlowski and R K Jain. Physiologically based pharmacokinetic modeling: principles and applications. *Journal of Pharmaceutical Sciences*, 72(10):1103–1127, Oktober 1983.
- [36] G H Golub and C F Van Loan. *Matrix computations*. Johns Hopkins University Press, Baltimore, 3rd edition, 1996.
- [37] M H Haddad, V S Chellaboina, and Q Hui. *Nonnegative and Compartmental Dynamical Systems*. Princeton University Press, New Jersey, 2010.
- [38] M Hartmann and W Kessler. Pharmacokinetics and endogenous production of isoprene in humans. *Naunyn-Schmiedberg's Arch Pharmacol*, 341 Suppl.:R13, 1990.
- [39] J Herbig, M Müller, S Schallhart, T Titzmann, M Graus, and Hansel A. On-line breath analysis with PTR-TOF. *J Breath Res*, 3:027004, 2009.
- [40] R Hermann and A J Krener. Nonlinear controllability and observability. *IEEE T Automat Contr*, 22:728–40, 1977.
- [41] H Heuser. *Lehrbuch der Analysis, Teil 2*. B. G. Teubner, Stuttgart, 11 edition, 2000.
- [42] M P Hlastala and A J Berger. *Physiology of Respiration*. Oxford University Press, New York, 2nd edition, 2001.
- [43] F C Hoppensteadt and C S Peskin. *Modeling and simulation in medicine and the life sciences*. Springer, New York, 2nd edition, 2002.
- [44] F Horn, M Moc, Isabelle, N Schneider, C Grillhösl, S Berghold, and G Lindenmeier. *Biochemie des Menschen*. Georg Thieme Verlag, Stuttgart, 2005.
- [45] J M B Hughes. Pulmonary gas exchange. *Eur Respir Mon*, 31(106-26), 2005.
- [46] J A Jacquez and T Perry. Parameter estimation: local identifiability of parameters. *Endocrinol Metab*, 21:E727–36, 1990.
- [47] J A Jacquez and C P Simon. Qualitative theory of compartmental systems. *SIAM Rev*, 35:43–79, 1993.
- [48] M L Johnson and L M Faunt. Parameter estimation by least-squares methods. *Method Enzymol*, pages 1–37, 1992.
- [49] M P Kalapos. On the mammalian acetone metabolism: from chemistry to clinical implications. *Biochim Biophys Acta*, 1621:122–39, 2003.

- [50] T Karl, P Prazeller, D Mayr, A Jordan, J Rieder, R Fall, and W Lindinger. Human breath isoprene and its relation to blood cholesterol levels: new measurements and modeling. *J Appl Physiol*, 91:762–70, 2001.
- [51] H K Khalil. *Nonlinear Systems*. Prentice Hall, New Jersey, 3rd edition, 2002.
- [52] J King, H Koc, K Unterkofler, P Mochalski, A Kupferthaler, G Teschl, S Teschl, H Hinterhuber, and A Amann. Physiological modeling of isoprene dynamics in exhaled breath. *J Theor Biol*, 267:626–37, 2010.
- [53] J King, A Kupferthaler, K Unterkofler, H Koc, S Teschl, G Teschl, W Miekisch, J Schubert, H Hinterhuber, and A Amann. Isoprene and acetone concentration profiles during exercise on an ergometer. *J Breath Res*, 3:027006, 2009.
- [54] J King, P Mochalski, A Kupferthaler, K Unterkofler, H Koc, W Filipiak, S Teschl, H Hinterhuber, and A Amann. Dynamic profiles of volatile organic compounds in exhaled breath as determined by a coupled PTR-MS/GC-MS study. *Physiol Meas*, 31:1169–84, 2010.
- [55] J King, K Unterkofler, G Teschl, S Teschl, H Koc, H Hinterhuber, and A Amann. A mathematical model for breath gas analysis of volatile organic compounds with special emphasis on acetone. *J Math Biol*, <http://dx.doi.org/10.1007/s00285-010-0398-9>, 2011.
- [56] H Koc, J King, G Teschl, K Unterkofler, S Teschl, P Mochalski, H Hinterhuber, and A Amann. The role of mathematical modeling in VOC analysis using isoprene as a prototypic example. *J Breath Res*, 5(3):037102, Jun 2011.
- [57] D E Koshland Jr. The molecule of the year. *Science*, 258:1861, 1992.
- [58] M Kupari, J Lommi, M Ventilä, and U Karjalainen. Breath acetone in congestive heart failure. *Am J Cardiol*, 76:1076–8, 1995.
- [59] I Kushch, B Arendacká, S Stolc, P Mochalski, W Filipiak, K Schwarz, L Schwentner, A Schmid, A Dzien, M Lechleitner, V Witkovský, W Miekisch, J Schubert, K Unterkofler, and A Amann. Breath isoprene—aspects of normal physiology related to age, gender and cholesterol profile as determined in a proton transfer reaction mass spectrometry study. *Clin Chem Lab Med*, 46:1011–8, 2008.
- [60] I Kushch, K Schwarz, L Schwentner, B Baumann, A Dzien, A Schmid, K Unterkofler, G Gastl, P Spaněl, D Smith, and A Amann. Compounds enhanced in a mass spectrometric profile of smokers' exhaled

- breath versus non-smokers as determined in a pilot study using PTR-MS. *J Breath Res*, 2:026002, 2008.
- [61] P Leenheer, D Angeli, and E Sontag. Monotone chemical reaction networks. *J Math Chem*, 41:295–314, 2007.
- [62] M G Levitzky. *Pulmonary Physiology*. Lange Medical Books/McGraw-Hill, New York, 7th edition, 2007.
- [63] J F Lewis and R A W Veldhuizen. Analyzing surfactant metabolism in humans: an important first step. *Am J Resp Crit Care*, 170:2–3, 2004.
- [64] T Ligor, M Ligor, A Amann, C Ager, M Bachler, A Dzien, and B Buszewski. The analysis of healthy volunteers' exhaled breath by the use of solid-phase microextraction and GC-MS. *J Breath Res*, 2:046006, 2008.
- [65] W Lindinger, Hansel A, and A Jordan. Proton-transfer-reaction mass spectrometry (PTR-MS): on-line monitoring of volatile organic compounds at pptv levels. *Chem Soc Rev*, 27:347–54, 1998.
- [66] P Lirk, F Bodrogi, H Raifer, K Greiner, H Ulmer, and J Rieder. Elective haemodialysis increases exhaled isoprene. *Nephrol Dial Transplant*, 18(5):937–41, 2003.
- [67] A B Lumb. *Nunn's Applied Respiratory Physiology*. Butterworth-Heinemann, Oxford, 6th edition, 2005.
- [68] T B Martonen and A F Wilson. Theoretical basis of single breath gas absorption tests. *J Math Biol*, 14:202–20, 1982.
- [69] A Mashir and R A Dweik. Exhaled breath analysis: The new interface between medicine and engineering. *Adv Powder Technol*, 20:420–425, 2009.
- [70] The MathWorks. *Optimization Toolbox User's Guide*. The MathWorks, Natick, 2nd edition, 1990-2000.
- [71] L T McGrath, R Patrick, and B Silke. Breath isoprene in patients with heart failure. *Eur J Heart Fail*, 3(4):423–7, 2001.
- [72] S Mendis, P A Sobotka, and D E Euler. Expired hydrocarbons in patients with acute myocardial infarction. *Free Radic Res*, 23(2):117–22, 1995.
- [73] W Miekisch, J K Schubert, and Gabriele F E Noeldge-Schomburg. Diagnostic potential of breath analysis—focus on volatile organic compounds. *Clin Chim Acta*, 347:25–39, 2004.

- [74] W Miekisch, J K Schubert, D A Vagts, and K Geiger. Analysis of volatile disease markers in blood. *Clin Chem*, 47:1053–60, 2001.
- [75] T A Miettinen. Diurnal variation of cholesterol precursors squalene and methyl sterols in human plasma lipoproteins. *J Lipid Res*, 23:466–73, 1982.
- [76] D E Mohrman and L J Heller. *Cardiovascular Physiology*. Lange Medical Books/McGraw-Hill, New York, 6th edition, 2006.
- [77] A K Mörk and Johanson G. A human physiological model describing acetone kinetics in blood and breath during various levels of physical exercise. *Toxicology Letters*, 164:6–15, 2006.
- [78] K Musa-Veloso, S S Likhodii, and S C Cunnane. Breath acetone is a reliable indicator of ketosis in adults consuming ketogenic meals. *Am J Clin Nutr*, 76:65–70, 2002.
- [79] K Musa-Veloso, E Rarama, F Comeau, R Curtis, and S Cunnane. Epilepsy and the ketogenic diet: assessment of ketosis in children using breath acetone. *Pediatr Res*, 52:443–8, Sep 2002.
- [80] O Nelles. *Nonlinear system identification: from classical approaches to neural networks and fuzzy models*. Springer, Heidelberg, 2001.
- [81] U.S Department of Health and Human Services. Report on carcinogens. Technical report, National Toxicology Program, 2011.
- [82] A J Olszowka. Can VA/Q distributions in the lung be recovered from inert gas retention data? *Resp Physiol*, 25:191–8, 1975.
- [83] J T Ottesen, M S Olufsen, and J K Larsen. *Applied Mathematical Models in Human Physiology*. SIAM, Philadelphia, 2004.
- [84] L Pauling, A B Robinson, R Teranishi, and P Cary. Quantitative analysis of urine vapor and breath by gas-liquid partition chromatography. *Proc Nat Acad Sci USA*, 68:2374–6, 1971.
- [85] M Phillips, J Greenberg, and J Awad. Metabolic and environmental origins of volatile organic compounds in breath. *J Clin Pathol*, 47:1052–3, 1994.
- [86] J D Pleil. Role of exhaled breath biomarkers in environmental health science. *J Toxicol Environ Health B Crit Rev*, 11:613–29, 2008.
- [87] G A Reichard, A C Haff, C Lutches Skutches, P Paul, C P Holroyde, and O E Owen. Plasma acetone metabolism in the fasting human. *J Clin Invest*, 63:619–26, 1979.

- [88] J G Reid. Structural identifiability in linear time-invariant systems. *IEEE T AUTOMAT CONTR*, 24:2-6, 1977.
- [89] R L Riley and A Cournaud. Ideal alveolar air and the analysis of ventilation-perfusion relationships in the lungs. *J Appl Physiol*, 1(12):825-47, Jun 1949.
- [90] T H Risby. Volatile organic compounds as markers in normal and diseased states. In *Disease markers in exhaled breath: basic mechanisms and clinical applications*, volume 346 of *Series I: Life and Behavioural Sciences*, pages 113-22. IOS Press, Amsterdam, 2002.
- [91] T H Risby. Critical issue for breath analysis. *J Breath Res*, 2:030302, 2008.
- [92] M Rodriguez-Fernandez, J A Egea, and J R Banga. Novel metaheuristic for parameter estimation in nonlinear dynamic biological systems. *BMC Bioinformatics*, 7:483, 2006.
- [93] S Roman. *Advanced Linear Algebra*. Graduate Texts in Mathematics. Springer, New York, 2nd edition, 2005.
- [94] M P Saccomani, S Audoly, and L D Angió. Parameter identifiability of nonlinear systems: the role of initial conditions. *Automatica*, 39:619-32, 2003.
- [95] E M Sakai, L A Connolly, and J A Klauck. Inhalation anesthesiology and volatile liquid anesthetics: focus on isoflurane, desflurane, and sevoflurane. *Pharmacotherapy*, 25:1773-88, 2005.
- [96] R Salerno-Kennedy and K D Cashman. Potential applications of breath isoprene as a biomarker in modern medicine: a concise overview. *Wiener Klinische Wochenschrift*, 117(5-6):180-186, 2005.
- [97] P Scheid, M P Hlastala, and J Piiper. Inert gas elimination from lungs with stratified inhomogeneity: theory. *Resp Physiol Physiology*, 44:299-309, 1981.
- [98] K Schwarz, W Filipiak, and A Amann. Determining concentration patterns of volatile compounds in exhaled breath by PTR-MS. *J Breath Res*, 3:027002 (15pp), 2009.
- [99] S T Senthilmohan, D B Milligan, M J McEwan, C G Freeman, and P F Wilson. Quantitative analysis of trace gases of breath during exercise using the new SIFT-MS technique. *Redox Rep*, 5:151-3, 2000.
- [100] T Sharkey. Isoprene synthesis by plants and animals. *Endeavour*, 20:74-8, 1996.

- [101] G M Silver and R Fall. Enzymatic synthesis of isoprene from dimethylallyl diphosphate in aspen leaf extracts. *Plant Physiol*, 97:1588–91, 1991.
- [102] G M Silver and R Fall. Characterization of aspen isoprene synthase, an enzyme responsible for leaf isoprene emission to the atmosphere. *J Biol Chem*, 270:13010–6, 1995.
- [103] D Smith, P Spanel, B Enderby, W Lenney, C Turner, and S J Davies. Isoprene levels in the exhaled breath of 200 healthy pupils within the age range 7–18 years studied using SIFT-MS. *J Breath Res*, 4:017101, 2010.
- [104] H L Smith. Monotone dynamical systems: an introduction to the theory of competitive and cooperative systems. *AMS, Providence*, 1995.
- [105] B G Stone, T J Besse, W C Duane, C D Evans, and E G DeMaster. Effect of regulating cholesterol biosynthesis on breath isoprene excretion in men. *Lipids*, 28:705–8, 1993.
- [106] C N Tassopoulos, D Barnett, and T R Fraser. Breath-acetone and blood-sugar measurements in diabetes. *Lancet*, 1:1282–6, 1969.
- [107] J Taucher, A Hansel, A Jordan, R Fall, J H Futrell, and W Lindinger. Detection of isoprene in expired air from human subjects using proton-transfer-reaction mass spectrometry. *Rapid Commun Mass Spectrom*, 11:1230–4, 1997.
- [108] P Tothill and A D Stewart. Estimation of thigh muscle and adipose tissue volume using magnetic resonance imaging and anthropometry. *J Sports Sci*, 20:563–76, 2002.
- [109] T Turányi and H Rabitz. Local methods. In A Saltelli, K Chan, and E M Scott, editors, *Sensitivity Analysis*, Series in probability and statistics. John Willey, Chichester, 2000.
- [110] C Turner, P Spanel, and D Smith. A longitudinal study of ammonia, acetone and propanol in the exhaled breath of 30 subjects using selected ion flow tube mass spectrometry, SIFT-MS. *Physiol Meas*, 27(321-7), 2006.
- [111] C Turner, P Spanel, and D Smith. A longitudinal study of breath isoprene in healthy volunteers using selected ion flow tube mass spectrometry (SIFT-MS). *Physiol Meas*, 27(1):13–22, 2006.
- [112] G N Vanderplaats. *Numerical Optimization Techniques for Engineering Design*. Series in Mechanical Engineering. McGraw-Hill, New York, 1984.

- [113] P D Wagner. Diffusion and chemical reaction in pulmonary gas exchange. *Physiol Rev*, 57(257-312), 1977.
- [114] P D Wagner, H A Saltzman, and J B West. Measurement of continuous distributions of ventilation-perfusion ratios: theory. *J Appl Physiol*, 36:588–98, 1974.
- [115] Peter D Wagner. The multiple inert gas elimination technique (MIGET). *Intensive Care Med*, 34:994–1001, Jun 2008.
- [116] P A Walravens, C Greene, and F E Frerman. Lovastatin, isoprenes and myopathy. *The Lancet*, 334:1097–8, 1989.
- [117] P M Wang, E Fujita, and J Bhattacharya. Mechanotransduction in the lung: vascular regulation of type II cell exocytosis. *Am J Physiol Lung Cell Mol Physiol*, 282:912–16, 2002.
- [118] J B West. *Respiratory Physiology: The Essentials*. Lippincott Williams and Wilkins, Baltimore, 8th edition, 2008.
- [119] B J Whipp and S A Ward. Cardiopulmonary coupling during exercise. *J Exp Biol*, 100:175–93, 1982.

Curriculum Vitae

PERSONAL DATA AND CONTACT INFORMATION

Name, First Name Koç Rauchenwald, Helin
Date and place of birth March 18, 1980, Ankara, Turkey
Citizenship Turkey
Working adress Process- and Product-Engineering research centre
Vorarlberg University of Applied Sciences
Hochschulstrasse 1, A-6850 Dornbirn, Austria
Phone +43 (0) 5572 7927123
E-mail helin.koc@fhv.at

EDUCATION AND EMPLOYEMENT

Vorarlberg University of Applied Sciences, Dornbirn

January 2007 - December 2008 Research Project "Breath Gas Analysis, Modeling, and Simulation"

March 2009 - Josef Ressel Centre
Project: "Optimization under uncertainty"

University of Vienna, Vienna

September 2001 - November 2007 Study of Mathematics.
Field of specialization: "Biomathematics"
Master thesis: "Selektions- und Migrationsmodelle in der Populationsgenetik"
supervised by R. Bürger

January 2007 - Oktober 2011 Doctoral studies supervised by G. Teschl and K. Unterkofler
Thesis title: "Compartmental Modeling for the Volatile Organic Compound Isoprene in Human Breath"

January 2009- December 2009 Fakultät für Mathematik
Scientific research in START-Project by G. Teschl

Gazi Üniversitesi, Ankara

September 1999 - June 2001 Study of mathematics

High school "Çankaya Anadolu Lisesi", Ankara

June 1998 Graduation

PUBLICATIONS

H Koc, J King, G Teschl, K Unterkofler, S Teschl, P Mochalski, H Hinterhuber, and A Amann. The role of mathematical modeling in VOC analysis using isoprene as a prototypic example. *J Breath Res.* 5(3):037102, 2011.

J King, H Koc, K Unterkofler, P Mochalski, A Kupferthaler, G Teschl, S Teschl, H Hinterhuber, and A Amann. Physiological modeling of isoprene dynamics in exhaled breath. *J Theor Biol.* 267:626–37, 2010

J King, A Kupferthaler, K Unterkofler, H Koc, S Teschl, G Teschl, W Miekisch, J Schubert, H Hinterhuber, and A Amann. Isoprene and acetone concentration profiles during exercise on an ergometer. *J Breath Res.* 3:027006, 2009.

CONFERENCE
CONTRIBUTIONS

FFH 2011, Vienna, Austria, April, 2011. *Mathematical modeling for breath gas analysis of VOCs* (Poster).

FFH 2009, Villach, Austria, April, 2009. *Mathematical modeling of blood-gas kinetics for validation of breath-gas diagnostics* (Poster).

Project Meeting BAMOD, Dortmund, Germany, March 27, 2008. *Breath Gas Analysis, Modeling, and Simulation* (Talk).

Project Meeting BAMOD, Cracow, Poland, September 23-25, 2007. *Breath Gas Analysis, Modeling, and Simulation* (Talk).